Project Final Report

Grant Agreement Number: 284405

"Analysis and Modelling of Multi-wavelength Observational Data from Protoplanetary Discs"

Project Acronym:	DiscAnalysis
SPA.2011.2.1-01:	exploitation of science and exploration data
Project Coordinator:	Dr. Peter Woitke

Project Duration: January 1$^{\rm st}$, 2012 – March 31$^{\rm st}$, 2016

Contents

1 Executive Summary

This European FP7-SPACE project (acronym *DiscAnalysis*; referred to hereafter as *DIANA*) has studied the birthplaces of planets, the so-called protoplanetary discs, both observationally and theoretically. We have collected multi-wavelength observational data from various space-borne instruments and combined them with ground-based data, from X-ray to centimetre wavelengths. The data include photometric fluxes, low and high resolution spectra, interferometric data and images, emission line fluxes, line velocity profiles and line maps, which probe both the dust and the gas in these objects.

We have developed novel 2D disc models that include continuum and line radiative transfer, disc chemistry, heating and cooling balance for both the gas and the dust, and coupled these to 3D diagnostic radiative transfer tools to simultaneously *predict all available observations based on a single model*, the *DIANA-standard* disc model.

With this powerful modelling strategy, we are providing new insights into the preconditions for planet formation in protoplanetary discs. Based on our original target list of 85 protoplanetary discs, we have identified about 45 objects suitable for detailed disc modelling (well-known stellar properties – also in UV and X-rays, sufficiently unobscured and isolated single stars) with suitable continuum and line observational data up to centimetre wavelengths. We have performed 24 continuum-fitting disc models, out of which we generated 11 detailed gas and dust *DIANA-standard* models which fit all observational data, line and continuum, as well as possible.

These models allowed us to draw new conclusions about the dust properties in discs, the PAHs, the total dust and gas masses, the radial and vertical distribution of the dust and the gas, the chemical structure including ices, and the gas and dust temperatures in protoplanetary discs, *just before the planets form*. Both the collected observational datasets and links to our disc modelling software are offered to the community via our website for further use and analysis. The modelling datasets include the full 2D physico-chemical structure in the discs and a large suite of predicted line and continuum observations for future purposes.

We have furthermore computed large grids of disc models in parameter space to identify the main physical and chemical mechanisms responsible for trends and correlations that we find between the physical disc parameters and the observable spectral appearance. Based on these results, we have revisited previously known disc diagnostics based on single observational quantities, such as mass determinations based on millimetre continuum fluxes and CO isotopologue lines, we have provided new robust diagnostics, and we have provided a large suite of predictions for yet unobserved spectral quantities for future observing facilities such as JWST and SPICA.

The investigations have been carried out between 01/2012 and 03/2016 by a team of about 20 senior scientists, postdoctoral researchers and PhD students at five European Universities: (i) the University of St Andrews, UK, (ii) the Universität Wien, Austria, (iii) the Université Grenoble Alpes, France, (iv) the Rijksuniversiteit Groningen, The Netherlands, and (v) the Universiteit van Amsterdam, The Netherlands.

Our dissemination efforts included 50 scientific papers, 74 scientific talks and 19 posters at international workshops and conferences, and about 70 public outreach talks and demonstrations. We published 7 press releases and a series of short YouTube videos about protoplanetary discs and planet formation. The Summer School *"Protoplanetary Discs: Theory and Modelling Meet Observations"* was held on Ameland, The Netherlands, June 16-20, 2014 (leading to the publication of a book with the same title) and the international scientific conference *"Protoplanetary Discussions"* was held in Edinburgh, Scotland, March 7-11, 2016.

2 Summary description of project context and objectives

One of the most exciting astrophysical realisations in the past decades is that our solar system is neither special nor rare. Planets are now expected to form regularly and robustly around most new-born stars, from the leftover gas and dust, which continues to rotate around the central objects in form of protoplanetary discs for about 3-10 Myrs.

However, how do these planets form? Which processes lead to a sufficient concentration of dust and gas in discs? *What are the chemical and physical preconditions for planet formation in protoplanetary discs?* Ultimately, our science field is driven by one of the most fundamental questions that mankind has ever formulated:

Are we alone in the universe?

Both possible answers to this intriguing question are simply breathtaking.

Consequently, astronomers have always pointed their telescopes towards the youngest stars, looking for evidence of circumstellar material and planet formation. First evidence for the existence of protoplanetary discs was derived from a "nebulosity" detected in optical images around young inter-mediate mass stars (Herbig, 1960). However, at that time, the concept of protoplanetary discs was not yet established, and astrophysicists thought about star formation with a more simplistic spherical infall model, thus expecting pre-main sequence stars to be enshrouded in a spherical envelope of dust and gas.

With the launch of the IRAS satellite in 1983 (InfraRed Astronomical Satellite), it became evident that most pre-main sequence stars possess a strong far infrared (far-IR) excess. Spherical infall models cannot explain both at the same time, the optical light received directly from the central objects as well as the strong IR excess, so the necessity to deviate from spherical geometry was becoming obvious. First images of millimetre dust emission in the late 1980s (e.g. Smith & Terrile, 1984), and double-peaked molecular line emission profiles at millimetre wavelengths showed the extended size and velocity profiles expected from a disc in Keplerian rotation. In the 1990s, NASA's Hubble Space Telescope (HST) clearly imaged the discs in reflected starlight, and in silhouette against the illuminated background of the Orion nebula (O'Dell & Wen, 1994). These were the first times astronomers directly *saw* the protoplanetary discs where planets form.

Ever since, the observation of star and planet formation has remained one of the main science drivers for the current design of telescopes and astronomical instrumentation, with the final goal to resolve the gas and dust, and find the planets in the discs.

Concerning the theoretical understanding of planet formation, the core-accretion theory (Pollack et al., 1996; Laughlin et al., 2004; Ida & Lin, 2005) posits collisional growth of submicron sized dust grains up to km-sized planetesimals on timescales of 10^5 to 10^7 years, and further growth to Earth-sized planets by gravitational interactions. Once solid protoplanetary cores of $\sim$10 Earth masses have formed, the surrounding gas is gravitationally captured to form gas giant planets. Alternatively, gravitational instabilities in discs may directly form planets on much shorter timescales (few 1000 years), but require fairly high densities and short cooling timescales at large distances from the star (Boss, 1997, 2009; Rice & Armitage, 2009).

However, what type of planetary system eventually forms, and whether these planets will become habitable, depends largely on the physico-chemical state in the discs at the time when the planets form (e.g. radial distribution of matter, the dust/gas ratio, opacities, temperatures, chemical composition, dust properties). Therefore, to understand planet formation requires us to study the protoplanetary discs both from an observational point of

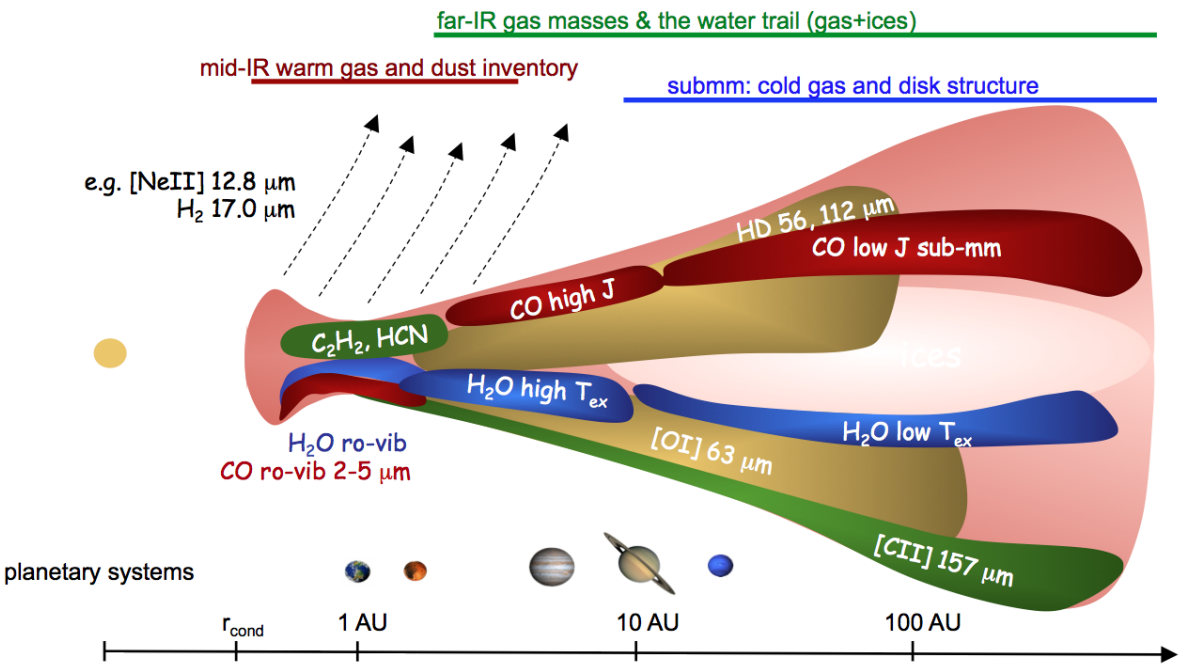

Figure 1: Sketch of the two-dimensional disc structure and the various disc components that we observe over the entire wavelength range. Note that the radial scale is logarithmic and refers to stars that are slightly more luminous than our Sun.

view and by modelling their internal physico-chemical structure and long-term evolution.

Observations of protoplanetary discs are challenging to interpret since physical densities in the discs span more than 10 orders of magnitude, ranging from about 10^{15} particles/cm^3 in the midplane close to the star to typical molecular cloud densities of 10^4 particles/cm^3 in the distant upper disc regions. At the same time, temperatures range from several 1000 K in the inner disc to only 10–20 K at distances of several 100 AU. The central star provides high-energy UV and X-ray photons which are scattered in complicated ways into the disc where they drive various non-equilibrium processes. The exact structure of the discs is not known, but it strongly affects the excitation of atoms and molecules and therefore their spectral appearance in form of emission lines. Figure 1 summarises our current understanding of the physical and chemical structure of protoplanetary discs. The figure illustrates the various disc regions as traced by different wavelengths and emission lines. As a rule of thumb, the short wavelengths (X-ray, UV, optical) tell us about the high-energy processes like mass accretion, stellar activity, and jet acceleration close to the star, intermediate wavelengths (near to mid-IR) tell us about the nature and distribution of dust and gas in the inner disc, and observations at longer wavelengths tell us about the total mass and chemistry of the gas and dust in the most extended parts of the disc. A better understanding of these multi-wavelength observations requires consistent models that are capable of treating all important physical and chemical processes in detail, simultaneously, in the entire disc.

This is where the FP7-SPACE project *DIANA* enters the quest for a better understanding of planet formation. Large amounts of survey data exist, but are seriously under-utilised in terms of systematic and coherent modelling. Most of the scientific projects working in this field are funding- and man-power limited, with the money usually being tied to a specific observational mission. The opportunity to involve data and modelling results from other wavelength regimes is often lacking. Our main project goals have been as follows:

- Collection of *as complete as possible datasets* from X-rays to cm wavelengths for a well selected sample of suitable protoplanetary discs to build an archive of standard data for further investigation. This includes high-quality spectra, photometry, visibility data and images from frontier instrumentation.
- Distillation of *model-friendly* observational data in uniform formats, permitting direct comparisons between different instruments and easy use in the subsequent modelling process.
- Development of high-quality, *cutting-edge disc models* including all relevant physical, chemical and radiative processes (dust opacities, PAHs, X-rays, separate dust and gas energy equations, non-LTE line formation, etc.) by a combination of Monte Carlo radiative-transfer programs (MCFOST, MCMax) and the radiation thermo-chemical gas modelling code ProDiMo.
- Development of a *standardised modelling procedure* leading to reproducible and well-documented fitting results. Application of this "*DIANA-standard* modelling procedure" to a well-selected subset of individual targets, aiming at *simultaneous fits* of all available multi-wavelength data, including complex near-IR molecular spectra and continuum visibilities, for example.
- *Calibration of the models* (e.g. adjustment of hidden modelling parameters, options and procedures) by analysis of systematic deviations between modelling results and data.
- *Statistical analyses* of the observational data and the modelling results, and the production of large *model grids* to identify, better understand and visualise the complex physical and chemical mechanisms responsible for observational trends.
- Identification of *correlations and robust trends* between observables and physical disc properties like the total disc mass, providing new *tools for disc diagnostics*.
- Offering the easy-to-use datasets, the detailed modelling results, and the systematic modelling grids to the community via a public database, for *further analysis and use in adjacent science areas*.

We are convinced that this FP7 project has provided a major contribution to the exploitation of European space mission data in the field of protoplanetary disc research. The following scientific questions have been addressed by the project.

1. How can we most reliably infer the physical/chemical disc structure from observations?
2. Which gas emission lines probe what process in which parts of the discs?
3. How can we derive the total gas mass, and the overall gas-to-dust mass ratio? How reliable are these results?
4. How can we recognise and diagnose disc anomalies, such as inner holes, gaps and spiral structures?
5. How do discs physically and chemically evolve in time?
6. What is the impact of planets on the disc structure?
7. What are the chemical pre-conditions for gas-planet formation, and those for rocky-planet formation?

3 Description of main S & T results/foregrounds

Figure 2 visualises the structure of this FP7-project in form of work packages and their inter-dependencies. The smaller work packages WP 3, WP 4 and WP 5 have studied particular physical processes and types of observations. These work packages have been finished early during the project (after 2 years) to extend the models' range of applicability and their capabilities to predict additional types of observations. In the following, we will summarise and review some highlights from the results of the scientific work packages WP 1 to WP 6, one by one.

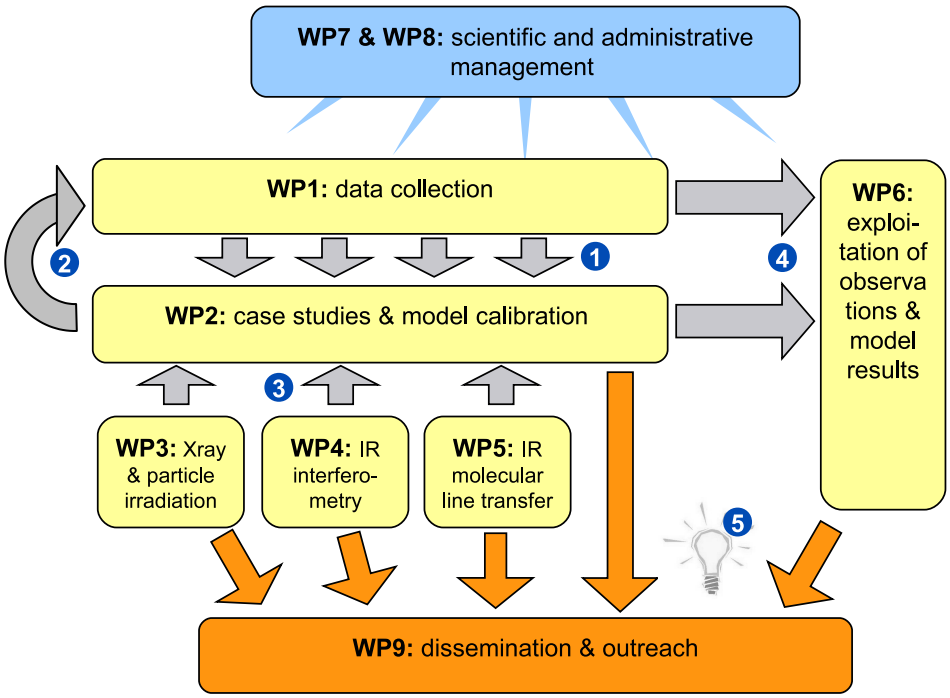

Figure 2: Structure and inter-dependencies of work packages.

① Selection of suitable target objects, compilation and reduction of multi-wavelength data.
② Using predictive power of models to optimise observing strategies and support proposal writing.
③ Extending model applicability by implementation of new physical modules.
④ Providing observational and modelling trends and conclusions for further analysis.
⑤ New scientific conclusions.

3.1 WP 1: Data Compilation

Work package 1 has been one of the two basic pillars of the DIANA project, providing the observational data test-bed to develop and refine the theoretical models (WP2) which would provide firm grounds for deriving global properties of protoplanetary discs (WP6). The initial requirement was to compile panchromatic data, ranging from X-rays to cm wavelengths on a set 40-50 targets known to host protoplanetary discs. The compiled, homogeneous datasets along with the modelling results are now publicly accessible through the DIANA Object Database (DIOD) (Deliverables D1.1, D2.2).

As a major part of DIANA, the compilation of multi-wavelength datasets was initiated at the very beginning of the project. The work involved two major functions: collection, evaluation and careful bookkeeping of existing (published) datasets as well as reduction of unpublished data by our team experts. An initial pool of 85 targets was initially compiled

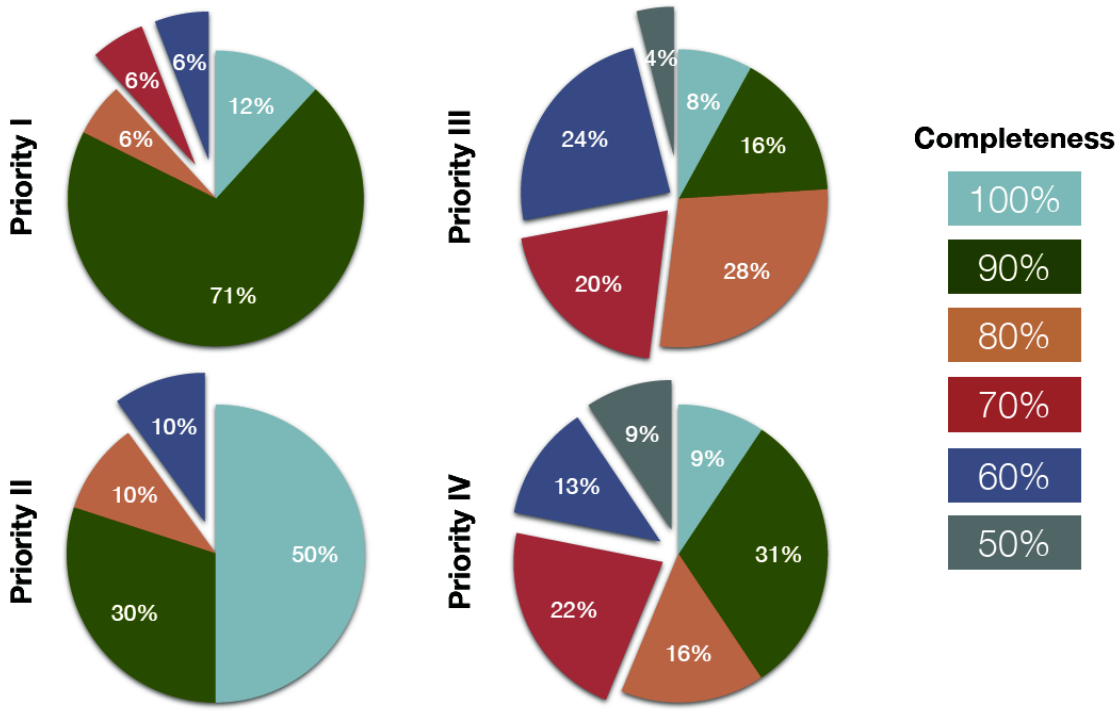

Figure 3: Completeness of observational data collection, separated for priority I-IV sources.

and sources were evaluated by scientific criteria into four priority groups. An analytical account of the types of sources per priority group is given in Table 1. In the lower part of the same table, we list the number of SED and full ProDiMo models for each priority group provided in the DIOD database. We aimed to compile complete datasets for $\sim$ 40-50 sources that would represent subjects of intense studies with models as part of WP2. This means that each source should have high-quality representative data delineating each part of the spectral energy distribution (SED) probing the central forming star and the dust content of the surrounding disc. Such data need to cover the electromagnetic spectrum, from X-rays to millimeter and centimetre wavelengths. In order to probe for the gas content of discs, the requirement for emission lines (and line shapes, if available) emerging from the inner and the outer parts of the disc was set. Additional data on the physical structure of the protostellar discs, such as high resolution (e.g. interferometric) images provide valuable constraints to models.

Table 1: Prioritisation of sources by type, and modelling coverage

Priority	Herbig Ae/Be	Transition Discs	T Tauri	Edge-on	Embedded	Total
I	5	1	14	1		**18**
II	3	4	3			**10**
III	3	2	15	2		**25**
IV	2	1	24	3	2	**32**
Total	**13**	**8**	**56**	**6**	**2**	**85**
SED models	8	4	11	1		**24**
DIANA standard models	5	3	3			**11**

The data compilation for the description of the SED represents an assembly of more than 150 individual filters and spectral chunks observed with $\sim$50 different facilities. Apart from unpublished data reduced by our group members (e.g. X-ray spectra) and provided to our group by collaborators, data were collected from more than 100 published articles.

Table 2: Target list and stellar parameters.

priority I ; priority II ; priority III ; priority IV ; 1 = SED-fitting model; 2 = DIANA standard model.

Source name	model	Spectral type	Av [mag]	log(L) [$L_\odot$]	$M_\star$ [$M_\odot$]	$T_{\rm eff}$ [K]	log(age) [yr]	L_X [$L_\odot$]	log($\dot{M}_{\rm acc}$) [$M_\odot$/yr]	$L_{\rm FUV}$ [$L_\odot$]	d [pc]
Herbig Ae/Be											
HD97048	1	B9.5[1] A0V[2] A0[3] B9[64]	0.87[2] 1.15[4] 1.24[3] 1.28[64]	1.84[1] 1.46[2] 1.53[3] 1.60[64]	2.5[3] 2.5[64]	10000[1] 10000[64]	6.8[4] >6.7[64]	8.26(−5)[5] 1.4(−5)[64]		7.2[64]	175[2] 158[4] 171
MWC480	1,2	A5[64]	0.16[64]	1.14[64]	1.97[64]	8250[64]	7.04[64]	2.5(−5)[64]		0.56[64]	137
HD142666	1,2	A8V[3] F1[64]	0.8[3] 0.81[64]	0.81[3] 0.80[64]	1.6[3] 1.6[64]	7590[6] 7297[3] 7050[64]	5.1[6] >7.1[64]	1.1(−5)[64]	−6.73[6]		145[6] 116
HD95881	1	B9[64]	0.89[64]	1.53[64]	2.5[64]	9900[64]	>6.9[64]			4.9[64]	171
HD169142	1,2	A7[64]	0.06[64]	0.99[64]	1.8[64]	7800[64]	7.11[64]	1.4(−6)[64]		0.22[64]	145
HD100546	1	B9V[2] B9[64]	0.09[7] 0.15[2] 0.36[3] 0.22[64]	1.47[2] 1.36[4] 1.63[3] 1.48[64]	2.5[3] 2.5[64]	10470[4] 11412[3] 10470[64]	>6.68[64]	2.08(−5)[5] 2.0(−5)[64]		8.0[64]	103[2] 97[4] 103
HD163296	1,2	A1(Ve)[3] A1[64]	0.5[3] 0.48[64]	1.58[3] 1.54[64]	2.47[3] 2.47	8907[3] 9000[64]	6.66[64]	4.4(−5)[64]	−6.3[64]	2.1[64]	122[3] 119
ABAur	1,2	A1[8] A0[9] B9[64]	0.55[8] 0.5[9] 0.25[4] 0.42[64]	1.39[8] 1.68[9] 1.62[64]	2.4[9] 2.31[8] 2.5[64]	9840[9] 9550[64]	6.6[8] >6.6[64]	8.26(−5)[5] 2.6(−5)[64]	−6.9[9] −6.9[64]	4.0[64]	140[9] 144
HD141569		B9.5[9]	0.37[4]	1.36[9] 1.47[4]	2.2[9]	9550[6]	6.7[6]	<3.29(−6)[5]	−6.89[6] −8.13[9]		99[6] 116[4]
HD104237		A0V[2] A4-5V[4]	0.08[7] 0.56[2] 0.16[4]	1.72[2] 1.45[4]		8550[4]	6.74[4]	4.14(−4)[5]			114[4]
HD144432		A5V[2]	0.62[2]	1.68[2] 1.17[9]	2[9]	7410[6]	5.3[6]		<−7.22[6] −7.69[9]		145[6] 253[2]
V380Ori		B8/A2[10] A1e[11]		1.99[11]							510[11]
HD150193		A1V[2] B9.5Ve[10]	1.15[2] 1.55[4]	1.26[2] 1.69[4]	2.2[9]	8970[6]	5[6] 6.58[4]	1.0(−4)[5]	−6.12[6]		203[6] 150[2] 216[4]
Transition Discs											
TWHya	1,2	K7[64]	0.20[64]	−0.61[64]	0.75[64]	4000[64]	7.11[64]	7.0(−5)[64]	−8.82[64]	0.011[64]	51
TCha								2.87(−4)[12]			
GMAur	1,2	K7[64]	0.30[64]	−0.22[64]	0.7[64]	4000[64]	6.41[64]	4.18(−4)[12] 1.2(−4)[64]		0.0066[64]	140
DMTau	1,2	M3[8] M1[9] M0[64]	0.1[8] 0.6[15] 0[17] 0.55[64]	−0.89[8] −0.49[9] −0.6[15] −0.63[64]	0.62[9] 0.35[8] 0.53[64]	3700[9] 3780[64]	6.6[8] 6.78[64]	5.23(−4)[12] 2.9(−4)[64]	−8.20[13] −8.54[16] −7.95[12]	0.0083[14] 0.0040[15] 0.00068[18] 0.0070[64]	140[15] 140
LkCa15											
49Cet	1	A1V[19] A4V[4] A2[64]	0.22[4] 0.0[64]	1.34[20] 1.22[64]	2.17[21] 2.0[64]	9970[21] 8770[64]	6.94[19] 6.9[4] 6.99[64]	5.3(−5)[64]		1.0[64]	59[20] 59.4
CoKuTau4		M1.1[8]	1.75[8]	−0.5[8]	0.53[8]	3720[22]	6.5[8]	<5.49(−5)[23]	<−10[12]		
UXTauA		K2[24]	0.51[7] 0.2[24] 1.3[25]	0[24] 0.338[25]	1.5[25]	5856[17]	6.43[27] 6.1[17]	0.00052[7]	−8.02[25]	0.00068[18]	140
T Tauri, F-type											
HD142527		F6IIIe[28]	0.6[27] 0.37[2]	1.18[27] 1.32[2]	2.2[28]	6250[27]	6.7[27] 6.3[4]		−6.85[30] −7.02[9]		198[2] 233[4]
HD135344B	1	F4V[30] F8V[3] F5V[3] F3[64]	0.4[30] 0.40[64]	0.91[3] 0.88[64]	1.65[30] 1.7[3] 1.65[64]	6620[31] 6950[3] 6620[64]	7.08[64]	5.3(−5)[64]		0.032[64]	140 140
RYTau		G0[8] F8[15] K1[17] F8V [3]	1.84[26] 1.8[15] 2.2[3]	1.03[8] 0.89[15] 1.04[3]	2.24[26]	5770[6] 5496[3]	6.7[8] 5.6[17]	1.44(−3)[31]	−7.19[33]	0.16[14] 0.072[15]	134[6] 131[8] 140[3]
CQTau		A8[33] F2[15]	2.85[34] 1.9[15] 1.4[4]	0.82[15] 1.05[36] 0.53[4]	1.5[35]	6750[35] 7200[36]	7[35] 6.6[4]		<−8.30[6]	0.094[15]	100[33] 140[36] 113[4]
HD181327		F5/6[37]		0.522[38]	1.36[38]		7.08[37]	<6.56(−5)[5]			51.9[38]

Table 2: continued

Source name	model	Spectral type	Av [mag]	log(L) [$L_\odot$]	$M_\star$ [$M_\odot$]	$T_{\rm eff}$ [K]	log(age) [yr]	L_X [$L_\odot$]	log($\dot{M}_{\rm acc}$) [$M_\odot$/yr]	$L_{\rm FUV}$ [$L_\odot$]	d [pc]
T Tauri, G-type											
DOTau		M0.3[8] M0[17] M6[3]	0.78[8] 1.35[24] 2.3[15] 2.6[17]	−0.64[8] 0[15] 0.11[3]	0.56[26] 0.37[9] 0.66[17]	3850[9] 3777[3]	6.9[8] 5.73[17]		−6.84[39] −7.28[9]	0.066[14] 0.0325[15]	140[9]
RULup	1	K7[64]	0.0[64]	0.13[64]	1.15[64]	4060[64]	6.08[64]	3.4(−4)[64]		0.00527[15] 0.012[64]	150
RYLup	1	G8[40] K4[41] G0V[11] K4[64]	0.65[41] 0.44[2] 2.48[3] 0.29[64]	0.1[41] −0.4[2] 0.42[15] 0.45[64]	1.71[40] 1.38[3] 1.38[64]	4590[42] 5200[3] 4420[64]	7.08[40] 6.48[64]	3.6(−4)[64]		0.0022[15] 0.0024[64]	108[41] 150[11] 120[3] 185
V1149Sco	1	K0III[42] G6[15] F9[64]	1.6[15] 0.71[64]	0.4[9] 0.45[64]	1.28[64]	5088[44] 6080[64]	7.28[64]	2.8(−5)[64]		0.0817[15] 0.051[64]	186[43] 145[15] 145
DLTau		K5.5[8] K7[9]	1.8[8] 1.3[15]	−0.3[8] 0.06[9]	0.92[8] 0.76[9]	4000[9]	6.7[8]		−7.41[9]	0.0041[14] 0.0010[15]	140[9]
RNO90		G5[44]	4.2[44]	0.82[45]	1.6[9]	5660[9]			−7.4[9]		120[9]
RWAur – RWAurA – RWAurB		K0[8] K4[15] K6.5[8] K4[15]	−0.25[8] 0.5[16] 0.1[8] 1.2[15]	−0.14[8] −0.35[8]	1.13[8] 1.4[36] 0.85[8] 0.86[17]	4900[36] 4350[17]	7.2[8] 5.85[36] 6.7[8] 6.4[17]	4.1(−4)[7]	−7.7[45]		140[8] 140[8] 140[8]
LkHa326		M0[47]					5.48[47]				250[9]
T Tauri, K-type											
VZCha		K7e[49] M0V[49]	0.44[2]	−0.54[49]	0.9[49]	3990[49]		1.38(−4)[12]	−8.28[12] −7.39[49]		168[2] 150[9]
DNTau		K6V[3]	0.5[3]	−0.1[3]	0.65[3]	3904[3]			−8.00[45]		140[3]
TWCha	1	K8[1] K0[2] K6[64]	2.11[2] 1.61[64]	−0.24[1] −0.23[64]	1.15[49] 1.0[64]	3990[1] 4110[64]	6.63[64]	3.66(−4)[12] 1.0(−4)[64]	−9.55[49]	0.072[64]	168[2] 160
BPTau	1,2	K7[64]	0.57[64]	−0.05[64]	0.65[64]	3950[64]	6.20[64]	3.60(−4)[12] 2.5(−4)[64]	−7.55[64]	0.013[64]	140 140
CITau	1	K5.5[8] K7[24] K6[64]	1.9[8] 1.2[24] 1.8[15] 1.77[64]	−0.2[8] −0.08[15] −0.04[64]	1.53[8] 0.74[17] 0.90[64]	4000[9] 4200[64]	6.6[8] 5.96[17] 6.45[64]	5.10(−5)[31] 8.26(−5)[5] 1.0(−5)[64]	−7.59[31] −7.19[31]	0.0016[14] 0.00092[15] 0.0020[64]	140[9] 140
DRTau		K6.0[8] K7[15]	0.45[8] 0.95[24] 1.2[15]	−0.51[8] 0.23[24]	0.87[8] 0.4[9]	4060[36]	7[8] 5.29[17]	0.0001[7]	−7.28[45] −6.86[9]	0.0083[14] 0.0011[15]	140[9]
Haro1-16		K2[13]	1.7[13]	−0.194[13]	0.97[13]	4900[13]		3.40(−4)[12]	−8.2[13]	0.0125[15]	125[13]
CWTau		K3[8]	1.8[8]	−0.35[8]	1.01[8]	4730[9]	7.2[8]	7.43(−4)[31]	−7.99[31]		140[9]
V4046Sgr		K5[15]	0.04[7] 0[15]	−0.41x2[11]	0.9[50]	4250[50]	1.08[50]	3.14(−4)[52]	−9.3[50]	7.23(−4)[15] 1.51(−3)[18]	73[51] 83[18]
LkHa327		K2[46]		0.96[53]			5.[50]				250[9]
PDS66		K1[16]	0.2[16] 1.2[15]	−0.046[16] 0.1[15]	1.1[16]			3.82(−4)[51]	−9.89[16] −9.1[51]	2.46(−2)[15]	103[51]
UScoJ1604-2130		K2[53]	1[54]	−0.118[54]	1[53]	4549[56]	6.7[53]	5.21(−4)[5]			145[54]
GOTau		M2.3[8] M0[17]	1.5[8] 1.2[17]	−0.7[8]	0.42[8] 0.72[17]	3850[36]	6.6[8] 6.81[17]	6.51(−5)[31]	−8.42[31]		140[8]
V1121Oph		K5[15]	1.2[15]	−0.06[2]	1.4[9]	4400[9]			−7.52[9]	0.00876[15]	95[2] 160[9]
WWCha		K5[1]	2.31[2]	0.74[1]		4350[1]					168[2]
FKSer		K6IVe[10]		0.2[11]							32[11]
TTauN		K0[15] K1[24]	1.5[15] 1.44[24] 1.25[8]	0.86[9] 1.03[24] 0.85[8]	2.11[9] 1.99[8]	5250[9]	5.9[8]	2.1(−3)[31]	−7.5[31] −7.24[31]	0.1[14] 0.061[15]	147[8]
AS205B		M0.1[8] K5[2] M3[9]	2.4[8] 1.09[2]	0.05[8] 0.34[2]	0.55[8] 0.3[9]	3450[9]	6.1[8]		−6.68[9]		145[2] 160[9] 121[8]
WaOph6		K[9]		−0.17[9]							120[9]
HTLup		K2[41]	1.45[41] 0.28[2]	0.78[41] 0.44[2] 1.16[9]	2.5[9]	4890[41]			−7.78[9]		159[2]
DoAr24E		K5[2]	2.16[2]	−0.45[2] 0.1[23]	0.47[23]			1.46(−4)[12] 1.31(−4)[23]	−8.46[23]		120[9]

Table 2: continued

Source name	model	Spectral type	Av [mag]	log(L) [$L_\odot$]	$M_\star$ [$M_\odot$]	$T_{\rm eff}$ [K]	log(age) [yr]	L_X [$L_\odot$]	log($\dot{M}_{\rm acc}$) [$M_\odot$/yr]	$L_{\rm FUV}$ [$L_\odot$]	d [pc]
UYAur		K7[8]	1[8]	−0.07[8]	0.7[8]		6.3[8]	1.04(−4)[12]	−7.18[39]		140[9]
– UYAurA		M0[17]	0.6[17]	0.49[22]	0.66[17]	3850[17]	5.56[17]				
– UYAurB		M2.5[17]	2.7[17]		0.62[17]	3485[17]	5.84[17]				
DGTau		K7[8]	1.6[8]	−0.31[8]	0.77[8]	4200[9]	6.6[8]	2.1(−3)[5]	−7.49[9]		140[9]
			1[24]	0.18[24]							
VWCha		K5[57]	2.39[57]	0.62[57]	1.4[57]	3955[1]		2.17(−3)[12]	−6.95[12]	0.041[14]	150[9]
		K8[1]	1.91[2]	0.48[1]	0.6[9]				−7.5[9]		168[2]
				0.22[2]							
T Tauri, M-type											
IMLup		K6[8]	0.4[8]	−0.03[8]	0.78[8]		6.3[8]	8.36(−4)[12]			
Haro6-13			5.43[56]	−0.159[56]		3850[56]		4.14(−5)[5]			140[5]
– Haro6-13E		M1.6[8]	2.2[8]	−0.57[8]	0.48[8]	3800[9]	6.5[8]		−7.02[9]		140[9]
– Haro6-13W		K5.5[8]	2.25[8]	−0.04[8]	[8]		6.3[8]				
CYTau	1,2	M1[26]	0.1[26]	−0.4[26]	0.48[26]	3628[3]	6.37[26]	3.47(−5)[31]	−8.86[31]		140[3]
		M2V[3]						5.07(−5)[31]	−8.12[31]		
		M1[64]	0.10[64]	−0.45[64]	0.43[64]	3640[64]	6.34[64]	6.9(−6)[64]	−8.12[64]	0.00073[64]	140
DFTau	1	M2.7[8]	0.1[8]	−0.35[8]	0.32[8]	3470[9]	5[8]	3.30(−5)[5]	−6.75[39]	0.00069[15]	140[9]
		M0.5[9]	0.6[15]	0.29[9]	0.27[9]						
		K7[64]	1.27[64]	0.39[64]	1.17[64]	3900[64]	6.34[64]			0.36[64]	140
– DFTauA		M2[17]	0.6[17]		0.61[17]	3560[17]	5.14[17]				
– DFTauB		M2.5[17]	0.8[17]		0.65[17]	3485[17]	5.74[17]				
RECX15	1,2	M3[16]	0.02[7]	−0.3[16]	0.3[16]				−9.1[16]	0.00030[18]	97[18]
		M3[64]	0.65[64]	−1.04[64]	0.28[64]	3400[64]	6.81[64]	8.2(−6)[64]	−9.0[64]	0.0063[64]	94.3
FTTau	1	M3[64]	1.09[64]	−0.53[64]	0.30[64]	3400[64]	6.28[64]	7.0(−6)[64]		0.0052[64]	140
EXLup		M0.5[57]	0[57]	−0.4[57]	0.5[57]	3800[41]		3.92(−4)[12]			147[2]
WXCha		M1.25[1]	1.99[2]	−0.076[1]	1.05[48]	3700[1]		1.20(−3)[12]	−8.47[12]		168[2]
				−0.37[2]							
XXCha		M2[1]		−0.43[1]	0.57[49]	3560[1]		2.87(−4)[12]	−9.07[12]		
GQLup		K5[8]	1.6[8]	−0.04[8]	0.89[8]	4000[9]	6.4[8]	1.93(−4)[12]	−7.5[12]		100[9]
		K7[9]							−8.15[9]		150[11]
Hen3-600A		M4Ve[10]	0[61]	−1.1[58]	0.37[58]	3350[58]	7[58]	4.14(−5)[5]	−9.6[58]		42[5]
		M3[58]									34[59]
UZTauE		M2-3[15]	0.3[15]	0.2[22]		3720[37]	5.3[22]	2.33(−4)[31]	−8.70[31]	0.00056[15]	140[5]
IQTau		M1.1[8]	0.85[8]	−0.72[8]	0.56[8]	3775[17]	6.9[8]	1.09(−4)[31]	−8.32[31]		140
		M0.5[17]	1.3[17]		0.64[17]		5.93[17]	8.26(−5)[5]			
HKTauB		M1[17]	2.3[17]	−0.33[22]	0.41[47]	3705[17]	7.7[17]	2.07(−5)[31]	−7.65[31]		
V853Oph		M2.5[2]	0.14[2]	−0.42[2]	0.42[24]			8.10(−4)[12]	−8.31[12]		128[2]
GGTauA		K7.5[8]	1.05[8]	0.14[8]	0.62[8]	4000[22]	6[8]				
– GGTauAB		K7.5[8]	1.05[8]	0.12[8]	0.63[8]		6[8]	1.04(−5)[5]	−7.76[39]		140[5]
– GGTauB		M5.8[8]	0[8]	−1.13[8]	0.07[8]	3760[22]	5.2[8]				
SXCha		M0[1]	0.79[2]	−0.38[1]		3850[1]			−8.37[12]		168[2]
		M3.5[1]		−1.4[1]		3340[1]					
TWA07		M3.2[8]	−0.1[8]	−0.94[8]	0.32[8]		6.7[8]	1.04(−4)[5]		6.0(−6)[15]	34[11]
		M1[15]	0[15]	−0.3[16]	0.5[16]						
				−1.09[15]							
FSTau		M2.4[8]	2.95[8]	−0.84[8]	0.41[8]		6.7[8]	8.43(−4)[31]	−9.50[31]		
– FSTauA		M0[17]	5[17]		0.66[17]	3850[17]	5.67[17]				
– FSTauB		M3.5[17]	5.2[17]		0.32[17]	3340[17]	6.4[17]				
Edge-on systems											
AATau	1	M0.6[8]	0.4[8]	−0.36[8]	0.58[8]	4000[9]	6.4[8]	3.24(−4)[31]	−8.48[39]	0.016[14]	140[9]
		K7[9]	0.74[15]	−0.15[24]	0.74[17]	4030[3]	6.16[17]	2.61(−4)[5]	−7.82[16]	0.002[16]	
		M0V[3]	0.93[24]	−0.97[3]	0.85[3]		5.98[40]			0.0022[18]	
			1.64[3]								
		K7[64]	0.99[64]	−0.11[64]	0.85[64]	4010[64]	6.36[64]	3.2(−4)[64]		0.0023[64]	140
IRAS04158+2805		M6[17]	8.6[17]	−0.39[22]	0.1[17]	2990[17]	5.91[17]	2.30(−4)[31]	<-9.5[31]		140[5]
		M3[5]				3470[23]					
IRAS04385+2550		M0.5[17]	10.2[17]	−0.425[56]	0.64[17]	3775[17]	5.91[17]	1.05(−4)[31]	−8.11[31]		140[5]
			5.24[56]								
HH30		M0[46]		−1[63]	0.45[62]	6-6.6[63]				140[62]	
HVTauC		M0[60]	1.72[56]	−1.56[56]	0.5-1[60]	4205[57]		9.71(−5)[5]			140[5]
					0.72[52]						
FlyingSaucer			2.1[61]	−0.85[61]		3500[60]					140[61]

Table 2: continued

Source name	model	Spectral type	Av [mag]	$\log(L)$ [$L_\odot$]	$M_\star$ [$M_\odot$]	$T_{\rm eff}$ [K]	log(age) [yr]	L_X [$L_\odot$]	$\log(\dot{M}_{\rm acc})$ [$M_\odot$/yr]	$L_{\rm FUV}$ [$L_\odot$]	d [pc]
Embedded sources											
HLTau		K3[8]	2.5[8]	−0.84[8]	0.55[9]	4350[9]	5.93[17]	1.0(−3)[31]	−8.83[32]		140[9]
IRAS04189+2650		K5[10]	9.96[47]	−1.33[47]	1.2[47]	4395[47]			−6.76[47]		

Entries as $a(b)$ mean $a \times 10^b$. (1) Luhman (2007); (2) Sartori et al. (2003); (3) Antonellini et al. (2015); (4) Meeus et al. (2012); (5) Dent et al. (2013); (6) Mendigutía et al. (2012); (7) McJunkin et al. (2014); (8) Herczeg & Hillenbrand (2014); (9) Salyk et al. (2013); (10) Skiff (2014); (11) Kraus et al. (2011); (12) Güdel et al. (2010); (13) Manara et al. (2014); (14) Ingleby et al. (2011); (15) Yang et al. (2012); (16) Ingleby et al. (2013); (17) Kraus & Hillenbrand (2009); (18) Schindhelm et al. (2012); (19) Roberge et al. (2013); (20) Montesinos et al. (2009); (21) Carmona et al. (2007); (22) White & Hillenbrand (2004); (23) Salyk et al. (2011); (24) Cabrit et al. (1990); (25) Espaillat et al. (2007); (26) Bertout et al. (2007); (27) Verhoeff et al. (2011); (28) Biller et al. (2012); (29) Mendigutía et al. (2014); (30) Carmona et al. (2014); (31) Güdel et al. (2007); (32) Calvet et al. (2004); (33) Trotta et al. (2013); (34) Alecian et al. (2013); (35) Testi et al. (2003); (36) Chapillon et al. (2008); (37) Stark et al. (2014); (38) Lebreton et al. (2012); (39) Gullbring et al. (1998); (40) Manset et al. (2009); (41) Hughes et al. (1994); (42) Pickles & Depagne (2010); (43) Ammons et al. (2006); (44) Chen et al. (1995); (45) Ingleby et al. (2013); (46) Pontoppidan et al. (2010); (47) Lahuis et al. (2007); (48) Torres et al. (2006); (49) Frasca et al. (2015); (50) Donati et al. (2011); (51) Sacco et al. (2012); (52) Cohen et al. (1989); (53) Zhang et al. (2014); (54) Mathews et al. (2012); (55) Palla & Stahler (2002); (56) Howard et al. (2013); (57) Johns-Krull et al. (2000); (58) Herczeg et al. (2009); (59) Duchêne et al. (2010); (60) Grosso et al. (2003); (61) Andrews et al. (2010); (62) Madlener et al. (2012);(63) Pety et al. (2006); (64) Derived from the DIANA photometric, UV spectral and X-ray data, where L_X refers to the unabsorbed 1-10 keV energy range and $L_{\rm FUV}$ refers to the de-reddened luminosity in the 91-205 nm wavelength interval. An entry under $\dot{M}_{\rm acc}$ marked with [64] means that this mass accretion rate was used in the model to compute viscous heating rates.

An example of these efforts is provided in Table 2, where we have compiled information on the parameters for the system and the central source from 64 refereed articles. Aiming towards an unbiased statistical approach in measuring the completeness of our data compilation, we have divided the electromagnetic spectrum into eight segments, assuming that individual wavelength regimes describing a source are of equal importance. We have assigned two additional bins for gas-line observations and high-angular-resolution observations. We then measured the data completeness per source based on the data availability of each field. For fields that are broken down into photometric and spectroscopic observations, we require that data are present for at least one of the two subgroups. Given the scarcity of data on particular fields (e.g. X-rays or high-resolution images), which, however, does not compromise our modelling efforts, we set a threshold of 80% above which data collection for a source is considered completed.

In Fig. 3, we provide a detailed account of the data collection completeness per priority group, as a measure of evaluating the success of the data collection efforts. The pie charts give the data completeness (as a percentage) for the relative number of sources per priority group. As an example, 28% of the sources in priority II group have 80% of the data collected. According to the data presented in Fig. 3, data collection has been extremely fruitful. We now have 54 sources over the 80% threshold set for data completeness, distributed in all priority groups, which surpasses our initial target of 40-50 sources with complete datasets. Data for the highest priority (I & II) sources reach completion rates above 82%, and among all 85 targets of our initial sample, there are only 3 sources at 50% completion rate and just one source below that level.

Our main principle for the data compilation is that "*what gets measured, gets managed*". What makes our datasets unique is not only the large volumes of data compiled into the datasets, but the characterisation of the individual data blocks. All data in our datasets are

accompanied by quality flags and in most of the cases additional comments, which provide direct information on quality concerns. Flags classify data in three quality domains: *good, questionable data* and *upper limits*. Depending on the data source, quality flags were applied as follows:

- Data from third sources (publications and/or survey data) in most of the cases bear the quality flags of their original source.
- Third-source flags were modified and warning comments were applied in case where systematic (e.g. calibration) errors were detected.
- Third-source data are accompanied by the original source reference so that re-assessment of the original data is always possible.
- Data cross-checks: multiple data in the same or adjacent wavelength regimes allow for direct comparisons. Special concerns on variability are discussed below.
- In particular cases of critical passbands (e.g. mid-IR, far-IR) special memos are compiled by data-reduction experts that will guide users in selecting the best possible data.
- Data reduced by our group members and collaborators are of high quality and always bear quality flags. Direct channels are established for resolving quickly and efficiently any quality concerns within the group.
- A paper discussing extensively the data collection and quality issues is under preparation (Dionatos et al. 2016, in prep.) and will serve as reference for future users of the datasets and the database.

3.1.1 The DIANA Object Database (DIOD)

We have designed the DIANA Object Database (DIOD) to provide a *one-stop-shop* toolbox allowing for comparison between observations and models. It is therefore a much more complicated and complete solution than the initial project requirement to distribute the complete observational datasets to the public. The multi-wavelength datasets available through the *DIANA Object Database* repository are processed end products "as opposed to raw data" that can be directly compared to models. Deriving meaningful physical quantities from raw astrophysical data is a complex process that requires good knowledge of the instrumentation involved, together with adequate experience and advanced programming skills. Therefore the dissemination of processed end-products has a greater impact within the community as they can be directly used for analysis and interpretation. As an example we mention the SDSS survey that has been up to now the most prolific project in terms of scientific outcome when compared to cost. We therefore anticipate that along with the advancements and increasing interest in the field, our database will become a point of reference for the study of protoplanetary discs.

The database provides *all available data and modelling results* to the end user. A schematic of the database design and implementation is provided in Fig. 4. The database itself has been designed in *MySQL* and the user front-end has been developed in *PHP*. The database toolbox provides additional functionality that allows the user to easily access and evaluate the datasets and models. For the collected data, quality flags, comments, and references, that allow backtracking of the data to their original sources, are readily available to

the end user of the database and are also included in the downloadable datasets. The plotting functionality allows direct graphical inspection of the data but also direct comparisons between datasets, or between datasets and models.

The database has been developed, and is hosted and maintained, at the University of Vienna. It is now public and can be accessed via the following URL: http://www.univie.ac.at/diana/index.php. An example of the dataset selection tool is provided in Fig. 5.

We will continue to upload new data and finished models even after the official end of the *DIANA* project, as it is also a useful tool to exchange data among the consortium and future collaborations.

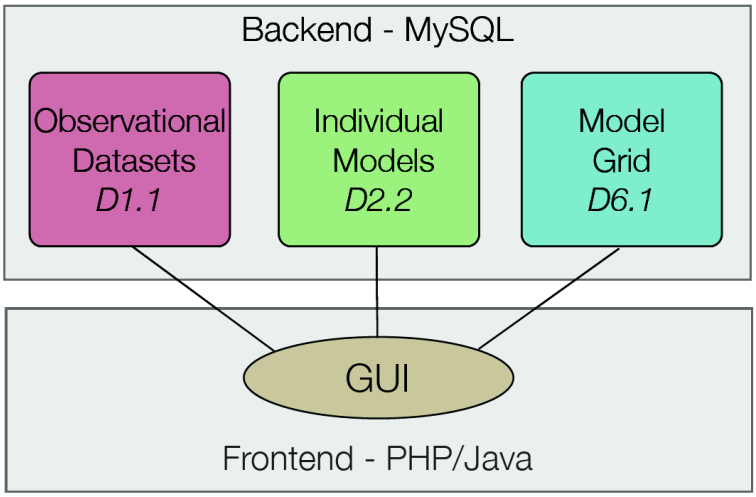

Figure 4: Design and purpose of DIANA Object Database (DIOD), offering multi-wavelength and multi-kind observational datasets of individual targets, along with modelling results, and results from model grids to extract systematic trends.

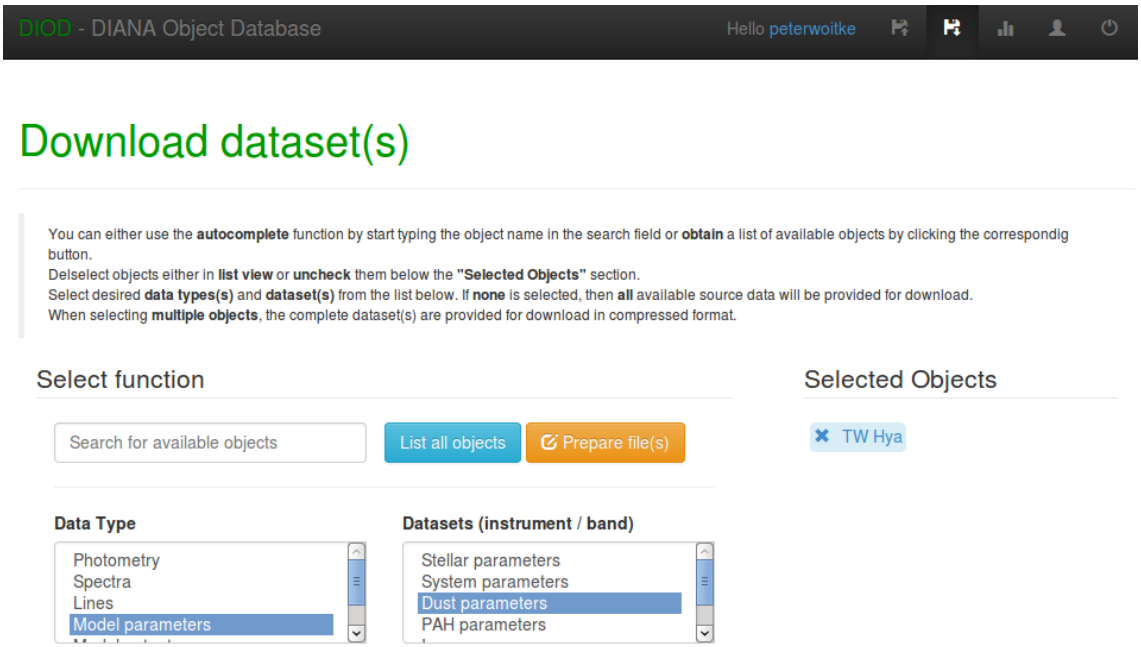

Figure 5: DIANA's web portal to our data collection and modelling results, the DIANA Object Database (DIOD).

3.2 WP 2: Case Studies and Model Calibration

Work package 2 has played a key role in the *FP7 DIANA project* in providing the main theoretical (modelling) framework for further analysis in WP 6, with three major aims:

1. to find a team consensus about the foundations of disc modelling concerning all physical, chemical and geometrical assumptions and approximations, to develop new disc-modelling standards,
2. to implement those *"DIANA standards"* into the three major modelling software products ProDiMo, MCFOST and MCMax, interface the codes, and provide well-tested and double-checked disc modelling tools along with robust fitting algorithms, capable of correctly predicting the most commonly observed continuum and line observables (*"model calibration"*),
3. to apply the models and procedures to as many datasets of individual target objects as possible, and fit all available multi-wavelength observational data, line and continuum, as well as possible (*"case studies"*).

These models allowed us to draw new conclusions about the dust properties in discs, the PAHs, the total dust and gas masses, the radial and vertical distribution of the dust and the gas, the chemical structure including the phase transitions between gases and ices, and the gas and dust temperatures in protoplanetary discs, *just before the planets form*, see WP 6.

3.2.1 The DIANA Modelling Standards

We have started a new series of scientific papers entitled *"Consistent dust and gas models for protoplanetary discs"* in the peer-reviewed journal *Astronomy & Astrophysics* where we present our consensus and conclusions about the disc-modelling assumptions, and results. We decided to split the presentation into three separate papers *"I. Disc shape, dust settling, opacities, and PAHs"* (Woitke et al., 2016), *"II. Chemical networks and rates"* (Kamp et al. in prep.) and *"III. The role of element abundances"* (Rab et al. , submitted). In these papers, we explain our modelling goals and assumptions step by step, and develop a reference model, which predicts a large number of continuum and line observations that reproduce the observations of class II T Tauri stars. Our new modelling standards are easy to implement, yet physically grounded, practical, and sufficiently motivated by observations.

The modelling standards presented in paper I show how we set up the disc zones, how to treat the irradiation by the UV and X-rays from the central star, how to treat the inner and outer disc edges with tapering, how to compute dust and PAH opacities, and how to take into account the gravitational settling of dust grains toward the midplane based on a simple but physically well-grounded approximation. In paper II we devise recommendations about the selection of gas-phase and ice species with updated chemical rates, and in paper III we discuss the role of element abundances and recommend standard abundances for discs.

Figure 6 gives an impression of the verification and calibration tests during model development. Only after equalisation of various program parts and adaptation of new dust and PAH opacities were we able to achieve agreement. The different parts of the figure show densities, temperatures, and the spectral energy distribution (SED), including emission features of polycyclic aromatic hydrocarbon molecules (PAHs).

We have run much more calibration and performance tests than shown here, including the validity of the so-called MCFOST-ProDiMo and MCMax-ProDiMo chain models (see e.g. Woitke et al., 2016, Appendix F), which include gas-modelling and emission-line

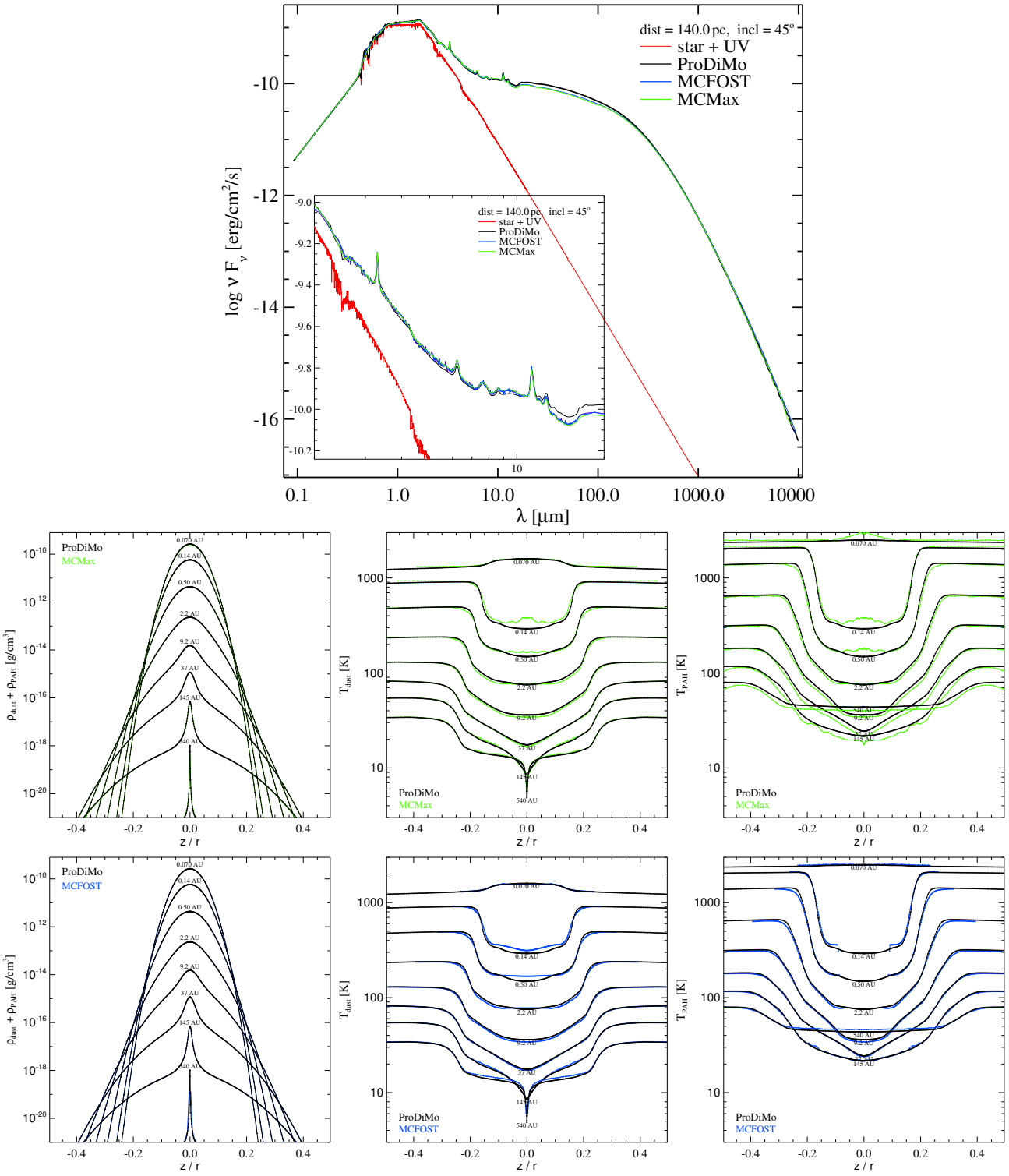

Figure 6: Results from 3 independent disc models for our T Tauri reference model with an artificially large PAH abundance (10× the standard ISM abundance). The figure compares independent results from ProDiMo, MCMax and MCFOST with PAHs in radiative equilibrium. The upper figure shows the computed SEDs with a zoom-in on the prominent PAH emission features at 3.3 μm, 6.2 μm, 7.6 μm, 8.6 μm, 11.3 μm and 13.5 μm. The lower two rows of plots compare the computed dust and PAH temperatures between MCMax (green), MCFOST (blue), and ProDiMo (black).

results. We are hence confident that we have achieved a new level of consistency and inter-coupled modelling of dust and gas, capable of predicting a large range of multi-wavelength observations simultaneously from one model.

3.2.2 DIANA Standard Dust Opacities

An important step towards more realistic models was the development of new *standard dust opacities*, which we consider as a major achievement of the FP7 project. Our assumptions for the dust opacity treatment are guided by a study of multi-wavelength optical properties of dust aggregates (Min et al., 2016) where the Discrete Dipole Approximation (DDA) is used to compute the interaction of light with inhomogeneous aggregate particles of complex shape. These opacity calculations are computationally too expensive to be applied in complex disc models, but Min et al. have developed a simplified, fast numerical treatment that allows us to reproduce these results reasonably well.

We consider a mixture of amorphous laboratory silicates (Dorschner et al., 1995, $Mg_{0.7}Fe_{0.3}SiO_3$) with amorphous carbon (Zubko et al., 1996, BE-sample). The dust grains are assumed to be composed of about 60% silicate, 15% amorphous carbon, and 25% porosity, well mixed on small scales. The effective refractive index of this porous material is calculated by applying the (Bruggeman, 1935) mixing rule. We use a distribution of hollow spheres (DHS) with a maximum hollow volume ratio $V_{\rm hollow}^{\rm max} = 0.8$. This approach avoids several artefacts of Mie theory (spherical resonances) and can account for the most important shape effects. In combination with our choice of the amorphous carbon optical constants (from Zubko et al., 1996, BE-sample), the DDA calculations highlight the "antenna effect"

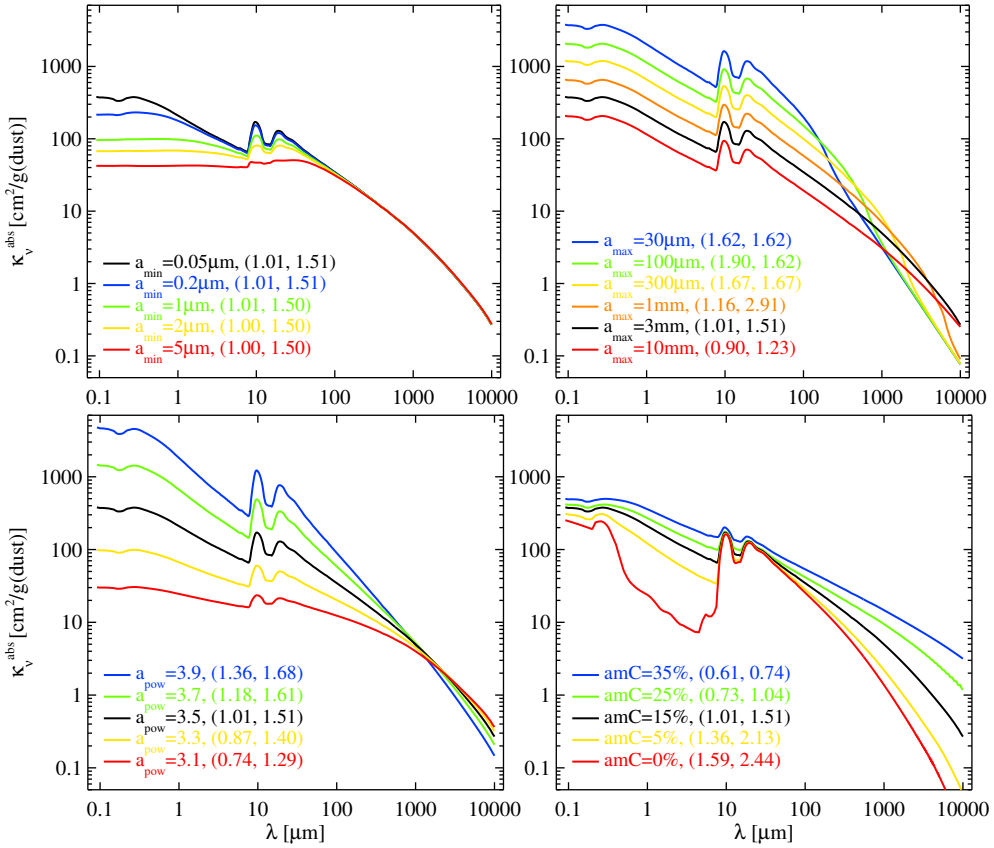

Figure 7: The *DIANA standard dust opacities*, showing here only the dust absorption coefficient per dust mass $\kappa_\nu^{\rm abs}$ as function of dust size and material parameters. The black line is identical in each subplot, with parameter values as used in the reference model, our *DIANA standard opacities*. The upper two figures show the dependencies on minimum and maximum particle size, $a_{\rm min}$ and $a_{\rm max}$. The lower two plots show the dependencies on dust size power-law index $a_{\rm pow}$ and on the volume fraction of amorphous carbon. 25% porosity and maximum hollow volume ratio $V_{\rm hollow}^{\rm max} = 0.8$ are assumed throughout. The two numbers in brackets represent the log-log dust absorption opacity slopes between 0.85 mm and 1.3mm, and between 5 mm and 1 cm.

observed from the aggregate particles, where irregularly shaped inclusions of conducting materials result in a considerable increase of mm-cm absorption opacities.

We have developed a stand-alone Fortran-90 package to compute the *DIANA standard dust opacities*, which we freely offer online via our internet portal https://dianaproject.wp.st-andrews.ac.uk/data-results-downloads/fortran-package.

3.2.3 Individual DIANA Standard Models

Based on our data collection (WP 1) we have performed 24 continuum-fitting disc models, and 11 detailed gas and dust *DIANA-standard* models to fit all available observational data, line and continuum, as well as possible. Some example results are shown in Figure 8. More details about the properties of the objects selected for the modelling can be found in Table 2. These results have been described in detail in the last two periodic reports, and in Deliverable 2.2.

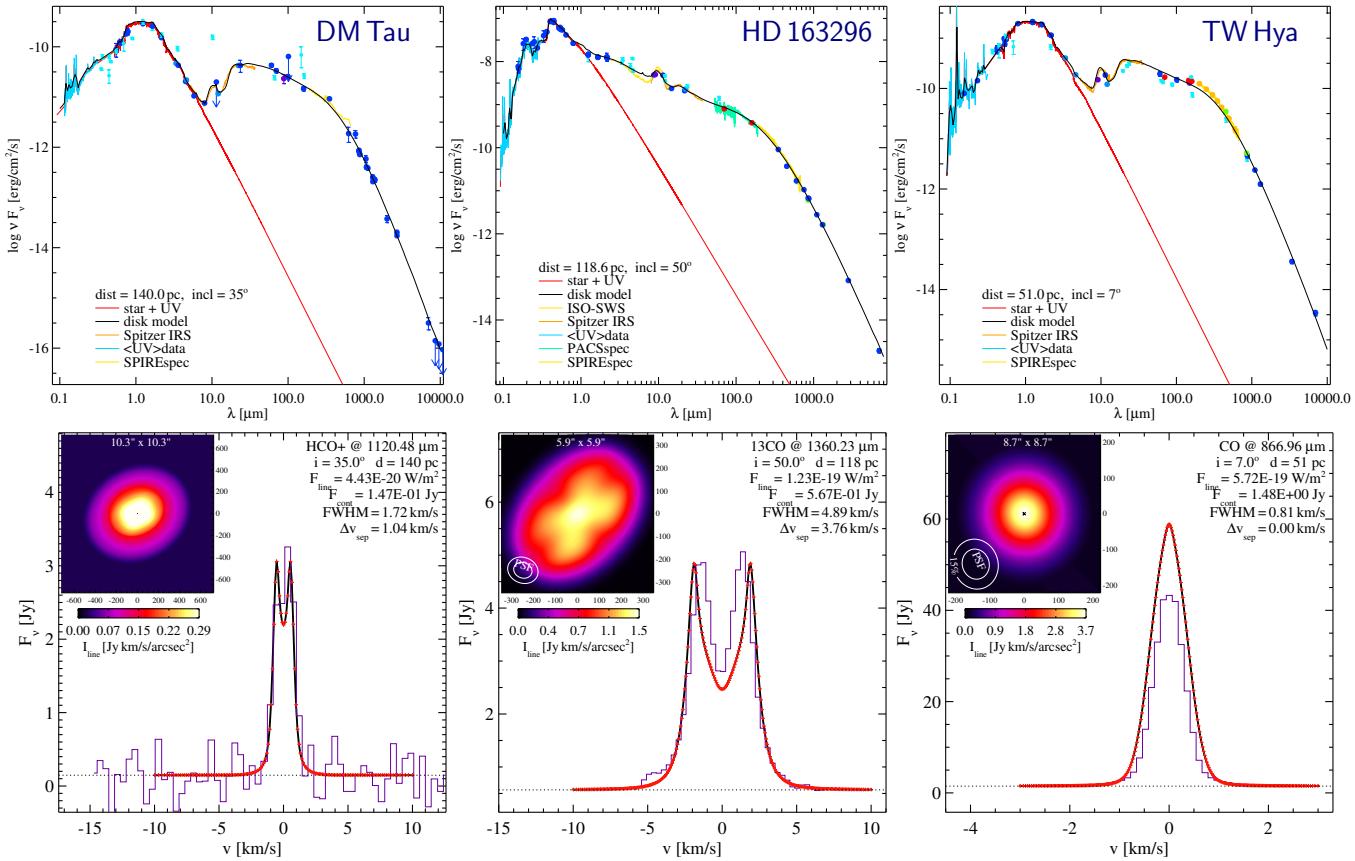

Figure 8: Example results from the individual object modelling of continuum and line observations, for the transitional disc around DM Tau, the Herbig Ae star HD 163296, and TW Hya.

All modelling results have been uploaded to our electronic database DIOD (see Fig. 5)

- complete physical disc parameters in generic format,
- full insight into the 2D internal physico-chemical structures of the discs (densities, chemical concentrations, temperatures, opacities, relaxation time scales, etc.), both the 2D numerical data and graphical figures,
- computed observables and derived quantities, such as the SED, near-IR excess, mean dust temperature across the disc, mm-slope, etc.,
- graphical analysis of SED and line-emission regions,

- complete continuum and line observational datasets in model-friendly formats,
- full set of input data-files to recompute the models with all three main modelling software tools, to be able to reproduce all computations if required, for example as soon as new observations become available,
- large suite of continuum and line predictions for proposal writing and other future purposes.

3.3 WP 3: Impact of X-ray and Particle Irradiation

The main goal of WP 3 was to study the influence of X-ray emission and high-energy particle irradiation (e.g. stellar winds) on the disc gas and dust. For this purpose, new physical processes had to be included into our modelling software to extend its range of applicability.

WP 3 was finished by 31/12/2013 in order to be in time for the large modelling effort ("mass production") of the *DIANA* project. The only deliverable D3.1 for this work package is *improved X-ray and particle irradiation modules for ProDiMo*. This includes the implementation of *X-ray radiative transfer* with scattering into ProDiMo based on the basic implementation of X-ray heating/cooling and chemistry of Aresu et al. (2011), Aresu et al. (2012) and Meijerink et al. (2012). The second task was to investigate the impact of *stellar particle irradiation* on the disc.

3.3.1 X-rays

The main task of WP 3 was the improvement of the X-ray physics/chemistry in ProDiMo. The main features of the new X-ray module in ProDiMo are

- new gas and dust opacities (absorption and scattering)
  (dust opacities for various compositions),
- consistent gas and dust X-ray radiative transfer, coupled with disc chemistry,
- X-ray scattering (Compton/Rayleigh), based on an approximation for anisotropic scattering,
- treatment for X-ray background fields,
- secondary FUV-fields caused by X-rays.

The new features allow us to study the impact of X-rays on the disc in great detail. The most important physical quantity affected is the ionisation fraction in the midplane of the disc, related to dead zones, viscosity and disc evolution. In Fig. 9 we compare the X-ray ionisation rate for models with X-ray absorption only, with absorption and scattering, and with absorption and scattering for gas and dust. From this figure, it becomes clear that a proper treatment of X-ray scattering is required to accurately derive the disc midplane ionisation fraction. The impact of the dust is in general lower; the dust mainly acts as an additional X-ray absorption agent.

The more detailed treatment of X-ray radiation transfer is computationally much more expensive (at least a factor of 5 compared to the old implementation). Therefore, the new X-ray radiative transfer module was not included in the general *DIANA* fitting approach. The X-rays are, however, still fully included, just with the old approximations. As the new module is an integral part of ProDiMo, it is easily possible to run the X-ray radiative transfer on top of an already fitted *DIANA* model in order to study the impact of X-rays in detail.

In addition to the improvements for the X-ray radiative transfer we have also added new chemical processes to the chemistry module of ProDiMo which are related to goals of WP 3:

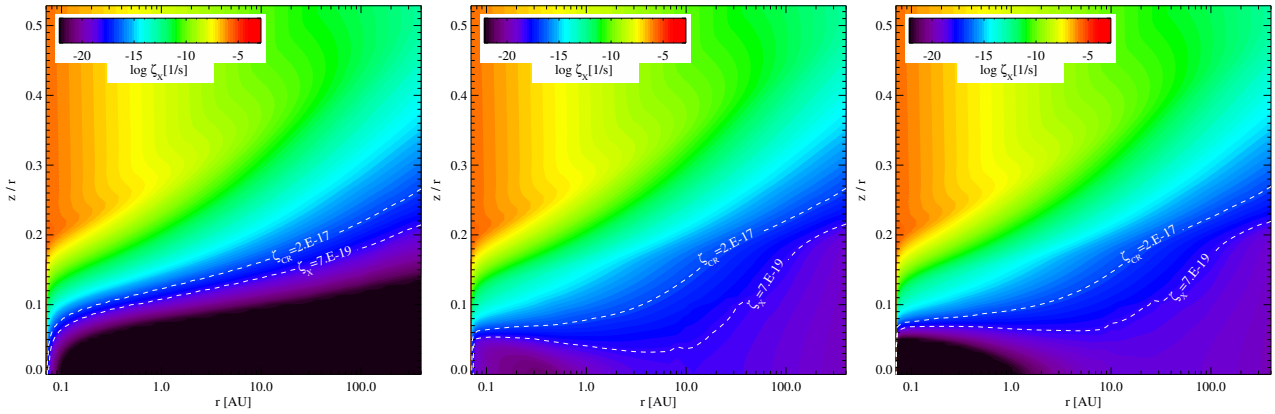

Figure 9: Comparison of the X-ray ionisation rate ζ_X throughout the disc. The x-axis shows the distance to the star in AU. The y-axis shows the height of the disc scaled by the radius (z/r). Shown are X-ray radiative transfer models considering gas absorption only (*left panel*), gas absorption and scattering (*middle panel*) and absorption/scattering for both the gas and the dust (*right panel*). The white *dashed* contours show the typical ionisation rates arising from cosmic rays and radioactive decay products.

- *FUV-field triggered by X-rays:* High-energy secondary electrons caused by X-ray ionisation excite H_2 and H. The subsequent de-excitation produces a secondary UV field which triggers local photo-ionisation and dissociation. This addition to the X-ray chemistry allows us to study the impact of X-rays on the midplane especially in comparison to cosmic rays (Chaparro Molano & Kamp, 2012a,b).
- *Radioactive Decay Ionisation:* We have added chemical reactions for the ionisation of H_2 and He due to high-energy products of radioactive decay processes in disc. This process can be important in the midplane of the disc (Umebayashi & Nakano, 2009; Umebayashi et al., 2013).
- *Cosmic ray absorption:* we implemented a treatment for cosmic ray absorption (e.g. Padovani et al., 2009; Cleeves et al., 2013) for a more accurate determination of the cosmic ray ionisation rate.

The combination of X-ray radiative transfer, with the unprecedentedly detailed treatment of X-ray chemistry, allows for profound investigations of the impact of X-rays on disc chemistry. ALMA will provide the necessary high-spatial-resolution data to compare our model results to observations (see also Fig. 11).

3.3.2 Stellar High-energy Particles

The young Sun was probably much more active than the Sun we know today (Feigelson et al., 2002). Thus, T Tauri stars can be expected to be more active as well. Based on observations of X-ray flares in young stars, Feigelson et al. (2002) estimated that the high-energy particle flux in the young Sun was $\approx 10^5$ times higher compared to the contemporary Sun (see also Glassgold et al., 2005).

To model the impact of the stellar particles on the disc chemistry, a proper treatment of the particle transport through the disc is required. Due to their high energies (see Fig. 10, left panel), the particles mainly ionise, and as a consequence, also heat the gas.

In collaboration with Marco Padovani, we applied the continuous-slowing-down approximation (e.g. Padovani et al., 2009) to calculate the particle transport through the disc and the stellar particle ionisation rate. This rate is used as an input for the chemical/thermal modelling, where we treat the stellar particles similar to cosmic rays.

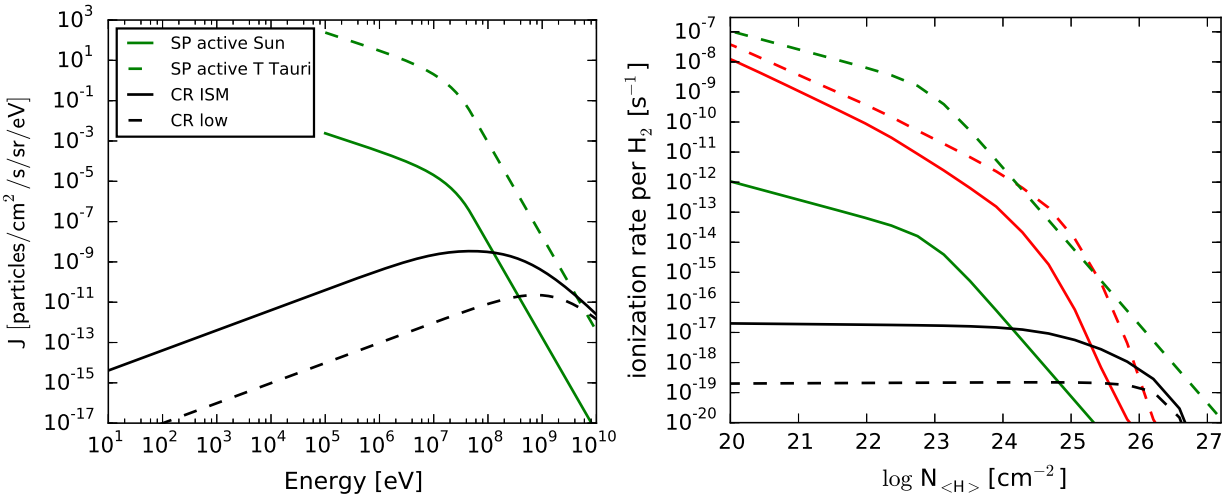

Figure 10: *Left Panel:* High-energy particle spectra. The green lines show the stellar high-energy particle spectra for the active Sun (solid) and an active T Tauri star (dashed). The black lines show the Galactic cosmic ray spectrum. The solid line represents the canonical interstellar-medium spectrum and the dashed line a modulated spectrum for an active T Tauri star (Cleeves et al., 2013). *Right panel:* Comparison of the molecular hydrogen ionisation rates for stellar particles (green), X-rays (red) and cosmic rays (black) as a function of hydrogen column density.

In Fig. 10 we show typical stellar-particle and cosmic ray spectra used as an input for our models. The right panel of Fig. 10 shows the comparison of the resulting ionisation rates (including also X-rays). From this Figure it becomes clear that stellar particles can dominate the ionisation in the upper layers of the disc (lower column densities). But it is also apparent that the general picture of disc ionisation is complex. In particular the fluxes of the various ionisation sources are not well known. Only the X-ray fluxes can be measured directly (but they are time-variable), particle fluxes can only be inferred indirectly from their impact on the disc.

A possible way to discriminate between the different ionisation sources is to use two different molecular ionisation tracers. We use HCO^+ and N_2H^+. These two molecules trace different vertical layers in the disc. N_2H^+ traces deeper layers where CO is frozen out (N_2H^+ is efficiently dissociated by CO, e.g. Qi et al. 2013) whereas HCO^+ traces higher layers (mainly the CO layer). In Fig. 11 we show synthetic ALMA observations of models including different ionisation sources. One can see that HCO^+ is affected by the stellar particles whereas N_2H^+ is mostly sensitive to X-rays and cosmic rays. The reason is that cosmic rays and X-rays can penetrate deeper into the disc: cosmic rays because of the high energy and the isotropic irradiation of the disc, and X-rays because they are scattered into the midplane of the disc. Stellar particles preferentially travel along straight lines and due their high energy are not scattered. As the particles originate from the star they can only penetrate the upper layers of the disc but not the midplane. Close to the midplane the radial column densities (typically $N_\mathrm{H} > 10^{26}\,\mathrm{cm}^{-2}$) are high enough to absorb the stellar particles already at the inner rim of the disc.

Fig. 11 nicely shows the applications of nearly all the new WP 3 features implemented in ProDiMo. The available (or soon to be available) capabilities of ALMA, in particular the high spatial resolution, will allow measurement of the chemical structure of the disc in great detail (vertical and radial). This kind of observation in combination with our model presented here makes it possible to discriminate between the different ionisation sources and indirectly measure the stellar particle fluxes of young stars.

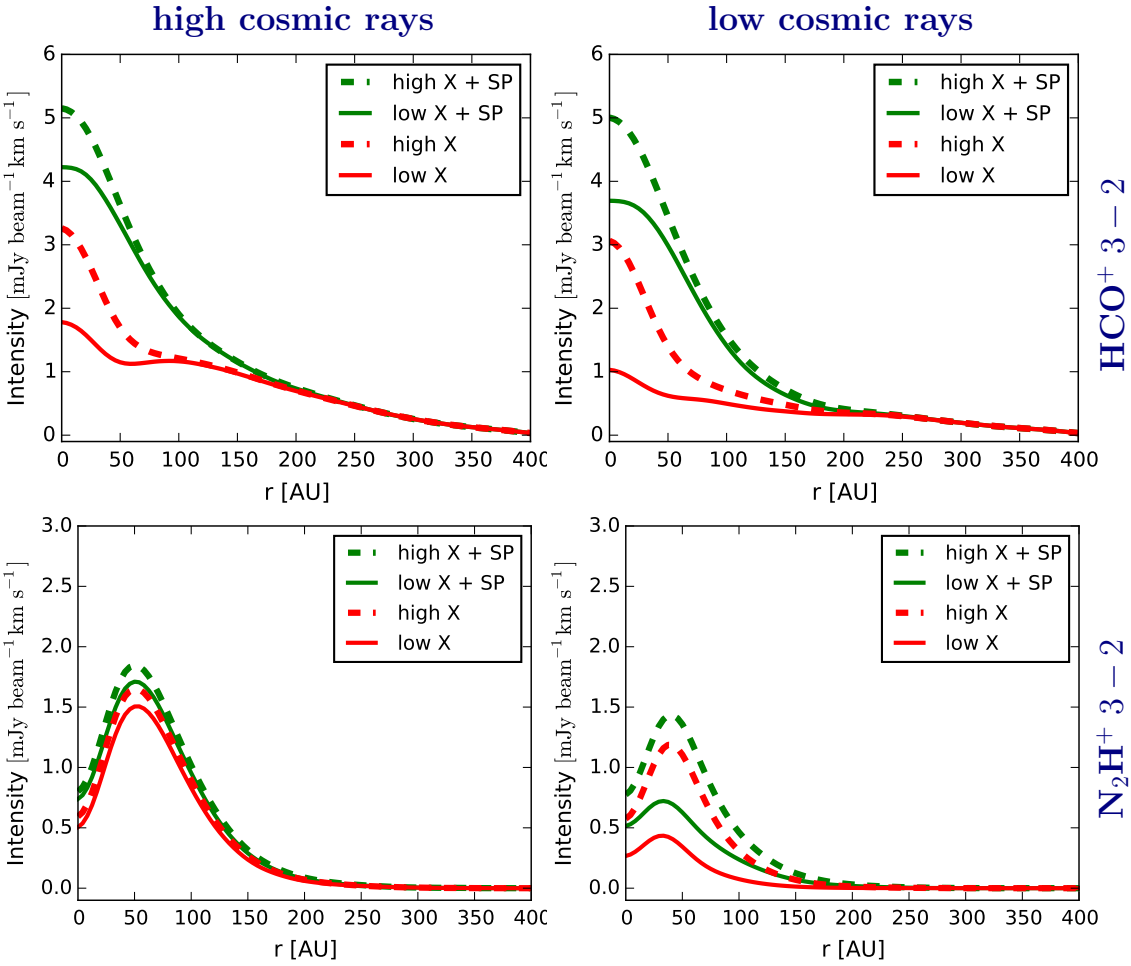

Figure 11: Synthetic ALMA (Cycle 4) radial intensity profiles for the HCO^+ $3-2$ (top row) and N_2H^+ $3-2$ (bottom row) spectral lines. The left column is for models with high cosmic ray flux (ISM like cosmic ray ionisation rate), the right column for low cosmic ray flux (modulated active T Tauri spectrum). Red lines are models with stellar X-rays (X) only, where the dashed line is for a higher X-ray luminosity. The green lines show models additionally including stellar-particle (SP) ionisation using the input spectrum for an active T Tauri star (see Fig. 10).

3.4 WP 4: Analysis with IR-interferometry

Work package 4 has focused on the collection, interpretation and analysis of near-IR interferometric data from protoplanetary discs. The interferometric data probe the innermost ∼(0.5-10) AU disc regions of the nearest star-forming regions, in particular the radial distance and shape of the inner rim, but also allow for some new conclusions about scattering from the more extended disc regions. This is a new emerging field, with the instrument VLT/PIONIER having been implemented and tested only during the FP7 project. Prior to *DIANA*, only the brightest Herbig Ae sources had been covered, with low sensitivity and low numbers of baselines. The PIONIER instruments allowed, for the first time, the analysis of near-IR interferometric data as a new component of the multi-wavelength modelling efforts in *DIANA*. The work package had three major scientific aims:

1. collection of near-IR interferometric data,
2. improved understanding and modelling of the inner rims of protoplanetary discs, and
3. individual fitting of targets with interferometric data.

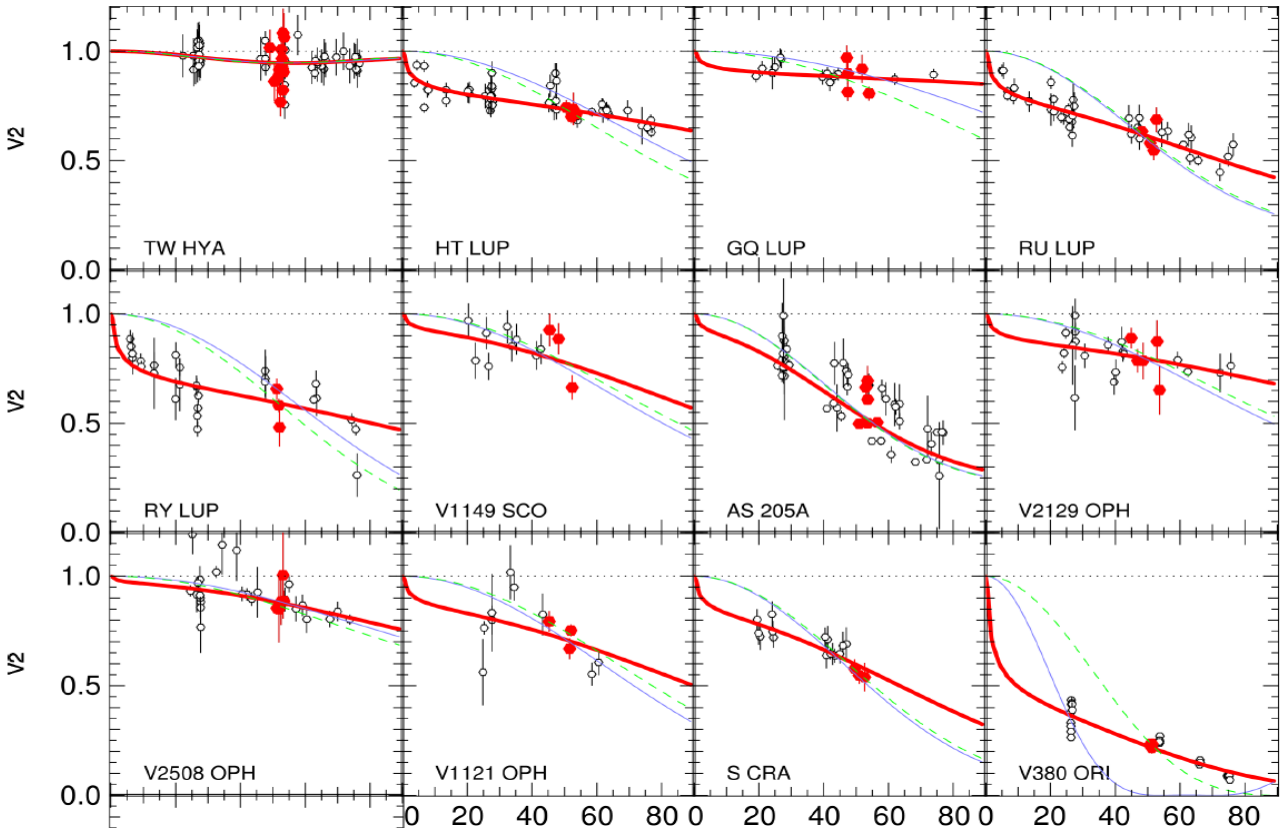

Figure 12: Visibility modelling of T Tauri stars with different pure thermal-emission models (blue and green dashed lines) and full radiative-transfer models including scattering (red lines). Figure taken from Anthonioz et al. (2015).

As described in Anthonioz et al. (2015), we have observed 21 T Tauri stars, and 2 Herbig Ae stars with PIONIER. Thirteen of these stars have a visibility profile showing clear signatures of a circumstellar disc. We fitted the data with two models: (i) a simple ring model with thermal emission and (ii) full radiative-transfer models including scattering, see Fig. 12.

The full radiative-transfer models improve the quality of the fits significantly in eight cases, with respect to the shape of the visibility curves at short baselines. In the models, the quick initial drop of the visibilities at small baselines is caused by extended scattering, before the visibilities decrease further due to thermal emission from the disc inner rim at longer baselines.

Further insight is given in Fig. 13. The small inserted figure in the middle right shows the contributions of direct starlight and thermal emission to the total flux at increasing wavelength across the H-band around 1.6 μm. At the blue end of the H-band, the direct stellar component is still dominant, whereas at slightly longer wavelengths, thermal emission from the inner rim becomes more important, simply because the Planck function increases so steeply. This means that the total initial drop of the visibilities at short baselines is deeper at the blue end of the H-band, and shallower at the red end, known as chromaticity effect. This is demonstrated on the right side of Fig. 13 for T Tauri stars where the inner rim is so close to the star that it is unresolved.

For larger inner rims (middle column) the PIONIER instrument starts to resolve the inner rim at longer baselines. Once it is resolved, the chromaticity effect reverses, because the signal from the inner rims kicks in earlier at the red end of the H-band than at the blue end. This inversion of the chromaticity effect is observed, for example, for T Tau N, which we

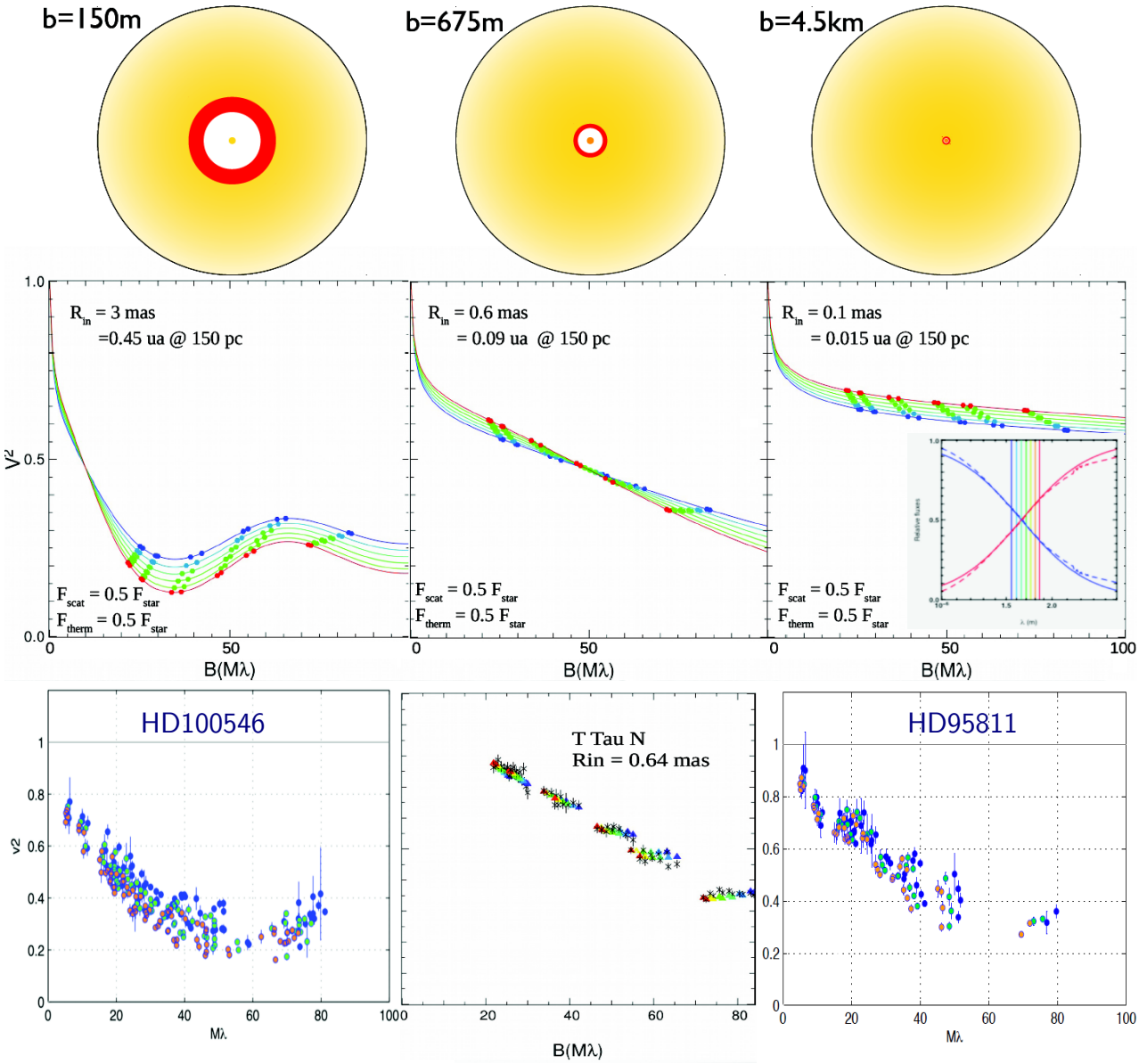

Figure 13: Visibilities and chromaticity effect. The top row of figures sketches the emission regions scattered light (yellow regions) and rim emission (red) for (from left to right) Herbig Ae, intermediate, and T Tauri stars. The second row of figures shows the expected visibility curves at the red end of the H-band (red lines and dots) and the blue end (blue lines and dots). The third row shows three examples of PIONIER measurements. Figure taken with permission from Anthonioz et al. in prep.

consider as a strong argument for our interpretation with thermal emission and scattering.

For even larger inner rims, typical for Herbig Ae stars (left column in Fig. 13), the visibilities are already dominated by rim emission at short baselines. The red visibility curves undergo deeper minima, because at the red end of the H-band the thermal emission from the rim is more dominant with respect to the stellar light than at the blue end. We see this effect clearly in the PIONIER data of HD 100546 and HD 95811. In the end, the crossover of the chromaticity effect is easy to understand. Signals which are caused by scattering are emphasised in the blue, and signals which are caused by thermal emission are emphasised in the red.

During the run-time of the FP7 *DIANA* project, we have made additional efforts to improve, equalise, and test the ways we compute visibilities in ProDiMo, MCFOST and MCMax. Figure 14 shows how near-IR, mid-IR and mm-visibilities are affected by the

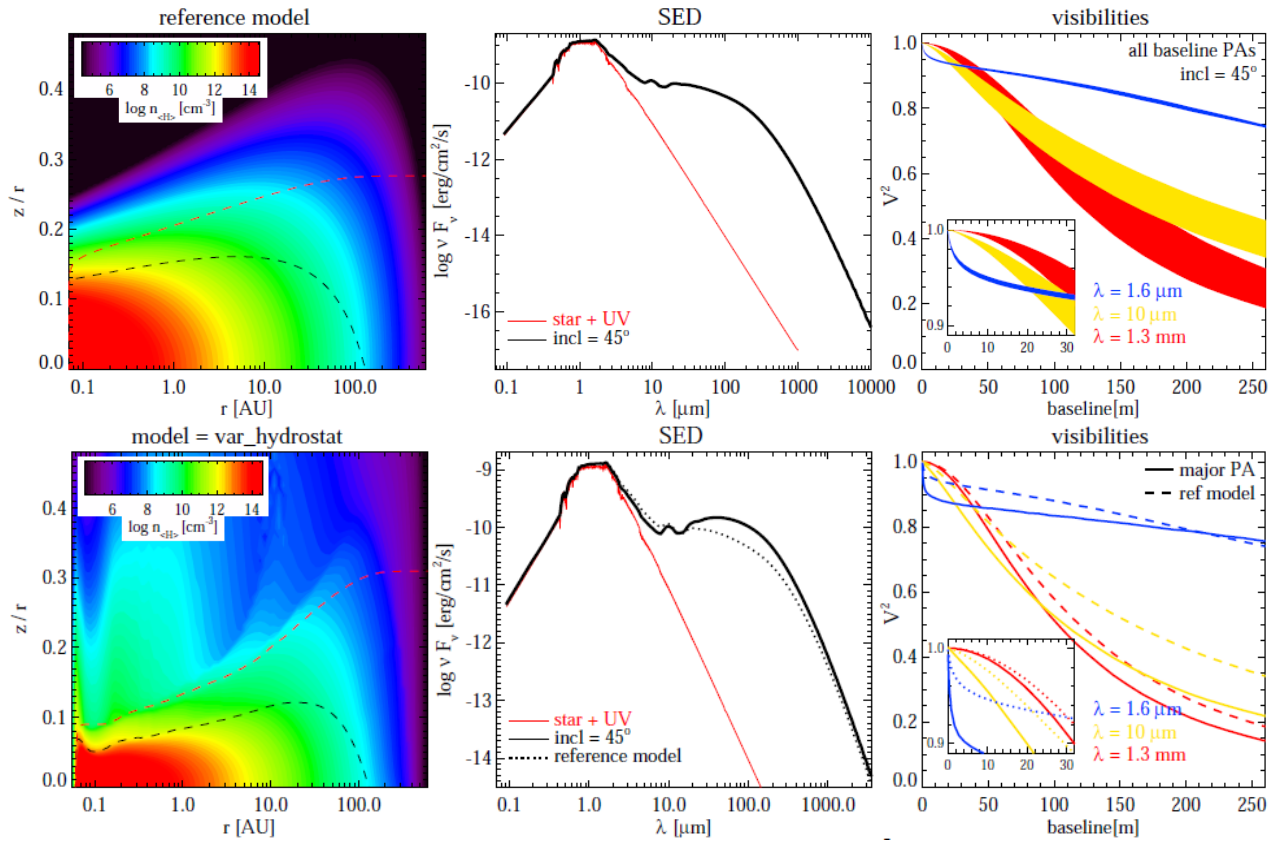

Figure 14: Effects of disc structure on SED and visibilities (Woitke et al., 2016). The upper row shows the parametric reference models, and the lower row shows a hydrostatic disc model.

assumed/calculated vertical disc structure. The hydrostatic disc model has a more strongly flared outer disc which enhances the initial drop of the near-IR visibilities at small baselines. It also leads to a more extended mid-IR emission region. Visibilities are hence a powerful tool to explore the disc structure, both radially and vertically.

In conclusion, IR interferometry is a powerful tool to probe the innermost disc regions. The contribution of extended scattered light from the disc is important and cannot be neglected. A full treatment of the light-scattering process is needed to correctly interpret the data, and we were able to demonstrate that not doing so had led researchers in the past to wrong conclusions, for example concerning the determination of the distances of inner rims from T Tauri stars. The analysis of the PIONIER data is still ongoing, and will be extended to Herbig Ae stars in the near future (Anthonioz et al. in prep.).

We expect the contribution of *DIANA* to have a large impact on the community with the on-going commissioning of the next-generation interferometric instrument GRAVITY that will be more sensitive than PIONIER, allowing the study of more, less-luminous T Tauri stars. GRAVITY, operating in the K-band, should be followed rapidly by MATISSE operating in the $5 - 10\,\mu$m window.

3.5 WP 5: Near-mid IR Molecular Line Transfer

The aim of work package 5 is to predict near-mid infrared molecular line emission spectra from protoplanetary discs and compare these predictions to CRIRES/VLT and Spitzer IRS observations, not only for isolated single lines, but also for a whole spectral region which contains thousands of such lines, possibly overlaping. Physically, this problem is separated into two parts

1. to determine the level populations of the ro-vibrational states of the molecules, and
2. to perform a formal solution of the line radiative-transfer problem in 3D to predict the continuum and line emission spectra under given disc inclination.

The terrestrial-planet-forming region of protoplanetary discs ($r < 10\,\mathrm{AU}$) is warm enough for molecules into be excited in their ro-vibrational levels. Observations by the Spitzer Space Telescope and ground-based telescopes (especially the VLT) have indeed revealed an unexpected rich forest of emission lines from molecules of pre-biotic interest like water, carbon dioxide, HCN, and C_2H_2. Those lines are well suited to constrain the inner disc densities, temperatures and compositional structures.

We endeavoured ourselves in this work-package to implement the capability of modelling those lines in the *DIANA* suite of software tools in conjunction with the warm gas photo-chemistry in a self-consistent manner. In previous versions of ProDiMo (version 2011) only the non-LTE populations for rotation levels were included (i.e. far-infrared to millimetre lines). The work-package has meet all its milestones.

3.5.1 Computation of the ro-vibrational level populations of complex molecules

The second novelty we have implemented in the ProDiMo-FLiTs software is the capability of computing non-LTE ro-vibrational population levels for CO and H_2O (see Kamp et al., 2013; Thi et al., 2013) and non-LTE vibrational levels of species for which no experimental or theoretical inelastic full ro-vibrational collisional data exist (C_2H_2, CO_2, HCN, OH).

For our purpose we devised a method to combine non-LTE vibrational populations with LTE-rotational populations within a vibrational level. At the large gas densities where the species emit the ro-vibrational lines, the rotational levels within one vibrational level are close

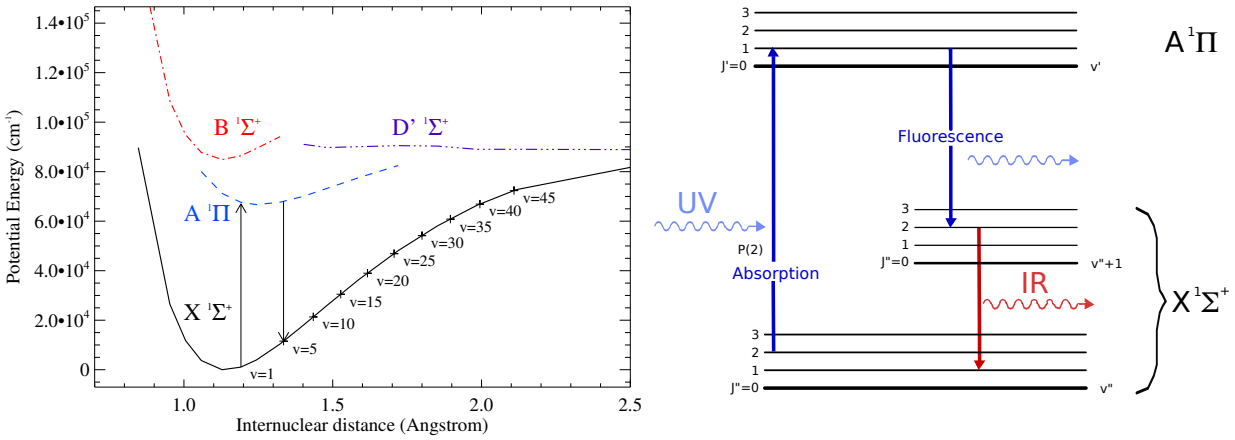

Figure 15: CO potential-energy curves on the left and a schematic of the UV fluorescence mechanism on the right (Thi et al., 2013). In the pseudo non-LTE level-population computation, the rotational levels are at LTE, while the vibrational-level populations are determined by the balance between de-excitation by spontaneous emissions and collisional excitations.

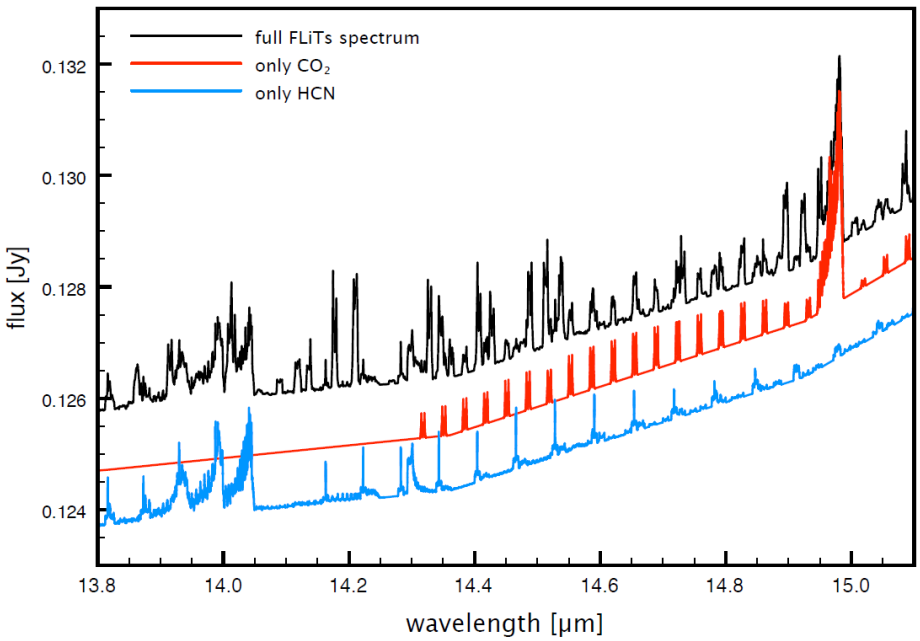

Figure 16: Simulated molecular line spectra for H_2O, CO_2 and HCN. The main features are the blends of Q-branch lines from HCN at 14 μm, and from CO_2 at 15 μm.

to LTE. The Einstein coefficients of vibrational transitions are much higher, of the order of 1 Hz compared to $(10^{-8} - 10^{-6})$ Hz for pure rotational transitions, such that the vibrational levels are not populated according to LTE. Despite the limitations, the computation with pseudo non-LTE populations constitutes a major advance compared to the assumption of full LTE. This implementation is so far unique among photochemical codes which model the protoplanetary disc environments. The inclusion of full or pseudo non-LTE populations permits us to simulate the effect of pumping by infrared photons emitted by the dust grains for all the species. We made intensive use of the *HITRAN* spectroscopic database which serves the planetary atmosphere community. The implementation of the CO molecular model is extensive and includes ro-vibrational levels in the first electronic excited state. Fluorescence pumping by UV photons from the star or from the accreting gas to the high vibrational levels of CO has been observed in the discs around Herbig Ae stars. Those UV-pumping effects can be reproduced in the ProDiMo code (see the schematics in Fig. 15). A recent work triggered by our first implementation of the CO collisional rates has resulted in more accurate quantum computations (Song et al., 2015; Walker et al., 2015).

3.5.2 FLiTs, a fast line ray-tracer for disc emission lines

The Amsterdam group lead by Prof. Waters took on the task of designing a code that overcomes the difficulties of line photon transfer in the near and mid-infrared. Inner discs are characterised by rapidly varying density, temperature and compositional structures. Therefore a very fine grid is usually required to maintain the accuracy in the calculations. The fine grid in combination with the high number of blended lines (>10000) requires a usually intractable amount of computation time with the previous generation of line ray-tracers implemented in ProDiMo. This would limit us in the context of the *DIANA* fitting projects where thousands of models have to be computed.

A new program called *FLiTs* (the Fast Line Tracer) has been developed by Dr. M. Min (at that time at the University of Amsterdam) that takes advantage of a special gridding as described by Pontoppidan et al. (2009) with additional performance-improvement tricks. The

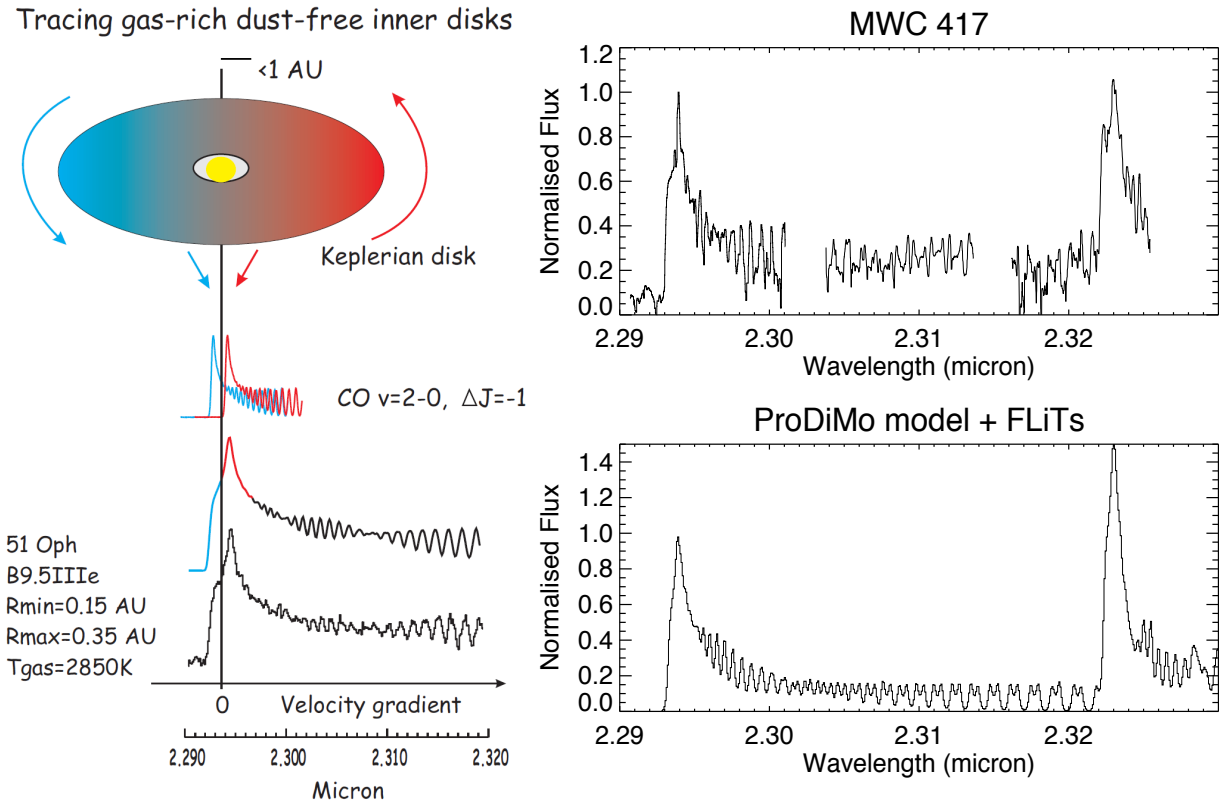

Figure 17: The left panel explains the shape of the CO-bandhead emitted by a Keplerian rotating discs. The right panel show the observed CO-bandhead spectrum towards MWC 417 and a ProDiMo + FLiTs model spectrum (J. Ilee).

FLiTs code computes several velocity bins simultaneously taking into account the thermal and scattered emission from the dust grains. The ProDiMo and *FLiTs* codes communicate with each other in a simple, transparent way allowing automatic fitting procedures to be performed. The *FLiTs* code achieves a speed-up factor of ~ 30 compared to the original ProDiMo ray-tracer. It has been benchmarked against ProDiMo and the agreement is within a few percent. An example of spectra produced by the *FLiTs* ray-tracer in combination with the molecule level populations computed by ProDiMo is given in Fig. 16. The CO model molecule is able to produce synthetic spectra of hot CO gas emission as traced by the CO-bandhead at 2.3 micron (see Fig. 17). In the future the *FLiTs* code together with ProDiMo will become a reference in near- and mid-infrared transfer when new data from the James Webb Space Telescope (the mid-infrared instrument MIRI is a European contribution), the E-ELT (e.g. METIS), and SPICA will be available. We plan a dedicated publication where the capabilities of the *FLiTs* code will be described.

3.5.3 A unique feature: combining warm gas chemistry, non-LTE population and a fast line ray-tracer

A major strength of our approach in the *DIANA* project is the combination of several state-of-the-art treatments in a self-consistent manner. In this work package, we combined a revised warm-gas-phase network adapted for the inner-disc chemistry, a (pseudo) non-LTE treatment of the line emission, and a fast line tracer. It should be noted that all spectral lines are automatically considered by *ProDiMo* as cooling agents. Likewise, ProDiMo would consider that photons emitted by dust grains and absorbed in the ro-vibrational levels (i.e. IR-pumping) are heating agents. Therefore our implementation of the near- and mid-

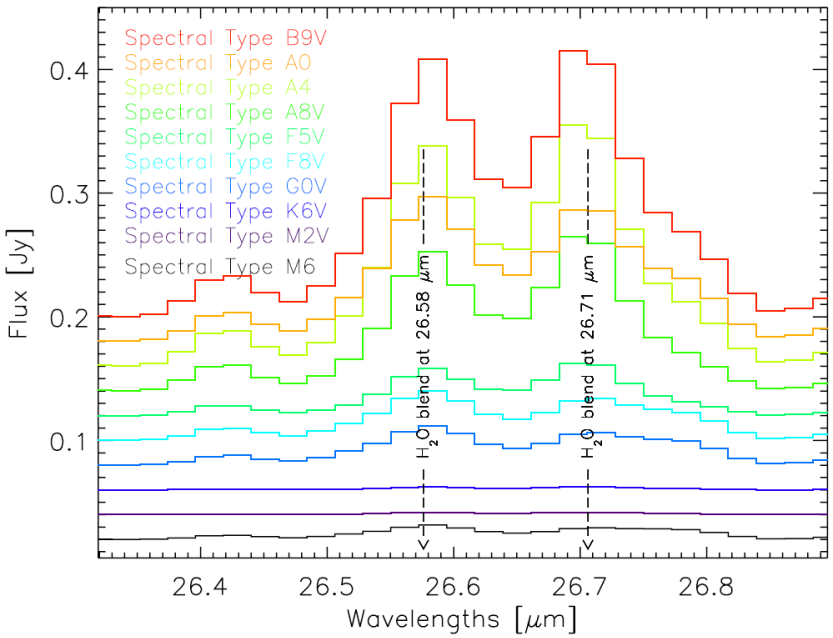

Figure 18: Two water line blends as modelled with ProDiMo emitted by a disc. The only difference between the various models is the spectral type of the central star, from Antonellini et al. (2016).

infrared lines automatically improves considerably the accuracy of the gas heating/cooling balance for the inner gas disc. Previous works by other researchers have focused only on one of those aspects. Comparison with archival and future observations of molecular lines will improve our understanding of the terrestrial-planet-forming region of discs.

3.5.4 Exploitation of the diagnostic value of molecular infrared bands

The question of the origin of water on Earth has always fascinated humanity. How much water is present on planets and how was it accumulated? What is the main reservoir of water in discs (ice or vapour)? For example, Kamp et al. (2013) have studied the diagnostic value of water lines to trace disc structure and ice formation. Similarly, Podio et al. (2013) use the water line spectra in combination with disc modelling to trace the water reservoir in the protoplanetary disc around DG Tau. They conclude the water line emission originates indeed in the outer disc around this system and find a large water reservoir of at least 10^4 Earth oceans.

Observations of the inner-disc emissions by the Spitzer Space Telescope have revealed the presence of a large reservoir of warm water. The water lines have been the subject of the PhD thesis of Stefano Antonellini (March 2016, funded by DIANA). He constrained the various disc parameters such as gas mass, gas-to-dust mass ratio and dust opacity, which strongly affect the strengths of the water lines (Antonellini et al., 2015). In a subsequent study, Antonellini et al. (2016) explored why ro-vibrational water lines are detected in 50% of discs around T Tauri stars (with mass less than 2 solar masses), but in only 5% of discs around Herbig Ae stars (which have masses between 2 and 4 solar masses). Figure 18 shows that an increasing stellar luminosity makes the water lines from the disc stronger according to our models, despite earlier proposed ideas that enhanced photodissociation by more luminous stars should make the water lines weaker. However, Antonellini et al. (2016) demonstrated that due to the dependence of the line S/N ratio on continuum flux in data reduction (like de-fringing), the Spitzer IRS instrument is actually likely to have missed the water lines from most Herbig Ae/Be discs, although they are intrinsically stronger.

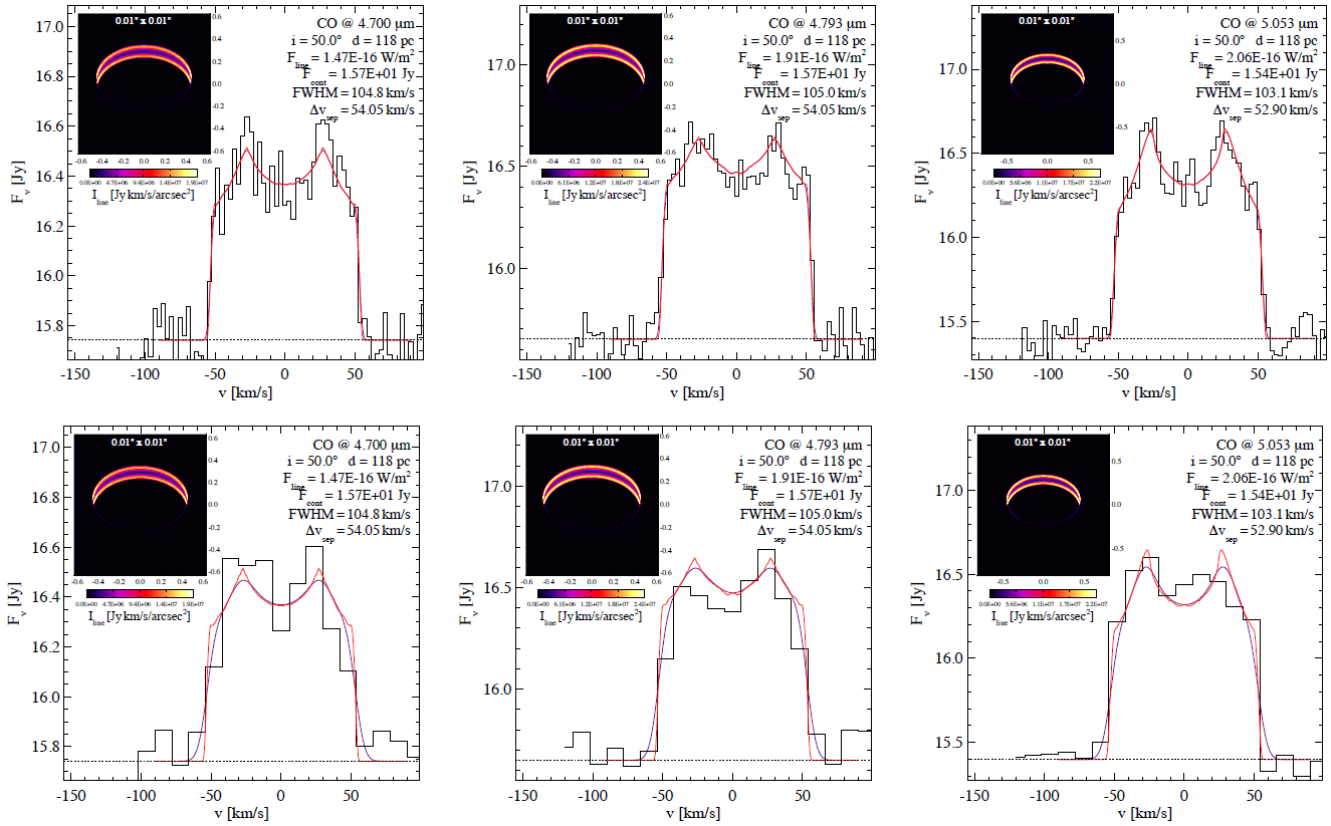

Figure 19: Observations with the CRIRES ($R = 100000$, left, taken 2012) and the NIRSPEC ($R = 25000$, right, taken 2001 and 2002) spectrometers and model predictions (rebinned to respective instrument resolution and noise added with S/N = 100) for the median CO ro-vibrational line profile from the disc around the Herbig Ae star HD 163296 (Hein Bertelsen et al., 2016b). The CO spectra show variability over a timescale of ten years and could show a additional variable central wind component.

CO ro-vibrational lines are detected in many protoplanetary discs. In a combined observational and modelling project, Rosina Hein Bertelsen used the full non-LTE module of ProDiMo to constrain the chemistry and excitation of the CO lines observed towards the transitional disc around HD100546 (Hein Bertelsen et al., 2014). A detailed model of the CO emission from the HD163296 disc has been compared to observations in Hein Bertelsen et al. (2016b), see also Fig. 19. The region within the inner 1 AU of protoplanetary discs is still poorly understood. CO overtone emission is excited in warm ($T = 2500 - 5000$K) and dense ($n \gtrsim 10^{15}\,\mathrm{cm}^{-3}$) gas - precisely the conditions expected close to the central star. Previous studies have only described the CO overtone emission in simplified ways. With our advanced tools, we have a much better handle on this unique observable to trace the inner disc regions (Fig. 16).

Other papers by members of the *DIANA* project have made use of the non-LTE population of CO or other species in their study (e.g. Carmona et al., 2014). Also, there is a wealth of archival VLT/CRIRES, VISIR and X-Shooter data to be re-analyzed. VISIR has just been upgraded and returned to the VLT, and CRIRES is currently upgraded as well.

3.5.5 Impact on the astrophysical community and beyond

The interest of the astronomers in molecular physics concerning near- and mid-infrared lines, collision rates and chemical rates has triggered new contacts with the molecular physics community (see Song et al., 2015; Walker et al., 2015). Within the next few years, it will be possible to compute more collisional data.

3.6 WP 6: Exploitation of Observations and Model Results

Work package 6 exploited the data collected in WP 1 and WP 4 in several ways: (1) search for correlations in the observational data, (2) analysis of disc-modelling results for individual targets and (3) computation of systematic disc model grids to find physical trends. The latter two approaches are based on the disc-modelling standards developed in WP 2 and the tools developed in WP 3 and WP 5. We selected four key questions listed on page 4 in Sect. 2 to illustrate the results obtained during the project and show the impact for future research and neighbouring fields.

3.6.1 Which gas emission lines probe what process in which part of the disc?

Only 21 molecules (plus some isotopologues) have been detected so far in discs compared to about ∼200 detected in the ISM. The overview in Table 3 illustrates that the molecules detected in discs are generally the simpler ones. It also shows that molecules in discs can be studied all the way from near-IR to sub-mm wavelengths. Figure 1 on page 3 summarises the knowledge gained over the past years on which atomic/molecular gas emission probes which part of the disc. The following paragraphs explain this sketch in more detail and apply to primordial discs that do not show substructure such as gaps, holes, protoplanets or spiral structure.

Atoms and ions trace the tenuous upper layers of the disc. Species that are easily ionised by UV/optical photons (stellar and interstellar) such as C^+, Fe^+ exist across the entire radial extent of the disc. Examples of emission lines are the [C II] 157 μm line, which originates in a thin 'PDR'-like layer on the disc surface. On the other hand species that require higher energies for ionisation such as Ne^+ and Ar^+ typically exist in the inner low-density surface regions of discs where stellar X-rays are strong and recombination with electrons is inefficient (Aresu et al., 2011). Hence these lines can be used to trace kinematic signatures of disc winds originating close to the star (Baldovin-Saavedra et al., 2011).

Neutral atoms exist in a transition layer between ions and molecules. The [C I] lines in the sub-mm come from a sandwich layer between C^+ and CO. The [O I] lines are among the strongest cooling lines for discs. They trace warm gas (∼ 50 K) and become optically thick in primordial discs. Hence, they trace gas in the surface out to typical distances of

Table 3: Observed species, red: near/mid-IR – green: far-IR – black: detected in sub-mm. A coloured * indicates a second detection in another wavelength band. Deuterated molecules are noted in addition since their spatial distribution can significantly differ from the main molecule.

1 atom	2 atoms	3 atoms	4 atoms	5 atoms	6 atoms
O	CO*	HCN*	H_2CO	HC_3N	CH_3CN
C^+	CN	NH_3	C_2H_2	CH_4	CH_3OH
C	H_2	HCO^+			
Fe^+	HD	N_2H^+			
Si	CH^+	DCO^+			
Si^+	CS	DCN			
Ne^+	SiO*	C_2H*			
Ar^+	OH*	CO_2			
	SO	H_2O*			
		N_2D^+			

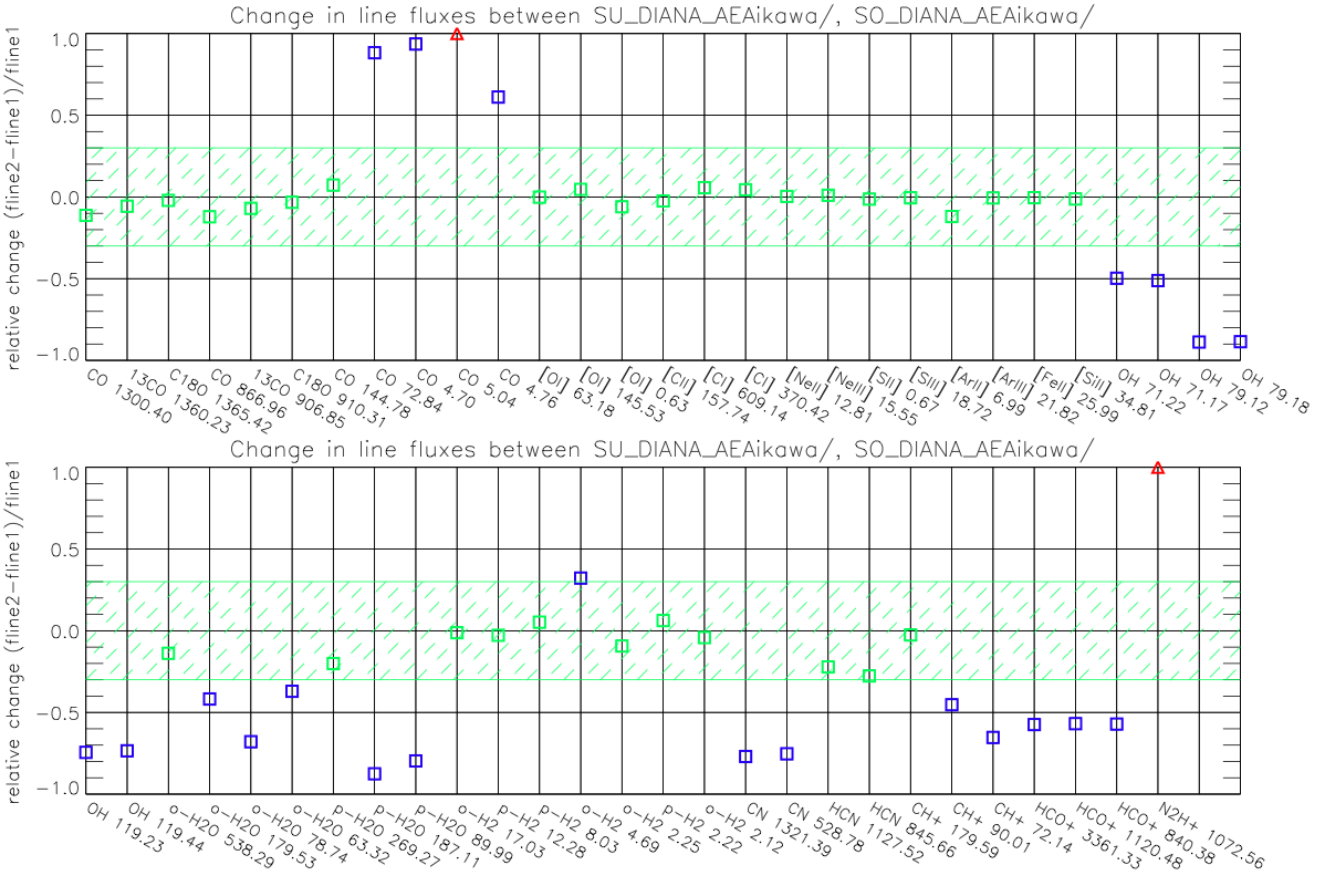

Figure 20: Comparison of line fluxes for two databases: UMIST2012 (fline1) and OSU (fline2). Blue squares and red triangles denote differences larger than a factor three and ten respectively.

$\sim$100 AU (Kamp et al., 2010). It is interesting to note that in the outer disc above the CO ice reservoir, atomic oxygen is the dominant oxygen-bearing species.

Molecular ions originate from efficient ion-molecule chemistry. This can be driven either by stellar/interstellar UV photons (closer to the disc surface) or by secondary ionisation from cosmic rays penetrating very deep into the disc. Hence, there are ion-molecules like HCO^+ which reside in thin surface layers 'around' the main CO ice reservoir (HCO^+ forms from gas phase CO). The thickness of this layer is influenced by the penetration depth of UV and X-rays (Kamp et al., 2013). On the other hand, N_2H^+ forms between the zones where CO and N_2 are frozen out as ice (strong dependence on the relative CO/N_2 binding energy). Its lines originate deep in the disc, but can be optically thick and hence not reach down all the way to the midplane (Rab et al. , submitted). Both lines are very sensitive to the ionisation fraction and hence not only the ionising radiation, but also the metal abundances in the disc (Rab et al. submitted).

Several molecules such as CO, HCN are detected in their rotational lines in the sub-mm, but also in their ro-vibrational lines in the near- to mid-IR. In those cases, the rotational lines generally probe the cold gas in the outer disc, while the ro-vibrational lines probe the planet-forming regions ($0.1-10$ AU). The ro-vibrational lines can be pumped by UV and/or IR fluorescence, thus requiring large model molecules and detailed 2D continuum radiative transfer including scattering for the quantitative interpretation of these lines (Thi et al., 2013; Bruderer et al., 2015). The CO rotational ladder scans the disc surface (the rarer isotopologues probe slightly deeper layers compared to the main one) and is thus sensitive to the radial temperature gradient of the disc (van der Wiel et al., 2014; Fedele et al., 2016).

Especially at earlier embedded evolutionary stages, gas line emission often originates both from larger-scale outflows and shocks as well as small-scale discs. Interferometers can help to disentangle the components spatially, but higher rotational lines of molecules with higher critical densities can also be good 'disc' tracers (e.g. CN 5-4, Podio et al., 2014).

The interpretation and understanding of this large suite of species hinges on chemical networks predicting the abundance distribution. A comparison study that involves the use of a small (100 species) and large (237 species) chemical networks and various databases (UMIST, KIDA, OSU, private collection) shows that within a set of 56 lines of 20 species (not all of them yet observed) ranging from the optical to the sub-mm, most of the line fluxes do not change by more than a factor of 2-3. Larger differences are seen for CN, OH and water pointing to (a) differences in the nitrogen chemistry and (b) three-body-reactions playing a role in water formation (Kamp et al. in prep, Fig. 20). The H_2 and CH^+ lines from the inner disc can also differ a lot. But overall, most of the differences in chemical structure are restricted to deeper, more opaque layers of the disc that are not directly accessible to gas line observations. And in turn **many of the gas emission lines frequently used in disc research are robust against changes and uncertainties in chemical networks**.

The most important conclusion is that we require multi-wavelength line observations in order to obtain a complete picture of these discs not only in the radial, but also in the vertical direction. Based on where specific species reside in a primordial homogeneous disc, they can be used to trace physical processes or local conditions such as disc winds, the degree of ionisation and the location of ice lines.

3.6.2 How can we derive the total gas mass, and the overall gas-to-dust mass ratio?

For many years, the holy grail of disc research has been the search for a suitable method to estimate gas masses and hence also gas-to-dust mass ratios. While gas-mass estimates are

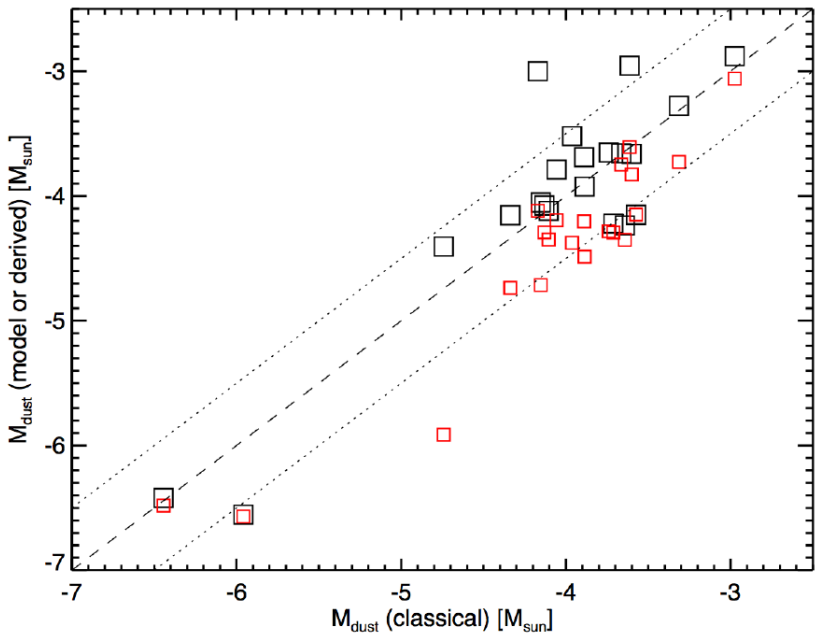

Figure 21: Dust masses derived from the 850 μm flux using the classical method (standard opacity of 3.5 cm^2/g, dust temperature of 20 K) versus actual dust masses used the SED-fitting DIANA standard models (black squares). Also shown are those derived in the classical way, but using the mean dust opacities and mean dust temperature as present in the models instead of the standard values (red squares).

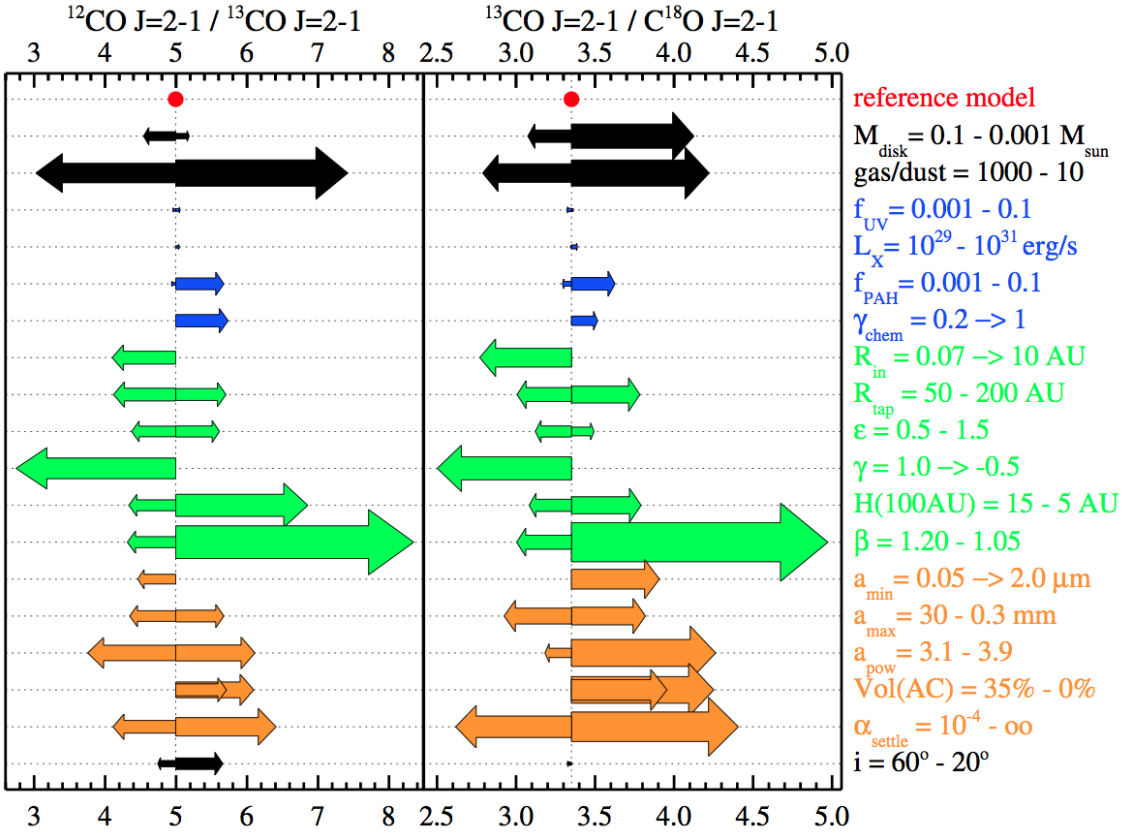

Figure 22: CO line ratio "impactogram" (from Woitke et al., 2016) shows the various physical disc model parameters and how changing them impacts the CO isotopologue line ratios. The right legend shows the disc model parameter and the ranges within which they were modified.

often seen as highly uncertain, dust masses are in general thought to be more robust. In DIANA, we reviewed both aspects and the results are summarised below.

Dust masses are generally derived from sub-mm or mm continuum fluxes using a fixed standard dust opacity of $\kappa_{850\mu m} = 3.5$ cm^2/g and a constant average dust temperature of 20 K. The new disc dust opacities calculated within DIANA (Min et al., 2016) are a factor of 2-3 higher and also the average dust temperature in the models is sometimes higher and sometimes lower than 20 K. This, together with the dust emission being composed of a series of blackbodies rather than a single one, leads to differences of up to one order of magnitude between the 'classical' mass-determination method and the approach using more realistic disc opacities and models (Fig. 21).

Gas masses are often estimated through CO isotopologue line ratios as explored by e.g. Thi et al. (2001) and more recently by Williams & Best (2014) and Miotello et al. (2014). A first comprehensive parameter study of the CO line ratio is done within DIANA by Woitke et al. (2016) showing clearly that detailed dust properties such as the grain size distribution also have a similar effect to that of the the gas mass on the isotopologue ratio (Fig. 22). Fig. 23 shows that the eleven discs that were analysed within the DIANA multi-wavelength standard approach indeed all fall on the CO isotopologue mass relation; however, the size of the symbol indicating the gas mass in the model is the same for low CO line ratios as well as high ratios. This is caused by the different dust properties and gas-to-dust mass ratios.

Hence, a more reliable path to estimate dust and gas masses is to have imaging of discs at two wavelengths to constrain the dust properties (grain size distribution and settling), and the two isotopologue lines ^{13}CO and C^{18}O (flaring and surface-density profile) to then

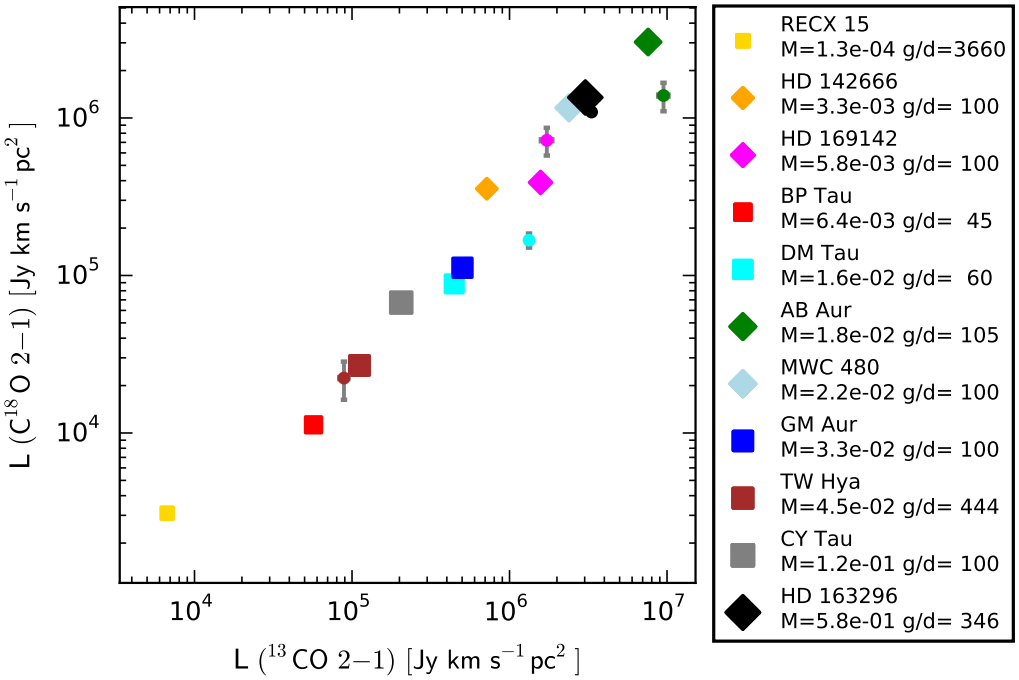

Figure 23: CO line flux results from the DIANA standard models (squares - size scaled to the disc gas mass) for the respective objects indicated in the legend (colour code). The observed fluxes are shown as dots of the same colour with error bars.

derive the gas mass consistently with the dust mass estimate/properties.

3.6.3 How can we recognise and diagnose disc anomalies, such as inner holes, gaps and spiral structures?

Several mechanisms have been proposed as explanation for inner-disc holes, gaps and/or spiral structure. Inner holes and gaps can originate from (1) photo-evaporation (UV, X-rays), which removes mostly gas and small dust grains entrained, (2) a massive planet opening a gap, and (3) dust grain growth which proceeds faster close to the star. A number of key measurements can help to distinguish between these scenarios:

- dust and gas inner-disc radii
- surface-density profiles in the inner disc,
- gas and dust column densities in the inner disc.

The analysis of PIONIER near-IR interferometry data for 21 T Tauri targets including thermal and scattered light emission shows that the inner radii are consistent with dust sublimation radii (Anthonioz et al., 2015). Gas inner radii can be measured from CO ro-vibrational line profiles (Carmona et al., 2014; van der Plas et al., 2015; Banzatti & Pontoppidan, 2015; Hein Bertelsen et al., 2016a). When we pull the various datasets together, we see that for a number of T Tauri discs, the dust and gas inner radii agree very well with the exception of GQ Lup which shows $R_{\rm gas,in} > R_{\rm dust,in}$ (Table 4). The picture is more diverse for the Herbig discs. Here Hein Bertelsen et al. (2016a) found that Herbig group I sources often have different gas and dust geometries (not co-spatial). The FWHM of the CO ro-vibrational lines versus J quantum number can be either constant or increase depending on the location of the CO inner radius (Fig. 24).

Carmona et al. (2014) and (2016, submitted) showed how the CO ro-vibrational line profiles can be used to derive the surface-density profile in the inner disc. In particular, the

Table 4: Dust inner radii from PIONIER data (Anthonioz et al., 2015) and CO rovibrational emission (v=1-0) radii for the broad (BC) and narrow (NC) component from CRIRES data (Banzatti & Pontoppidan, 2015).

object	BC $R_{\rm CO}$ [au]	NC $R_{\rm CO}$ [au]	$R_{\rm in,dust}$ [au]
AS205N	0.17	2.3	$0.176^{+0.002}_{-0.001}$
GQ Lup	0.20	0.6	$0.041^{+0.013}_{-0.034}$
HT Lup	0.05	1.6	$0.055^{+0.004}_{-0.004}$
RU Lup	0.07	2.5	$0.102^{+0.003}_{-0.004}$
S CrA N	0.05	1.1	$0.078^{+0.007}_{-0.008}$

optically thinner isotopologues of ^{13}CO and C^{18}O (if detectable) probe the full column of gas. From these types of analysis evidence is emerging that the gas column density in the inner disc is increasing with radius rather than decreasing, a scenario that would be compatible with hydrodynamical simulations of gap opening due to a massive planet.

In the outer disc, the surface-density distribution of gas and dust can be shaped by a series of other processes. Viscous spreading of the disc will create an exponentially tapered edge in contrast to binary interaction and dynamical encounters which could produce sharp outer edges. Dust radial migration can lead to a size sorting of grains at the outer radius and dust radii being systematically smaller compared to gas radii. ALMA continuum and line images are excellent in disentangling these scenarios. de Gregorio-Monsalvo et al. (2013) have shown from ALMA images of HD 163296 that the surface-brightness profiles require different radial dust and gas profiles consistent with a scenario of grain growth and radial migration. Woitke et al. (2016) demonstrated that the difference in radial extent between the two isotopologues ^{12}CO and ^{13}CO is a powerful tool to probe the shape of the gas outer-disc truncation.

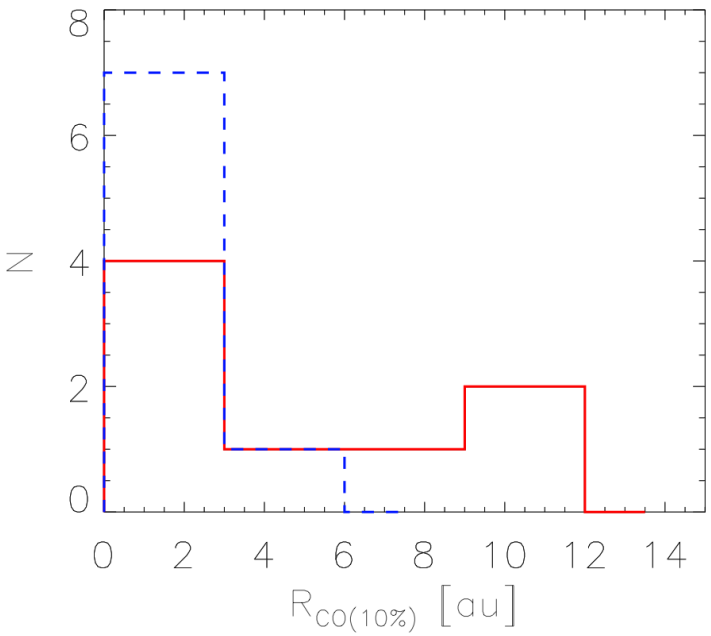

Figure 24: Histogram for the distribution of $R_{\rm CO,10\%}$, the radius which corresponds to the velocity at 10% of the peak flux, in sources with increasing FWHM versus J (red) and constant FWHM versus J (blue dashed).

3.6.4 Preparation and planning of future instruments and missions

Within DIANA extensive testing and comparison with observations (WP 2 and e.g. Rab et al. submitted) have led to a level of reliability never reached before. That now enables, for the first time, robust predictions for currently unexplored spectral windows and types of observations. Below a few examples are highlighted.

JWST/MIRI: Antonellini et al. (2015, 2016) investigated the mid-IR water spectra of T Tauri and Herbig discs and compared them with existing Spitzer data. They found that Herbig discs are likely not "drier" than T Tauri discs, but that JWST/MIRI's higher spectral resolution will be required to detect abundant water in those systems.

METIS: This is a proposed first-generation mid-infrared imager and spectrograph for the upcoming European Extremely Large Telescope (E-ELT). Using ProDiMo together with FLiTs, John Ilee calculated a synthetic spectrum for a canonical Herbig Ae disc (Fig. 25). This model spectrum was used by the design review team to recommend an increase in wavelength coverage in order to maximise the scientific output of the instrument.

SPICA: This is the proposed next IR space mission (ESA/JAXA collaboration) hosting two instruments SMI (mid-IR) and SAFARI (far-IR). Vicente (in prep.) provided re-assessments of SPICA's capability to detect the [O I] fine-structure lines, CO lines and water lines in discs around T Tauri and Herbig stars (based on GASPS target samples and our large disc-modelling grids from WP 6). This led to a re-design of the SAFARI instrument which is now much better tuned to (a) detect faint lines on bright continua and (b) look at brighter sources up to ∼1 Jy.

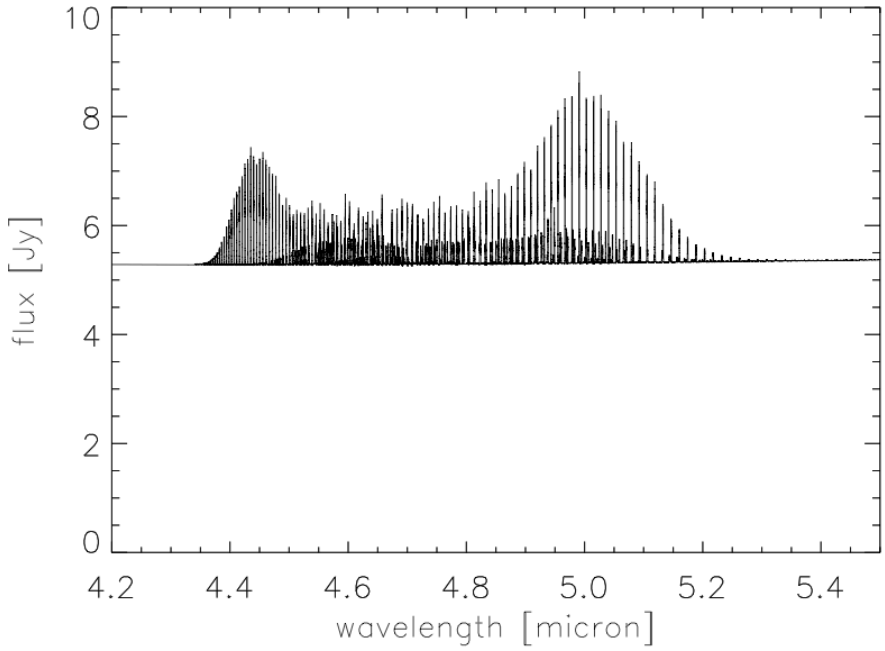

Figure 25: Simulated FLiTs 4.7 μm spectrum for a Herbig Ae star. This shows the richness of this spectral band including CO ro-vibrational lines of the fundamental and various excited bands; the spectral band also contains lines of several other simple molecules like H_2O.

4 Main Dissemination Activities, Exploitation and Impact

4.1 Peer-reviewed Articles

During the lifetime of *DIANA* we published 50 papers in peer-reviewed journals like *Nature*, *Astronomy & Astrophysics*, *Monthly Notices of the Royal Astronomical Society*, the *Astrophysical Journal*, and *Publications of the Astronomical Society of the Pacific* (see full list of publications in Deliverable 7.1). Table 5 shows that about half of those papers have been written in teamwork, with at least two contributing authors from two different *DIANA* institutions, and the proportion of papers with contributions from at least three different *DIANA* institutions is as high as 40 %, showing our sustained level of good collaboration throughout the project.

Table 5: Summary of peer-reviewed journal articles written by *DIANA* team members between 01/2012 and 03/2016.

1 author 1 institution	≥ 2 authors 1 institution	≥ 2 authors ≥ 2 institutions	≥ 3 authors ≥ 3 institutions	total
13	14	23	19	50

4.2 Talks and Posters at International Conferences

Team members have represented our project ideas, strategies and results in 74 talks and 19 posters altogether at international conferences and workshops, see Table 6.

Table 6: Overview of talks given and posters shown at international conferences by members of the *DIANA* team.

	2012	2013	2014	2015	2016	total
talks	12	17	22	16	7	74
posters	2	7	8	1	1	19

4.3 Public Talks, Demonstrations, Exhibitions

Questions about the birth and death of stars, and the formation of the Earth and planetary systems, easily catch the interest of society, from school-age children to passionate pensioners. This works to our advantage as our research is directly related to important philosophical questions. For example, everybody wants to know what life might look like on planets

Table 7: Summary of outreach activities by *DIANA* members

	2012	2013	2014	2015-16	total
public talks	7	5	11	11	34
exhibitions / demonstrations	5	3	16	12	36
press releases / interviews / TV	1	0	3	3	7

Figure 26: **Left:** The *road show* of St Andrews University. An inflatable planetarium, among other demonstration material, is brought to local schools by astronomers from St Andrews University, including FP7 DIANA members Laura Rigon and John Ilee. We estimate that in its first three years of operation altogether some 10,000 visitors had crawled into the "dome" to see the virtual universe sparkle around them, see http://star-www.st-and.ac.uk/planetarium. **Right:** Peter Woitke during the *Open Days* 2013 at St Andrews University - junior visitors view their pictures taken by an infra-red camera (top), which shows surface temperature variations http://www.vision4thefuture.org.

Figure 27: **Left:** *Make your own comet* during the "Nacht van de Nacht" at Groningen University. **Right:** Watching the solar eclipse on 20 March 2015 in front of the "Infoversum" in Groningen.

orbiting other suns, and how water came to planet Earth. Between January 2012 and March 2016, we organised a number of outreach activities, partly in collaboration with our host universities. Altogether, 34 public talks have been delivered by *DIANA* members (see Table 7), we have participated in 36 demonstrations/exhibitions (see e.g. Figure 26), and we managed to publish seven press releases/interviews (Table 8).

It is important to realise that taking part in existing outreach activities like the bi-annual *Open Night at the Observatory*, *Ask an Astronomer* or the Planetarium Show in St Andrews (see Figure 26), or the *Nacht van de Nacht* and *Sterrenkijkdagen* at the Blaauw Observatory

Table 8: *DIANA* press releases

1. *"Levenskansen in het zonnestelsel"*, 09/09/2012, article published in the popular press, article in 'Zenit', Amsterdam, NL, 5 pages in Dutch (by Michiel Min)
2. *"Entre Terre et Ciel"*, Arte TV documentary about ALMA and dust in discs, episode 7, aired 09/09/2014 (featuring Francois Ménard)
3. *"De kennis van nu: Philae landing on comet"*, 12/11/2014, radio interview in 'Radio 5', NL (Carsten Dominik)
4. *"ALMA image of HL Tau"*, 15/11/2014, interview for article in 'De Volkskrant' by Govert Schilling, Amsterdam, NL (Carsten Dominik)
5. *"De zon: Die kennen we nu zo langzamerhand toch wel?"*, 02/05/2015, interview in 'Dagblad van het Norden', NL, newspaper interview (Inga Kamp)
6. *"Astronomers see pebbles poised to make planets"*, 05/07/2015, https://www.ras.org.uk/news-and-press/2656-astronomers-see-pebbles-poised-to-make-planets (Jane Greaves)
7. *"Astronomers peer into the 'amniotic sac' of a planet-hosting star"*, 14/09/2015, http://www.ras.org.uk/news-and-press/2709-astronomers-peer-into-the-amniotic-sac-of-a-planet-hosting-star (John Ilee)

in Groningen (see Figure 27), are well-established and very effective opportunities to reach local children and interested laymen, with some 300 visitors every year. Such numbers would be difficult to achieve, for example, if something different had been "invented" by us instead, from scratch.

Similar activities have been carried out in Groningen and Amsterdam, using their inflatable planetaria, and in Vienna and Grenoble concerning their Open Days.

The EU funding of the *FP7 DIANA project* has therefore not only resulted in a number of self-organised outreach activities, but has also added value to existing outreach programmes of our host universities, where the science questions raised by the FP7 *DIANA* project have been successfully incorporated.

4.4 Series of Educational YouTube Videos

A series of seven YouTube movies has been delivered in December 2013, see Figure 28 and see https://www.youtube.com/channel/UCbpJQukyO7U1MMdi-36Y5Gg. The scripts were written by *DIANA* team members and discuss the following questions

- "Observing dust grains grow into planets"
- "Why are all the planets aligned?"
- "Transition Discs and Planet Formation"
- "Exoplanets"
- "Models in Astronomy"
- "Chemistry in Space"
- "Water in Protoplanetary Discs"

The actual filming was done during the *DIANA* team meeting in Amsterdam (September 2013) in three different locations. The short videos feature eight *DIANA* team members,

Laura Rigon: Observing dust grains grow into planets
202 views • 2 years ago

John Ilee: Why are all the planets aligned?
410 views • 2 years ago

Andres Carmona: Transition Disks and Planet Formation
1,055 views • 2 years ago

Michiel Min: Exoplanets
207 views • 2 years ago

Christian Rab: Models in Astronomy
202 views • 2 years ago

Stefano Antonellini: Chemistry in Space
238 views • 2 years ago

Inga Kamp: Water in Protoplanetary Disks and the ...
305 views • 2 years ago

Figure 28: DIANA's prize-winning series of YouTube videos about star and planet formation, see https://www.youtube.com/channel/UCbpJQukyO7U1MMdi-36Y5Gg.

preferentially the PhD students and postdoctoral researchers, from all five participating institutions. The second movie in this series entitled "Why are all planets aligned?", featuring postdoctoral researcher John Ilee (University of St Andrews), won the second prize of Scotland's SUPA video competition in 2014.

4.5 Provision of School Material

Astronomy is often a minor or even missing part of the standard school curriculum in many European countries. Obviously, astronomy needs to compete here with other natural sciences which are equally important. However, astronomy is special in that it can teach us about the vastness of the universe, the possible existence of other worlds, and the enormous contrast between very large and very small scales, both in time and in space. Studying the universe means to analyse, model and understand the light we receive with wavelengths that our eyes cannot even see, without being able to touch the objects of study. And here, young

Figure 29: In-service training for physics school teachers at Kirkcaldy High School, Scotland, in November 2015.

schoolchildren seem to soak up such questions and explanations like sponges.

In 2015, a new curriculum for advanced highers in physics at Scottish secondary schools was released (see details from the Scottish Qualifications Authority http://www.sqa.org.uk/sqa/48460.html) which includes, for the first time, stellar physics and general relativity.

In November 2015, PI Woitke was invited to provide in-service training for teachers (INSET meeting), reaching about 60 high-school physics teachers in Fife, Scotland. After the three training sessions (see Figure 29), it became clear that the school teachers are right now actively looking for suitable lecturing material, so Woitke created this webpage http://www-star.st-and.ac.uk/~pw31/education.html. The link provides some selected lecturing material covering the Sun, basic stellar parameters (stellar radius, luminosity, effective temperature, spectral flux, Stefan-Boltzmann law, apparent and absolute brightness), basic assumptions in stellar atmosphere and stellar structure theory, including nuclear fusion reactions, position and classification in the Hertzsprung-Russell (H-R) diagram, as well as some insight into stellar evolution, final stages of stellar evolution, and the cosmic cycle of matter. It includes a selection of simple astronomical questions about stars and provides answers in an extra document.

This is an example of an impact made by *DIANA* on education and society, how to make small improvements to the education system for our children.

4.6 Lecture Notes

Our "book" about the physics and chemistry of protoplanetary discs is publicly available via the EPJ Web of Conferences, see https://dianaproject.wp.st-andrews.ac.uk/summer-school/lecture-notes/. The book aims at more advanced education for students and PhD students at university level. The book is a compilation of 15 peer-reviewed lectures presented at the Summer School "Protoplanetary Discs: Theory and Modelling Meet Observations", Ameland, The Netherlands, June 16-20, 2014, I. Kamp, P. Woitke and J.D. Ilee (eds.), ISBN: 978-2-7598-1875-4.

1. Carsten Dominik: "Disc formation and structure"
2. Rens Waters: "Dust in protoplanetary discs: observations"
3. Carsten Dominik: "Disc evolution: dust and gas"
4. Michiel Min: "Dust Opacities"
5. Christophe Pinte: "Continuum radiative transfer"
6. Peter Woitke: "Modelling and interpretation of SEDs"
7. Odysseas Dionatos: "Gas line observations of discs"
8. John Ilee, Jane Greaves: "Interferometry and the study of protoplanetary discs"
9. Inga Kamp: "Line radiative transfer and statistical equilibrium"
10. Peter Woitke: "Heating and cooling processes in discs"
11. Wing-Fai Thi: "Disc Chemistry"
12. Inga Kamp: "Modelling and interpretation of line observations"
13. Wing-Fai Thi: "Chemical networks"
14. Manuel Güdel: "Ionisation and heating by X-rays and cosmic rays"
15. Michiel Min: "Modelling and interpretation of images"

The long-term aim of this initiative is to disseminate our theories, tools and methods to the next generation of scientists, and to help higher-education institutions to develop new lecture courses about star and planet formation.

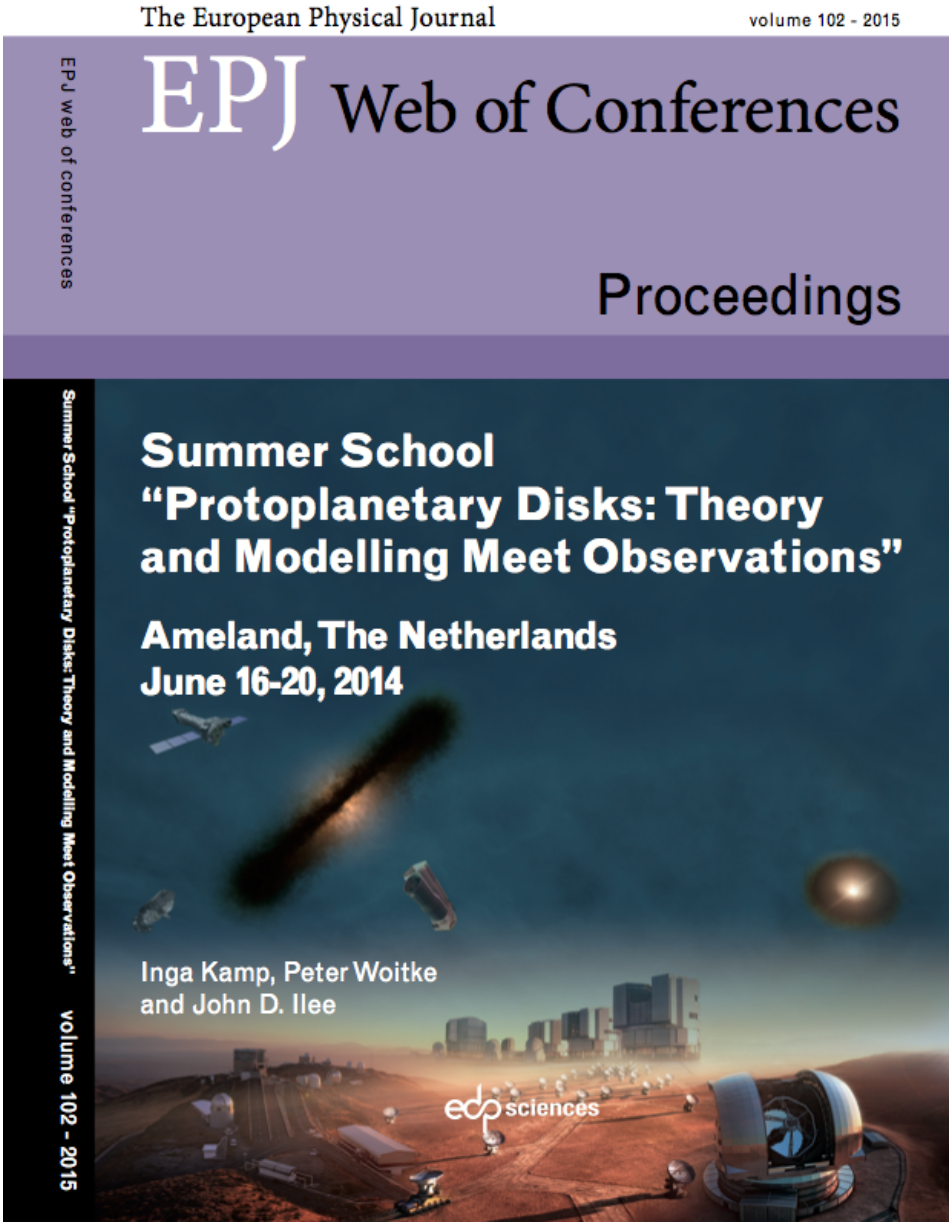

Figure 30: DIANA's book – a collection of lectures from our summer school.

4.7 International Conference

We have organised an international conference entitled "Protoplanetary Discussions" held in the John Mc Intyre Conference Centre, Edinburgh, UK, 7^{th} – 11^{th} March 2016, see http://www-star.st-and.ac.uk/ppdiscs/index.html and Fig. 31. The Local Organising Committee (LOC) was led by *DIANA* member J. Ilee (in collaboration with the University of Edinburgh) and the Scientific Organising Committee (SOC) by PI Woitke. F. Ménard and R. Waters were also SOC members, together with five external international experts.

The aim of this conference was to invite observers from all wavelength regimes to share their latest results with modellers from the thermo-chemical and hydrodynamic communities in order to foster collaboration across this exciting and rapidly expanding field. Recent observations of protoplanetary discs have revealed intriguing and frequently non-symmetric structures including spiral arms, gaps and rings, holes, and warps. These structures have been detected in the gas and dust, in scattered light and thermal emission. Identifying their nature, whether they are caused by disc-planet interactions or by other physical pro-

cesses, remains challenging and controversial. What observational quantities are essential to constrain the models? How can models help to guide future observational campaigns? What do different wavelength regimes reveal? What are the possible interpretations from hydrodynamic, chemical and radiative-transfer modelling? What are the signposts for planet formation?

We had 110 participants, and the SOC selected 53 international expert speakers in the field, including 6 reviews, 9 highlight talks and 38 contributed talks. Six speakers were selected from the *DIANA* team.

The conference included ample time for six participant-led open discussion and collaboration sessions, with the goal of exploring common ground between the different communities and discovering new avenues for investigation. The goal of these "discussions" was to stimulate active knowledge transfer between experts in the field, to discuss the latest observations and to see what current models are lacking, and how, for example, hydrodynamics can be merged with astrochemistry and radiative transfer.

With the rapid development of disc models in these merging theoretical fields, and the new observational facilities revealing the next level of complexity in discs right now, we believe our group is well positioned to face all future challenges, and to possibly apply again for

Figure 31: International Conference "Protoplanetary Discussions", held in March 2016 in Edinburgh.

European support in the Horizon 2020 framework. The new data, in particular from ALMA and SPHERE, reveal that discs include 3D features that have not been taken into account in *DIANA*. We have identified the coupling between hydrodynamics and chemistry with proper heating/cooling and radiative transfer as the most important future developments to better understand and account for these new structures.

4.8 Impact on Related Science Fields

Our impact and scientific knowledge exchange efforts can be measured, for example, by looking at publications that have used our main modelling tools ProDiMo, MCFOST or MCMax, but do **NOT** have the *DIANA* acknowledgement included, because they focus on adjacent science topics. Usually, these papers are led by first authors from other institutions, but have at least one of the *DIANA* members as co-author, to ensure proper usage of the modelling software.

The following list shows that applications are widespread, from active galactic nuclei, to N-particle simulations for debris discs to the molecular gas in the centre of our Galaxy, from the red supergiant Betelgeuse to the dusty winds of asymptotic giant branch stars and post-AGB stars to the discs around brown dwarfs. There are also some papers which focus on predictions for new astronomical instruments.

- structure of active galactic nuclei (Meijerink et al., 2013)
- dense gas in the Galactic central molecular zone (Ginsburg et al., 2016)
- N-body simulations of debris discs (Thilliez & Maddison, 2015), and predictions of planets (Thilliez & Maddison, 2016)
- interpreting scattered-light images of debris discs taken by the Gemini Planet Imager (Hung et al., 2015)
- protoplanetary disc lifetimes and giant planet populations (Ribas et al., 2015)
- polarimetry with the Gemini Planet Imager at first light (Perrin et al., 2015)
- predicting polarisation of light by protoplanetary discs (Canovas et al., 2015)
- discs around brown dwarfs (Broekhoven-Fiene et al., 2014; van der Plas et al., 2016)
- radial drift in protoplanetary discs (Pinte & Laibe, 2014)
- near-IR integral field spectra of young M-L dwarfs (Bonnefoy et al., 2014)
- newly resolved debris discs in scattered light from the HST/NICMOS archive (Moerchen et al., 2014)
- proto-stellar disc around Radio Source I with Keck Adaptive Optics (Sitarski et al., 2013)
- flows of gas through gaps in protoplanetary discs (Casassus et al., 2013)
- post-AGB binary stars (Hillen et al., 2015b)
- the evolved circumbinary disc of AC Herculis (Hillen et al., 2015a)
- dusty winds of oxygen-rich AGB stars (Khouri et al., 2015)
- detection of an equatorial dust lane on the AGB star IRC+10216 (Jeffers et al., 2014)
- theoretical intensity and polarised intensity images of transitional discs (de Juan Ovelar et al., 2014)
- structure of circumstellar envelope surrounding Betelgeuse (Decin et al., 2012)
- massive dust clouds around post-AGB star R Coronae Borealis (Jeffers et al., 2012)

5 Public website and contact details

The main project website is located at https://dianaproject.wp.st-andrews.ac.uk/ with further links to the *DIANA's database* (DIOD), the model grids, a Fortran tool to compute dust opacities, our summer school and conference, and outreach.

The main project contact details are:

scientific coordinator / PI:	**Dr. Peter Woitke** University of St Andrews School of Physics & Astronomy North Haugh St Andrews KY16 9SS, Scotland, UK Peter.Woitke@st-andrews.ac.uk (+44) 1334 46 1681
administrative officer:	**Dr. Irina Leonhardt** University of St Andrews School of Physics & Astronomy il4@st-andrews.ac.uk Tel: (+44) 1334 46 3103
scientific contact for Vienna:	**Prof. Manuel Güdel** University of Vienna Department of Astrophysics Türkenschanzstrasse 17 A-1180 Vienna, Austria manuel.guedel@univie.ac.at (+43) 1 4277 53814
scientific contact for Grenoble:	**Prof. François Ménard** Université Grenoble Alpes Institut de Planetologie et d'Astrophysique (IPAG) CS 40700 F-38058 Grenoble cedex 9, France francois.menard@univ-grenoble-alpes.fr (+33) 476 63 5601
scientific contact for Groningen:	**Prof. Inga Kamp** Rijksuniversiteit Groningen Kapteyn Instituut Postbus 800 9700 AV Groningen, The Netherlands kamp@astro.rug.nl (+31) 50 363 4070
scientific contact for Amsterdam:	**Prof. Carsten Dominik** Universiteit van Amsterdam Anton Pannekoek Institute for Astronomy Science Park 904, PO Box 94249 1090 GE Amsterdam, The Netherlands dominik@uva.nl (+31) 20 525 7477

References

Alecian, E., Wade, G. A., Catala, C., Grunhut, J. H., Landstreet, J. D., Bagnulo, S., Böhm, T., Folsom, C. P., Marsden, S., Waite, I. (2013, February). A high-resolution spectropolarimetric survey of Herbig Ae/Be stars - I. Observations and measurements. *MNRAS* **429**, 1001–1026.

Ammons, S. M., Robinson, S. E., Strader, J., Laughlin, G., Fischer, D., Wolf, A. (2006, February). The N2K Consortium. IV. New Temperatures and Metallicities for More than 100,000 FGK Dwarfs. *ApJ* **638**, 1004–1017.

Andrews, S. M., Czekala, I., Wilner, D. J., Espaillat, C., Dullemond, C. P., Hughes, A. M. (2010, February). Truncated Disks in TW Hya Association Multiple Star Systems. *ApJ* **710**, 462–469.

Anthonioz, F., Ménard, F., Pinte, C., Le Bouquin, J.-B., Benisty, M., Thi, W.-F., Absil, O., Duchêne, G., Augereau, J.-C., Berger, J.-P., Casassus, S., Duvert, G., Lazareff, B., Malbet, F., Millan-Gabet, R., Schreiber, M. R., Traub, W., Zins, G. (2015, January). The VLTI/PIONIER near-infrared interferometric survey of southern T Tauri stars. I. First results. *A&A* **574**, A41.

Antonellini, S., Kamp, I., Lahuis, F., Woitke, P., Thi, W.-F., Meijerink, R., Aresu, G., Spaans, M., Güdel, M., Liebhart, A. (2016, January). Mid-IR spectra of pre-main sequence Herbig stars: An explanation for the non-detections of water lines. *A&A* **585**, A61.

Antonellini, S., Kamp, I., Riviere-Marichalar, P., Meijerink, R., Woitke, P., Thi, W.-F., Spaans, M., Aresu, G., Lee, G. (2015, October). Understanding the water emission in the mid- and far-IR from protoplanetary disks around T Tauri stars. *A&A* **582**, A105.

Aresu, G., Kamp, I., Meijerink, R., Woitke, P., Thi, W.-F., Spaans, M. (2011, February). X-ray impact on the protoplanetary disks around T Tauri stars. *A&A* **526**, A163.

Aresu, G., Meijerink, R., Kamp, I., Spaans, M., Thi, W.-F., Woitke, P. (2012, November). Far-ultraviolet and X-ray irradiated protoplanetary disks: a grid of models. II. Gas diagnostic line emission. *A&A* **547**, A69.

Baldovin-Saavedra, C., Audard, M., Güdel, M., Rebull, L. M., Padgett, D. L., Skinner, S. L., Carmona, A., Glauser, A. M., Fajardo-Acosta, S. B. (2011, April). Searching for gas emission lines in Spitzer Infrared Spectrograph (IRS) spectra of young stars in Taurus. *A&A* **528**, A22.

Banzatti, A., Pontoppidan, K. M. (2015, August). An Empirical Sequence of Disk Gap Opening Revealed by Rovibrational CO. *ApJ* **809**, 167.

Bertout, C., Siess, L., Cabrit, S. (2007, October). The evolution of stars in the Taurus-Auriga T association. *A&A* **473**, L21–L24.

Biller, B., Lacour, S., Juhász, Benisty, M., Chauvin, G., Olofsson, J., Pott, J.-U., Müller, A., Sicilia-Aguilar, A., Bonnefoy, M., Tuthill, P., Thebault,

P., Henning, T., Crida, A. (2012, July). A Likely Close-in Low-mass Stellar Companion to the Transitional Disk Star HD 142527. *ApJL* **753**, L38.

Bonnefoy, M., Chauvin, G., Lagrange, A.-M., Rojo, P., Allard, F., Pinte, C., Dumas, C., Homeier, D. (2014, February). A library of near-infrared integral field spectra of young M-L dwarfs. *A&A* **562**, A127.

Boss, A. P. (1997). Giant planet formation by gravitational instability. *Science* **276**, 1836–1839.

Boss, A. P. (2009, March). Analytical Solutions for Radiative Transfer: Implications for Giant Planet Formation by Disk Instability. *ApJ* **694**, 107–114.

Broekhoven-Fiene, H., Matthews, B., Duchêne, G., Di Francesco, J., Scholz, A., Chrysostomou, A., Jayawardhana, R. (2014, July). The Disk around the Brown Dwarf KPNO Tau 3. *ApJ* **789**, 155.

Bruderer, S., Harsono, D., van Dishoeck, E. F. (2015, March). Ro-vibrational excitation of an organic molecule (HCN) in protoplanetary disks. *A&A* **575**, A94.

Bruggeman, D. A. G. (1935). Berechnung verschiedener physikalischer Konstanten von heterogenen Substanzen. I. Dielektrizitätskonstanten und Leitfähigkeiten der Mischkörper aus isotropen Substanzen. *Annalen der Physik* **416**, 636–664.

Cabrit, S., Edwards, S., Strom, S. E., Strom, K. M. (1990, May). Forbidden-line emission and infrared excesses in T Tauri stars - Evidence for accretion-driven mass loss? *ApJ* **354**, 687–700.

Calvet, N., Muzerolle, J., Briceño, C., Hernández, J., Hartmann, L., Saucedo, J. L., Gordon, K. D. (2004, September). The Mass Accretion Rates of Intermediate-Mass T Tauri Stars. *AJ* **128**, 1294–1318.

Canovas, H., Ménard, F., de Boer, J., Pinte, C., Avenhaus, H., Schreiber, M. R. (2015, October). Nonazimuthal linear polarization in protoplanetary disks. *A&A* **582**, L7.

Carmona, A., Pinte, C., Thi, W. F., Benisty, M., Ménard, F., Grady, C., Kamp, I., Woitke, P., Olofsson, J., Roberge, A., Brittain, S., Duchêne, G., Meeus, G., Martin-Zaïdi, C., Dent, B., Le Bouquin, J. B., Berger, J. P. (2014, July). Constraining the structure of the transition disk HD 135344B (SAO 206462) by simultaneous modeling of multiwavelength gas and dust observations. *A&A* **567**, A51.

Carmona, A., van den Ancker, M. E., Henning, T., Goto, M., Fedele, D., Stecklum, B. (2007, December). A search for near-infrared molecular hydrogen emission in the CTTS LkHα 264 and the debris disk 49 Ceti. *A&A* **476**, 853–862.

Casassus, S., van der Plas, G., M, S. P., Dent, W. R. F., Fomalont, E., Hagelberg, J., Hales, A., Jordán, A., Mawet, D., Ménard, F., Wootten, A., Wilner, D., Hughes, A. M., Schreiber, M. R., Girard, J. H., Ercolano, B., Canovas, H., Román, P. E., Salinas, V. (2013, January). Flows of gas through a protoplanetary gap. *Nature* **493**, 191–194.

Chaparro Molano, G., Kamp, I. (2012a, January). The role of OH in the chemical evolution of protoplanetary disks. I. The comet-forming region. *A&A* **537**, A138.

Chaparro Molano, G., Kamp, I. (2012b, November). The role of OH in the chemical evolution of protoplanetary disks. II. Gas-rich environments. *A&A* **547**, A7.

Chapillon, E., Guilloteau, S., Dutrey, A., Piétu, V. (2008, September). Disks around CQ Tauri and MWC 758: dense PDR or gas dispersal? *A&A* **488**, 565–578.

Chen, H., Myers, P. C., Ladd, E. F., Wood, D. O. S. (1995, May). Bolometric temperature and young stars in the Taurus and Ophiuchus complexes. *ApJ* **445**, 377–392.

Cleeves, L. I., Adams, F. C., Bergin, E. A. (2013, July). Exclusion of Cosmic Rays in Protoplanetary Disks: Stellar and Magnetic Effects. *ApJ* **772**, 5.

Cohen, M., Emerson, J. P., Beichman, C. A. (1989, April). A reexamination of luminosity sources in T Tauri stars. I - Taurus -Auriga. *ApJ* **339**, 455–473.

de Gregorio-Monsalvo, I., Ménard, F., Dent, W., Pinte, C., López, C., Klaassen, P., Hales, A., Cortés, P., Rawlings, M. G., Tachihara, K., Testi, L., Takahashi, S., Chapillon, E., Mathews, G., Juhasz, A., Akiyama, E., Higuchi, A. E., Saito, M., Nyman, L.-Å., Phillips, N., Rodón, J., Corder, S., Van Kempen, T. (2013, September). Unveiling the gas-and-dust disk structure in HD 163296 using ALMA observations. *A&A* **557**, A133.

de Juan Ovelar, M., Min, M., Dominik, C., Thalmann, C., Pinilla, P., Benisty, M., Birnstiel, T. (2014, January). The different faces of transitional discs. In M. Booth, B. C. Matthews, & J. R. Graham (eds.), *Exploring the Formation and Evolution of Planetary Systems*, Vol 299 of *IAU Symposium*, pp. 155–156.

Decin, L., Cox, N. L. J., Royer, P., Van Marle, A. J., Vandenbussche, B., Ladjal, D., Kerschbaum, F., Ottensamer, R., Barlow, M. J., Blommaert, J. A. D. L., Gomez, H. L., Groenewegen, M. A. T., Lim, T., Swinyard, B. M., Waelkens, C., Tielens, A. G. G. M. (2012, December). The enigmatic nature of the circumstellar envelope and bow shock surrounding Betelgeuse as revealed by Herschel. I. Evidence of clumps, multiple arcs, and a linear bar-like structure. *A&A* **548**, A113.

Dent, W. R. F., Thi, W. F., Kamp, I., Williams, J. P., Menard, F., Andrews, S., Ardila, D., Aresu, G., Augereau, J.-C., Barrado y Navascues, D., Brittain, S., Carmona, A., Ciardi, D., Danchi, W., Donaldson, J., Duchene, G., Eiroa, C., Fedele, D., Grady, C., de Gregorio-Molsalvo, I., Howard, C., Huélamo, N., Krivov, A., Lebreton, J., Liseau, R., Martin-Zaidi, C., Mathews, G., Meeus, G., Mendigutía, I., Montesinos, B., Morales-Calderon, M., Mora, A., Nomura, H., Pantin, E., Pascucci, I., Phillips, N., Pinte, C., Podio, L., Ramsay, S. K., Riaz, B., Riviere-Marichalar, P., Roberge, A., Sandell, G., Solano, E., Tilling, I., Torrelles, J. M., Vandenbusche, B., Vicente, S., White, G. J., Woitke, P. (2013, May). GASPS - A Herschel Survey of Gas and Dust in Protoplanetary Disks: Summary and Initial Statistics. *PASP* **125**, 477–505.

Donati, J.-F., Gregory, S. G., Montmerle, T., Maggio, A., Argiroffi, C., Sacco, G., Hussain, G., Kastner, J., Alencar, S. H. P., Audard, M., Bouvier, J., Damiani, F., Güdel, M., Huenemoerder, D., Wade, G. A. (2011, November).

The close classical T Tauri binary V4046 Sgr: complex magnetic fields and distributed mass accretion. *MNRAS* **417**, 1747–1759.

Dorschner, J., Begemann, B., Henning, T., Jaeger, C., Mutschke, H. (1995, August). Steps toward interstellar silicate mineralogy. II. Study of Mg-Fe-silicate glasses of variable composition. *A&A* **300**, 503.

Duchêne, G., McCabe, C., Pinte, C., Stapelfeldt , K. R., Ménard, F., Duvert, G., Ghez, A. M., Maness, H. L., Bouy, H., Barrado y Navascués, D., Morales-Calderón, M., Wolf, S., Padgett, D. L., Brooke, T. Y., Noriega-Crespo, A. (2010, March). Panchromatic Observations and Modeling of the HV Tau C Edge-on Disk. *ApJ* **712**, 112–129.

Espaillat, C., Calvet, N., D'Alessio, P., Hernández, J., Qi, C., Hartmann, L., Furlan, E., Watson, D. M. (2007, December). On the Diversity of the Taurus Transitional Disks: UX Tauri A and LkCa 15. *ApJL* **670**, L135–L138.

Fedele, D., van Dishoeck, E. F., Kama, M., Bruderer, S., Hogerheijde, M. (2016, April). Probing the 2D temperature structure of protoplanetary disks with Herschel observations of high-J CO lines. *ArXiv e-prints*, 1604.02055.

Feigelson, E. D., Garmire, G. P., Pravdo, S. H. (2002, June). Magnetic Flaring in the Pre-Main-Sequence Sun and Implications for the Early Solar System. *ApJ* **572**, 335–349.

Frasca, A., Biazzo, K., Lanzafame, A. C., Alcalá , J. M., Brugaletta, E., Klutsch, A., Stelzer, B., Sacco, G. G., Spina, L., Jeffries, R. D., Montes, D., Alfaro, E. J., Barentsen, G., Bonito, R., Gameiro, J. F., López-Santiago, J., Pace, G., Pasquini, L., Prisinzano, L., Sousa, S. G., Gilmore, G., Randich, S., Micela, G., Bragaglia, A., Flaccomio, E., Bayo, A., Costado, M. T., Franciosini, E., Hill, V., Hourihane, A., Jofré, P., Lardo, C., Maiorca, E., Masseron, T., Morbidelli, L., Worley, C. C. (2015, March). The Gaia-ESO Survey: Chromospheric emission, accretion properties, and rotation in γ Velorum and Chamaeleon I. *A&A* **575**, A4.

Ginsburg, A., Henkel, C., Ao, Y., Riquelme, D., Kauffmann, J., Pillai, T., Mills, E. A. C., Requena-Torres, M. A., Immer, K., Testi, L., Ott, J., Bally, J., Battersby, C., Darling, J., Aalto, S., Stanke, T., Kendrew, S., Kruijssen, J. M. D., Longmore, S., Dale, J., Guesten, R., Menten, K. M. (2016, February). Dense gas in the Galactic central molecular zone is warm and heated by turbulence. *A&A* **586**, A50.

Glassgold, A. E., Feigelson, E. D., Montmerle, T., Wolk, S. (2005, December). X-Ray Flares of Sun-like Young Stellar Objects and Their Effects on Protoplanetary Disks. In A. N. Krot, E. R. D. Scott, & B. Reipurth (eds.), *Chondrites and the Protoplanetary Disk*, Vol 341 of *Astronomical Society of the Pacific Conference Series*, pp. 165.

Grosso, N., Alves, J., Wood, K., Neuhäuser, R., Montmerle, T., Bjorkman, J. E. (2003, March). Spatial Study with the Very Large Telescope of a New Resolved Edge-on Circumstellar Dust Disk Discovered at the Periphery of the ρ Ophiuchi Dark Cloud. *ApJ* **586**, 296–305.

Güdel, M., Briggs, K. R., Arzner, K., Audard, M., Bouvier, J., Feigelson, E. D., Franciosini, E., Glauser, A., Grosso, N., Micela, G., Monin, J.-L., Montmerle, T., Padgett, D. L., Palla, F., Pillitteri, I., Rebull, L., Scelsi, L., Silva, B., Skinner, S. L., Stelzer, B., Telleschi, A. (2007, June). The XMM-Newton extended survey of the Taurus molecular cloud (XEST). *A&A* **468**, 353–377.

Güdel, M., Lahuis, F., Briggs, K. R., Carr, J., Glassgold, A. E., Henning, T., Najita, J. R., van Boekel, R., van Dishoeck, E. F. (2010, September). On the origin of [NeII] 12.81 μm emission from pre-main sequence stars: Disks, jets, and accretion. *A&A* **519**, A113.

Gullbring, E., Hartmann, L., Briceño, C., Calvet, N. (1998, January). Disk Accretion Rates for T Tauri Stars. *ApJ* **492**, 323–341.

Hein Bertelsen, R. P., Kamp, I., Goto, M., van der Plas, G., Thi, W.-F., Waters, L. B. F. M., van den Ancker, M. E., Woitke, P. (2014, January). CO ro-vibrational lines in HD 100546. A search for disc asymmetries and the role of fluorescence. *A&A* **561**, A102.

Hein Bertelsen, R. P., Kamp, I., van der Plas, G., van den Ancker, M. E., Waters, L. B. F. M., Thi, W.-F., Woitke, P. (2016a, March). A proposed new diagnostic for Herbig disc geometry: FWHM versus J of CO ro-vibrational lines. *ArXiv e-prints*, 1603.03546.

Hein Bertelsen, R. P., Kamp, I., van der Plas, G., van den Ancker, M. E., Waters, L. B. F. M., Thi, W.-F., Woitke, P. (2016b, May). Variability in the CO ro-vibrational lines from HD163296. *MNRAS* **458**, 1466–1477.

Herbig, G. H. (1960, March). The Spectra of Be- and Ae-Type Stars Associated with Nebulosity. *ApJS* **4**, 337.

Herczeg, G. J., Cruz, K. L., Hillenbrand, L. A. (2009, May). Measuring Tiny Mass Accretion Rates Onto Young Brown Dwarfs. *ApJ* **696**, 1589–1599.

Herczeg, G. J., Hillenbrand, L. A. (2014, May). An Optical Spectroscopic Study of T Tauri Stars. I. Photospheric Properties. *ApJ* **786**, 97.

Hillen, M., de Vries, B. L., Menu, J., Van Winckel, H., Min, M., Mulders, G. D. (2015a, June). The evolved circumbinary disk of AC Herculis: a radiative transfer, interferometric, and mineralogical study. *A&A* **578**, A40.

Hillen, M., Menu, J., de Vries, B. L., Van Winckel, H., Min, M., Mulders, G. D., Gielen, C., Wevers, T., Regibo, S., Verhoelst, T. (2015b, August). A Tale of Two Stars: Interferometric Studies of Post-AGB Binaries. In F. Kerschbaum, R. F. Wing, & J. Hron (eds.), *Why Galaxies Care about AGB Stars III: A Closer Look in Space and Time*, Vol 497 of *Astronomical Society of the Pacific Conference Series*, pp. 175.

Howard, C. D., Sandell, G., Vacca, W. D., Duchêne, G., Mathews, G., Augereau, J.-C., Barrado, D., Dent, W. R. F., Eiroa, C., Grady, C., Kamp, I., Meeus, G., Ménard, F., Pinte, C., Podio, L., Riviere-Marichalar, P., Roberge, A., Thi, W.-F., Vicente, S., Williams, J. P. (2013, October). Herschel/PACS Survey of Protoplanetary Disks in Taurus/Auriga Observations of [O I] and [C II], and Far-infrared Continuum. *ApJ* **776**, 21.

Hughes, J., Hartigan, P., Krautter, J., Kelemen, J. (1994, September). The stellar population of the Lupus clouds. *AJ* **108**, 1071–1090.

Hung, L.-W., Duchêne, G., Arriaga, P., Fitzgerald, M. P., Maire, J., Marois, C., Millar-Blanchaer, M. A., Bruzzone, S., Rajan, A., Pueyo, L., Kalas, P. G., De Rosa, R. J., Graham, J. R., Konopacky, Q., Wolff, S. G., Ammons, S. M., Chen, C. H., Chilcote, J. K., Draper, Z. H., Esposito, T. M., Gerard, B., Goodsell, S., Greenbaum, A., Hibon, P., Hinkley, S., Macintosh, B., Marchis, F., Metchev, S., Nielsen, E. L., Oppenheimer, R., Patience, J. L., Perrin, M. D., Rantakyrö, F. T., Sivaramakrishnan, A., Wang, J. J., Ward-Duong, K., Wiktorowicz, S. J. (2015, December). First Scattered-light Image of the Debris Disk around HD 131835 with the Gemini Planet Imager. *ApJL* **815**, L14.

Ida, S., Lin, D. N. C. (2005, June). Toward a Deterministic Model of Planetary Formation. III. Mass Distribution of Short-Period Planets around Stars of Various Masses. *ApJ* **626**, 1045–1060.

Ingleby, L., Calvet, N., Herczeg, G., Blaty, A., Walter, F., Ardila, D., Alexander, R., Edwards, S., Espaillat, C., Gregory, S. G., Hillenbrand, L., Brown, A. (2013, April). Accretion Rates for T Tauri Stars Using Nearly Simultaneous Ultraviolet and Optical Spectra. *ApJ* **767**, 112.

Ingleby, L., Calvet, N., Hernández, J., Briceño, C., Espaillat, C., Miller, J., Bergin, E., Hartmann, L. (2011, April). Evolution of X-ray and Far-ultraviolet Disk-dispersing Radiation Fields. *AJ* **141**, 127.

Jeffers, S. V., Min, M., Waters, L. B. F. M., Canovas, H., Pols, O. R., Rodenhuis, M., de Juan Ovelar, M., Keller, C. U., Decin, L. (2014, December). Surprising detection of an equatorial dust lane on the AGB star IRC+10216. *A&A* **572**, A3.

Jeffers, S. V., Min, M., Waters, L. B. F. M., Canovas, H., Rodenhuis, M., de Juan Ovelar, M., Chies-Santos, A. L., Keller, C. U. (2012, March). Direct imaging of a massive dust cloud around R Coronae Borealis. *A&A* **539**, A56.

Johns-Krull, C. M., Valenti, J. A., Linsky, J. L. (2000, August). An IUE Atlas of Pre-Main-Sequence Stars. II. Far-Ultraviolet Accretion Diagnostics in T Tauri Stars. *ApJ* **539**, 815–833.

Kamp, I., Thi, W.-F., Meeus, G., Woitke, P., Pinte, C., Meijerink, R., Spaans, M., Pascucci, I., Aresu, G., Dent, W. R. F. (2013, November). Uncertainties in water chemistry in disks: An application to TW Hydrae. *A&A* **559**, A24.

Kamp, I., Tilling, I., Woitke, P., Thi, W., Hogerheijde, M. (2010, February). Radiation thermo-chemical models of protoplanetary disks. II. Line diagnostics. *A&A* **510**, A18.

Khouri, T., Waters, L. B. F. M., de Koter, A., Decin, L., Min, M., de Vries, B. L., Lombaert, R., Cox, N. L. J. (2015, May). Dusty wind of W Hydrae. Multi-wavelength modelling of the present-day and recent mass loss. *A&A* **577**, A114.

Kraus, A. L., Hillenbrand, L. A. (2009, October). The Coevality of Young Binary Systems. *ApJ* **704**, 531–547.

Kraus, A. L., Ireland, M. J., Martinache, F., Hillenbrand, L. A. (2011, April). Mapping the Shores of the Brown Dwarf Desert. II. Multiple Star Formation in Taurus-Auriga. *ApJ* **731**, 8.

Lahuis, F., van Dishoeck, E. F., Blake, G. A., Evans, II, N. J., Kessler-Silacci, J. E., Pontoppidan, K. M. (2007, August). c2d Spitzer IRS Spectra of Disks around T Tauri Stars. III. [Ne II], [Fe I], and H_2 Gas-Phase Lines. *ApJ* **665**, 492–511.

Laughlin, G., Bodenheimer, P., Adams, F. C. (2004, September). The Core Accretion Model Predicts Few Jovian-Mass Planets Orbiting Red Dwarfs. *ApJL* **612**, L73–L76.

Lebreton, J., Augereau, J.-C., Thi, W.-F., Roberge, A., Donaldson, J., Schneider, G., Maddison, S. T., Ménard, F., Riviere-Marichalar, P., Mathews, G. S., Kamp, I., Pinte, C., Dent, W. R. F., Barrado, D., Duchêne, G., Gonzalez, J.-F., Grady, C. A., Meeus, G., Pantin, E., Williams, J. P., Woitke, P. (2012, March). An icy Kuiper belt around the young solar-type star HD 181327. *A&A* **539**, A17.

Luhman, K. L. (2007, November). The Stellar Population of the Chamaeleon I Star-forming Region. *ApJS* **173**, 104–136.

Madlener, D., Wolf, S., Dutrey, A., Guilloteau, S. (2012, July). The circumstellar disk of HH 30. Searching for signs of disk evolution with multi-wavelength modeling. *A&A* **543**, A81.

Manara, C. F., Testi, L., Natta, A., Rosotti, G., Benisty, M., Ercolano, B., Ricci, L. (2014, August). Gas content of transitional disks: a VLT/X-Shooter study of accretion and winds. *A&A* **568**, A18.

Manset, N., Bastien, P., Ménard, F., Bertout, C., Le van Suu, A., Boivin, L. (2009, May). Photometric and polarimetric clues to the circumstellar environment of RY Lupi. *A&A* **499**, 137–148.

Mathews, G. S., Williams, J. P., Ménard, F. (2012, July). 880 μm Imaging of a Transitional Disk in Upper Scorpius: Holdover from the Era of Giant Planet Formation? *ApJ* **753**, 59.

McJunkin, M., France, K., Schneider, P. C., Herczeg, G. J., Brown, A., Hillenbrand, L., Schindhelm, E., Edwards, S. (2014, January). Direct Measurement of Interstellar Extinction toward Young Stars Using Atomic Hydrogen Lyα Absorption. *ApJ* **780**, 150.

Meeus, G., Montesinos, B., Mendigutía, I., Kamp, I., Thi, W. F., Eiroa, C., Grady, C. A., Mathews, G., Sandell, G., Martin-Zaïdi, C., Brittain, S., Dent, W. R. F., Howard, C., Ménard, F., Pinte, C., Roberge, A., Vandenbussche, B., Williams, J. P. (2012, August). Observations of Herbig Ae/Be stars with Herschel/PACS. The atomic and molecular contents of their protoplanetary discs. *A&A* **544**, A78.

Meijerink, R., Aresu, G., Kamp, I., Spaans, M., Thi, W.-F., Woitke, P. (2012, November). Far-ultraviolet and X-ray irradiated protoplanetary disks: a grid of models. I. The disk structure. *A&A* **547**, A68.

Meijerink, R., Spaans, M., Kamp, I., Aresu, G., Thi, W.-F., Woitke, P. (2013, October). Tracing the Physical Conditions in Active Galactic Nuclei with Time-Dependent Chemistry. *Journal of Physical Chemistry A* **117**, 9593–9604.

Mendigutía, I., Fairlamb, J., Montesinos, B., Oudmaijer, R. D., Najita, J. R., Brittain, S. D., van den Ancker, M. E. (2014, July). Stellar Parameters and Accretion Rate of the Transition Disk Star HD 142527 from X-Shooter. *ApJ* **790**, 21.

Mendigutía, I., Mora, A., Montesinos, B., Eiroa, C., Meeus, G., Merín, B., Oudmaijer, R. D. (2012, July). Accretion-related properties of Herbig Ae/Be stars. Comparison with T Tauris. *A&A* **543**, A59.

Min, M., Rab, C., Woitke, P., Dominik, C., Ménard, F. (2016, January). Multiwavelength optical properties of compact dust aggregates in protoplanetary disks. *A&A* **585**, A13.

Miotello, A., Bruderer, S., van Dishoeck, E. F. (2014, December). Protoplanetary disk masses from CO isotopologue line emission. *A&A* **572**, A96.

Moerchen, M., Perrin, M. D., Chen, C., Choquet, E., Debes, J. H., Golimowski, D. A., Hagan, J., Hines, D. C., Mittal, T., N'Diaye, M., Pueyo, L., Reid, I. N., Schneider, G., Wolff, S., Soummer, R. (2014, January). Archival Legacy Investigations of Circumstellar Environments (ALICE): Debris Disks Newly Resolved in Scattered Light from the HST NICMOS Archive. In *American Astronomical Society Meeting Abstracts #223*, Vol 223 of *American Astronomical Society Meeting Abstracts*, pp. 350.

Montesinos, B., Eiroa, C., Mora, A., Merín, B. (2009, March). Parameters of Herbig Ae/Be and Vega-type stars. *A&A* **495**, 901–917.

O'Dell, C. R., Wen, Z. (1994, November). Postrefurbishment mission Hubble Space Telescope images of the core of the Orion Nebula: Proplyds, Herbig-Haro objects, and measurements of a circumstellar disk. *ApJ* **436**, 194–202.

Padovani, M., Galli, D., Glassgold, A. E. (2009, July). Cosmic-ray ionization of molecular clouds. *A&A* **501**, 619–631.

Palla, F., Stahler, S. W. (2002, December). Star Formation in Space and Time: Taurus-Auriga. *ApJ* **581**, 1194–1203.

Perrin, M. D., Duchene, G., Millar-Blanchaer, M., Fitzgerald, M. P., Graham, J. R., Wiktorowicz, S. J., Kalas, P. G., Macintosh, B., Bauman, B., Cardwell, A., Chilcote, J., De Rosa, R. J., Dillon, D., Doyon, R., Dunn, J., Erikson, D., Gavel, D., Goodsell, S., Hartung, M., Hibon, P., Ingraham, P., Kerley, D., Konapacky, Q., Larkin, J. E., Maire, J., Marchis, F., Marois, C., Mittal, T., Morzinski, K. M., Oppenheimer, B. R., Palmer, D. W., Patience, J., Poyneer, L., Pueyo, L., Rantakyrö, F. T., Sadakuni, N., Saddlemyer, L., Savransky, D., Soummer, R., Sivaramakrishnan, A., Song, I., Thomas, S., Wallace, J. K., Wang, J. J., Wolff, S. G. (2015, February). Polarimetry with the Gemini Planet Imager: Methods, Performance at First Light, and the Circumstellar Ring around HR 4796A. *ApJ* **799**, 182.

Pety, J., Gueth, F., Guilloteau, S., Dutrey, A. (2006, November). Plateau de Bure interferometer observations of the disk and outflow of HH 30. *A&A* **458**, 841–854.

Pickles, A., Depagne, É. (2010, December). All-Sky Spectrally Matched UBVRI-ZY Magnitudes for Stars in the Tycho2 Catalog. *PASP* **122**, 1437–1464.

Pinte, C., Laibe, G. (2014, May). Diversity in the outcome of dust radial drift in protoplanetary discs. *A&A* **565**, A129.

Podio, L., Kamp, I., Codella, C., Cabrit, S., Nisini, B., Dougados, C., Sandell, G., Williams, J. P., Testi, L., Thi, W.-F., Woitke, P., Meijerink, R., Spaans, M., Aresu, G., Ménard, F., Pinte, C. (2013, March). Water Vapor in the Protoplanetary Disk of DG Tau. *ApJL* **766**, L5.

Podio, L., Kamp, I., Codella, C., Nisini, B., Aresu, G., Brittain, S., Cabrit, S., Dougados, C., Grady, C., Meijerink, R., Sandell, G., Spaans, M., Thi, W.-F., White, G. J., Woitke, P. (2014, March). Probing the Gaseous Disk of T Tau N with CN 5-4 Lines. *ApJL* **783**, L26.

Pollack, J. B., Hubickyj, O., Bodenheimer, P., Lissauer, J. J., Podolak, M., Greenzweig, Y. (1996, November). Formation of the Giant Planets by Concurrent Accretion of Solids and Gas. *Icarus* **124**, 62–85.

Pontoppidan, K. M., Meijerink, R., Dullemond, C. P., Blake, G. A. (2009, October). A New Raytracer for Modeling AU-Scale Imaging of Lines from Protoplanetary Disks. *ApJ* **704**, 1482–1494.

Pontoppidan, K. M., Salyk, C., Blake, G. A., Meijerink, R., Carr, J. S., Najita, J. (2010, September). A Spitzer Survey of Mid-infrared Molecular Emission from Protoplanetary Disks. I. Detection Rates. *ApJ* **720**, 887–903.

Qi, C., Öberg, K. I., Wilner, D. J., D'Alessio, P., Bergin, E., Andrews, S. M., Blake, G. A., Hogerheijde, M. R., van Dishoeck, E. F. (2013, August). Imaging of the CO Snow Line in a Solar Nebula Analog. *Science* **341**, 630–632.

Ribas, Á., Bouy, H., Merín, B. (2015, April). Protoplanetary disk lifetimes vs. stellar mass and possible implications for giant planet populations. *A&A* **576**, A52.

Rice, W. K. M., Armitage, P. J. (2009, July). Time-dependent models of the structure and stability of self-gravitating protoplanetary discs. *MNRAS* **396**, 2228–2236.

Roberge, A., Kamp, I., Montesinos, B., Dent, W. R. F., Meeus, G., Donaldson, J. K., Olofsson, J., Moór, A., Augereau, J.-C., Howard, C., Eiroa, C., Thi, W.-F., Ardila, D. R., Sandell, G., Woitke, P. (2013, July). Herschel Observations of Gas and Dust in the Unusual 49 Ceti Debris Disk. *ApJ* **771**, 69.

Sacco, G. G., Flaccomio, E., Pascucci, I., Lahuis, F., Ercolano, B., Kastner, J. H., Micela, G., Stelzer, B., Sterzik, M. (2012, March). High-resolution Spectroscopy of Ne II Emission from Young Stellar Objects. *ApJ* **747**, 142.

Salyk, C., Herczeg, G. J., Brown, J. M., Blake, G. A., Pontoppidan, K. M., van Dishoeck, E. F. (2013, May). Measuring Protoplanetary Disk Accretion with H I Pfund β. *ApJ* **769**, 21.

Salyk, C., Pontoppidan, K. M., Blake, G. A., Najita, J. R., Carr, J. S. (2011, April). A Spitzer Survey of Mid-infrared Molecular Emission from Protoplanetary Disks. II. Correlations and Local Thermal Equilibrium Models. *ApJ* **731**, 130.

Sartori, M. J., Lépine, J. R. D., Dias, W. S. (2003, June). Formation scenarios for the young stellar associations between galactic longitudes l = 280degr - 360degr. *A&A* **404**, 913–926.

Schindhelm, E., France, K., Herczeg, G. J., Bergin, E., Yang, H., Brown, A., Brown, J. M., Linsky, J. L., Valenti, J. (2012, September). Lyα Dominance of the Classical T Tauri Far-ultraviolet Radiation Field. *ApJL* **756**, L23.

Sitarski, B. N., Morris, M. R., Lu, J. R., Duchêne, G., Stolte, A., Becklin, E. E., Ghez, A. M., Zinnecker, H. (2013, June). Keck Adaptive Optics Observations of the Protostellar Disk around Radio Source I in the Orion Kleinmann-Low Nebula. *ApJ* **770**, 134.

Skiff, B. A. (2014, October). VizieR Online Data Catalog: Catalogue of Stellar Spectral Classifications (Skiff, 2009-2014). *VizieR Online Data Catalog* **1**, 2023.

Smith, B. A., Terrile, R. J. (1984, December). A circumstellar disk around Beta Pictoris. *Science* **226**, 1421–1424.

Song, L., Balakrishnan, N., Walker, K. M., Stancil, P. C., Thi, W. F., Kamp, I., van der Avoird, A., Groenenboom, G. C. (2015, November). Quantum Calculation of Inelastic CO Collisions with H. III. Rate Coefficients for Ro-vibrational Transitions. *ApJ* **813**, 96.

Stark, C. C., Schneider, G., Weinberger, A. J., Debes, J. H., Grady, C. A., Jang-Condell, H., Kuchner, M. J. (2014, July). Revealing Asymmetries in the HD 181327 Debris Disk: A Recent Massive Collision or Interstellar Medium Warping. *ApJ* **789**, 58.

Testi, L., Natta, A., Shepherd, D. S., Wilner, D. J. (2003, May). Large grains in the disk of CQ Tau. *A&A* **403**, 323–328.

Thi, W. F., Kamp, I., Woitke, P., van der Plas, G., Bertelsen, R., Wiesenfeld, L. (2013, March). Radiation thermo-chemical models of protoplanetary discs. IV. Modelling CO ro-vibrational emission from Herbig Ae discs. *A&A* **551**, A49.

Thi, W. F., van Dishoeck, E. F., Blake, G. A., van Zadelhoff, G. J., Horn, J., Becklin, E. E., Mannings, V., Sargent, A. I., van den Ancker, M. E., Natta, A., Kessler, J. (2001, November). H_2 and CO Emission from Disks around T Tauri and Herbig Ae Pre-Main-Sequence Stars and from Debris Disks around Young Stars: Warm and Cold Circumstellar Gas. *ApJ* **561**, 1074–1094.

Thilliez, E., Maddison, S. T. (2015, October). The Impact of Initial Conditions in N-Body Simulations of Debris Discs. *PASA* **32**, e039.

Thilliez, E., Maddison, S. T. (2016, April). Numerical predictions for planets in the debris discs of HD 202628 and HD 207129. *MNRAS* **457**, 1690–1701.

Torres, C. A. O., Quast, G. R., da Silva, L., de La Reza, R., Melo, C. H. F., Sterzik, M. (2006, December). Search for associations containing young stars (SACY). I. Sample and searching method. *A&A* **460**, 695–708.

Trotta, F., Testi, L., Natta, A., Isella, A., Ricci, L. (2013, October). Constraints on the radial distribution of the dust properties in the CQ Tauri protoplanetary disk. *A&A* **558**, A64.

Umebayashi, T., Katsuma, N., Nomura, H. (2013, February). Effects of Dust Growth and Settling on the Ionization by Radionuclides. I. Formulation and Results in a Quiescent State of Protoplanetary Disks. *ApJ* **764**, 104.

Umebayashi, T., Nakano, T. (2009, January). Effects of Radionuclides on the Ionization State of Protoplanetary Disks and Dense Cloud Cores. *ApJ* **690**, 69–81.

van der Plas, G., Ménard, F., Ward-Duong, K., Bulger, J., Harvey, P. M., Pinte, C., Patience, J., Hales, A., Casassus, S. (2016, March). Dust Masses of Disks around 8 Brown Dwarfs and Very Low-mass Stars in Upper Sco OB1 and Ophiuchus. *ApJ* **819**, 102.

van der Plas, G., van den Ancker, M. E., Waters, L. B. F. M., Dominik, C. (2015, February). The structure of disks around Herbig Ae/Be stars as traced by CO ro-vibrational emission. *A&A* **574**, A75.

van der Wiel, M. H. D., Naylor, D. A., Kamp, I., Ménard, F., Thi, W.-F., Woitke, P., Olofsson, G., Pontoppidan, K. M., Di Francesco, J., Glauser, A. M., Greaves, J. S., Ivison, R. J. (2014, November). Signatures of warm carbon monoxide in protoplanetary discs observed with Herschel SPIRE. *MNRAS* **444**, 3911–3925.

Verhoeff, A. P., Min, M., Pantin, E., Waters, L. B. F. M., Tielens, A. G. G. M., Honda, M., Fujiwara, H., Bouwman, J., van Boekel, R., Dougherty, S. M., de Koter, A., Dominik, C., Mulders, G. D. (2011, April). The complex circumstellar environment of HD 142527. *A&A* **528**, A91.

Walker, K. M., Song, L., Yang, B. H., Groenenboom, G. C., van der Avoird, A., Balakrishnan, N., Forrey, R. C., Stancil, P. C. (2015, September). Quantum Calculation of Inelastic CO Collisions with H. II. Pure Rotational Quenching of High Rotational Levels. *ApJ* **811**, 27.

White, R. J., Hillenbrand, L. A. (2004, December). On the Evolutionary Status of Class I Stars and Herbig-Haro Energy Sources in Taurus-Auriga. *ApJ* **616**, 998–1032.

Williams, J. P., Best, W. M. J. (2014, June). A Parametric Modeling Approach to Measuring the Gas Masses of Circumstellar Disks. *ApJ* **788**, 59.

Woitke, P., Min, M., Pinte, C., Thi, W.-F., Kamp, I., Rab, C., Anthonioz, F., Antonellini, S., Baldovin-Saavedra, C., Carmona, A., Dominik, C., Dionatos, O., Greaves, J., Güdel, M., Ilee, J. D., Liebhart, A., Ménard, F., Rigon, L., Waters, L. B. F. M., Aresu, G., Meijerink, R., Spaans, M. (2016, February). Consistent dust and gas models for protoplanetary disks. I. Disk shape, dust settling, opacities, and PAHs. *A&A* **586**, A103.

Yang, H., Herczeg, G. J., Linsky, J. L., Brown, A., Johns-Krull, C. M., Ingleby, L., Calvet, N., Bergin, E., Valenti, J. A. (2012, January). A Far-ultraviolet Atlas of Low-resolution Hubble Space Telescope Spectra of T Tauri Stars. *ApJ* **744**, 121.

Zhang, K., Isella, A., Carpenter, J. M., Blake, G. A. (2014, August). Comparison of the Dust and Gas Radial Structure in the Transition Disk [PZ99] J160421.7-213028. *ApJ* **791**, 42.

Zubko, V. G., Mennella, V., Colangeli, L., Bussoletti, E. (1996, October). Optical constants of cosmic carbon analogue grains - I. Simulation of clustering by a modified continuous distribution of ellipsoids. *MNRAS* **282**, 1321–1329.